2015

HETEROATOM-DOPED NANOPOROUS CARBONS: SYNTHESIS, CHARACTERIZATION AND APPLICATION TO GAS STORAGE AND SEPARATION

Babak Ashourirad
Virginia Commonwealth University

HETEROATOM-DOPED NANOPOROUS CARBONS: SYNTHESIS, CHARACTERIZATION AND APPLICATION TO GAS STORAGE AND SEPARATION

A dissertation submitted in partial fulfillment of the requirements for the degree of Doctor of Philosophy at Virginia Commonwealth University.

By
Babak Ashourirad

Bachelor of Science
Sharif University of Technology, 2005

Master of Science
Tarbiat Modares University, 2008

Director: Hani M. El-Kaderi,
Associate Professor, Department of Chemistry

Virginia Commonwealth University
Richmond, Virginia
December, 2015

Acknowledgment

I would like to express my deepest gratitude to my advisor, Professor Hani M. El-Kaderi, for his excellent guidance, caring, patience, and providing me with a great atmosphere for doing research. I wish to express my sincere appreciation for my committee members Prof. Massimo F. Bertino, Prof. Indika U. Arachchige, and Prof. Julio C. Alvarez for their willingness to assist whenever needed. I am also indebted to the previous and current members of the El-Kaderi research group with whom I have interacted during the course of my graduate studies. It would have been a lonely lab without them. I certainly share the credit of my work with Department of Chemistry at Virginia Commonwealth University for giving me a chance to peruse my study toward doctorate degree as well as for the financial support. I am eternally grateful to my caring parents for raising me to be the man that I am today as well as my lovely sister, Sara, for her never-ending support and encouragement. Additionally, I would like to thank my dear friend Leah M. Ley for always being just a phone call away when I needed her. This research was supported by the U. S. Department of Energy, Office of Basic Energy Sciences under award number (DE-SC0002576).

Table of Contents

Abstract

HETEROATOM-DOPED NANOPOROUS CARBONS: SYNTHESIS, CHARACTERIZATION AND APPLICATION TO GAS STORAGE AND SEPARATION

By Babak Ashourirad, Ph.D.

A dissertation submitted in partial fulfillment of the requirements for the degree of Doctor of Philosophy at Virginia Commonwealth University.

Virginia Commonwealth University, 2015

Director: Hani M. El-Kaderi, Associate Professor, Department of Chemistry

Activated carbons as emerging classes of porous materials have gained tremendous attention because of their versatile applications such as gas storage/separations sorbents, oxygen reduction reaction (ORR) catalysts and supercapacitor electrodes. This diversity originates from fascinating features such as low-cost, lightweight, thermal, chemical and physical stability as well as adjustable textural properties. More interestingly, sole heteroatom or combinations of various elements can be doped into their framework to modify the surface chemistry. Among all dopants, nitrogen as the most frequently used element, induces basicity and charge delocalization into the carbon network and enhances selective adsorption of CO_2. Transformation of a task-specific and single source precursor to heteroatom-doped carbon through a one-step activation process is considered a novel and efficient strategy.

With these considerations in mind, we developed multiple series of heteroatom doped porous carbons by using nitrogen containing carbon precursors. Benzimidazole-linked polymers

(BILP-5), benzimidazole monomer (BI) and azo-linked polymers (ALP-6) were successfully transformed into heteroatom-doped carbons through chemical activation by potassium hydroxide. Alternative activation by zinc chloride and direct heating was also applied to ALP-6. The controlled activation/carbonization process afforded diverse textural properties, adjustable heteroatom doping levels and remarkable gas sorption properties. Nitrogen isotherms at 77 K revealed that micropores dominate the porous structure of carbons. The highest Brunauer-Emett-Teller (BET) surface area (4171 $m^2 g^{-1}$) and pore volume (2.3 $cm^3 g^{-1}$) were obtained for carbon synthesized by KOH activation of BI at 700 °C. In light of the synergistic effect of basic heteroatoms and fine micropores, all carbons exhibit remarkable gas capture and selectivity. Particularly, BI and BIPL-5 derived carbons feature unprecedented CO_2 uptakes of 6.2 mmol g^{-1} (1 bar) and 2.1 mmol g^{-1} (0.15 bar) at 298 K, respectively. The ALP-6 derived carbons retained considerable amount of nitrogen dopants (up to 14.4 wt%) after heat treatment owing to the presence of more stable nitrogen-nitrogen bonds compared to nitrogen-carbon bonds in BILP-5 and BI precursors. Subsequently, the highest selectivity of 62 for CO_2/N_2 and 11 for CO_2/CH_4 were obtained at 298 K for a carbon prepared by KOH activation of ALP-6 at 500 °C.

Chapter 1: Introduction

1.1 Significance of Carbon Dioxide Capture

The sharp increase of carbon dioxide (CO_2) concentration in the atmosphere in recent decades is believed to be the main cause of climate change and global warming.[1-3] The majority of the CO_2 emissions into the atmosphere originate from the combustion of fossil fuels in order to provide power for industrial plants. To fight against global warming, the world's energy dependency on fossil fuels needs to be cut and replaced by renewable green sources. Meanwhile, carbon dioxide capture and sequestration (CCS) is regarded as a short-term solution until sustainable clean energy is applicable.[3-6] Power plant exhaust gas is a mixture which consists of N_2 (78-80 % by volume), CO_2 (3-15% by volume) and H_2O (5-7% by volume).[7] Therefore, to develop materials for CCS applications several key parameters need to be satisfied such as large CO_2 adsorption capacity at low working pressure, stability in presence of water vapor, high sorption rate and more importantly good selectivity for CO_2 over other competing gases in the stream. Additionally, good recyclability and a low energy consumption for regeneration process should be taken into consideration. However, finding a material that meets all these requirements might not be realistic. In the next section, we will discuss the most widely applied candidates for CO_2 adsorption as well as their advantages and disadvantages.

1.2 Classification of CCS Technologies

Currently, three main technology processes are used to capture CO_2. 1) Post-combustion, which involves collecting of CO_2 from the exhaust gas of a power plant (also known as flue gas). 2) In oxyfuel process, nearly pure oxygen will be used for combustion instead of air. 3) Pre-combustion technology collects CO_2 from the reformed synthesis gas of an upstream gasification unit. The fuel conversion before combustion is a complex and expensive process, but the high density and pressure of CO_2 in the gas allows for easy separation (Figure 1.1).[8]

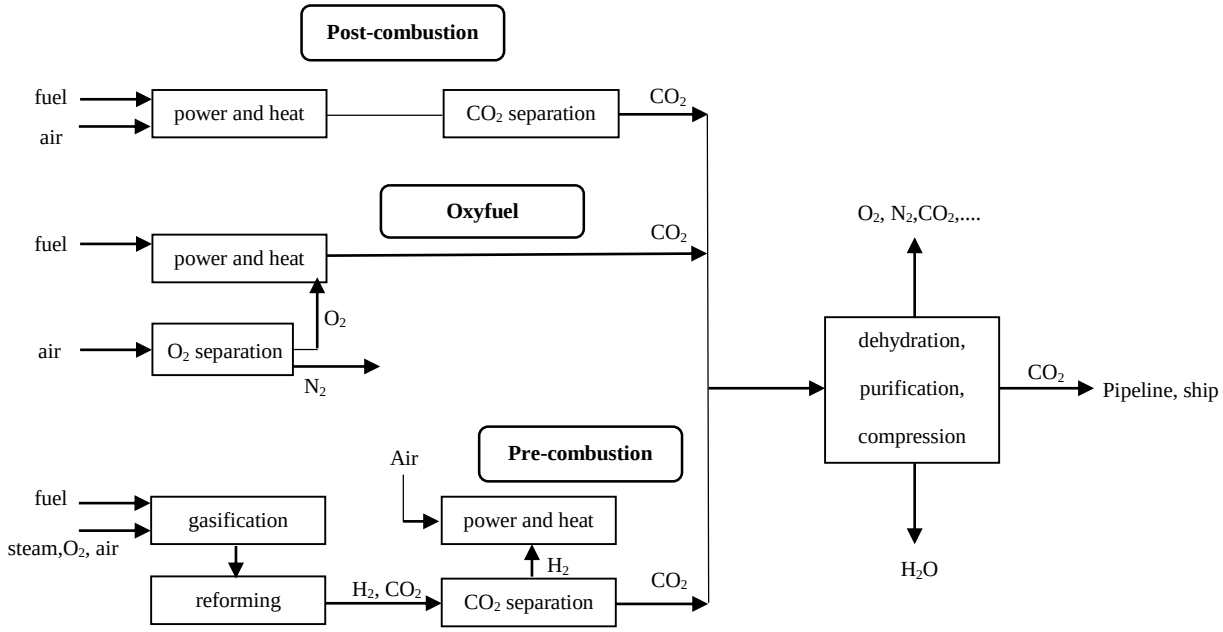

Figure 1.1. Schematic diagrams of currently favored CCS technologies

1.3 Major Mechanisms for Carbon Dioxide Capture

1.3.1 Chemical Absorption by Amine Solutions. Absorption is defined as a process in which guest molecules completely enter into or dissolve in the bulk of host substance (absorbent). Amine scrubbing is based on chemical interaction of CO_2 molecules with the basic amine-containing sites through formation of carbamate species with N-C covalent bond (Figure 1.2). The amine moieties are regenerated by applying heat (stripping with water at 100-120 °C) followed by breaking of covalent C-N bond and release of CO_2.[9] Chemical absorption by amine-based solution is realized as the benchmark and the most effective process for CO_2 capture and sequestration to date. However, this process suffers from severe drawbacks including high energy output for regeneration, instability and volatility of solvent (degradation and evaporation during regeneration processes) and corrosion of equipment (by the high pH liquid amine solution).[10]

1.3.2 Physical Adsorption by Porous Solids. Physisorption (physical adsorption) takes place whenever a gas (adsorptive) is brought into contact with a solid surface (adsorbent). Here, we have to clarify the terms adsorbate and adsorptive. The former is the material in an adsorbed state while the latter is a molecule, which is going to be adsorbed. Long-range London dispersion forces and the short-range intermolecular repulsion are always defined as the major forces in physisorption. The easy regeneration by means of pressure swing or vacuum swing can be done at much lower costs than chemisorption processes. Accordingly, the design and development of numerous solid sorbents during past decades well proves that adsorption can be considered as a promising alternative for amine scrubbing technology. In the following section, we have classified the most frequently studied porous solids that might serve as potential candidates for carbon dioxide capture. However, before that, it is necessary to discuss porous parameters and the most accepted methods for pore characterization.

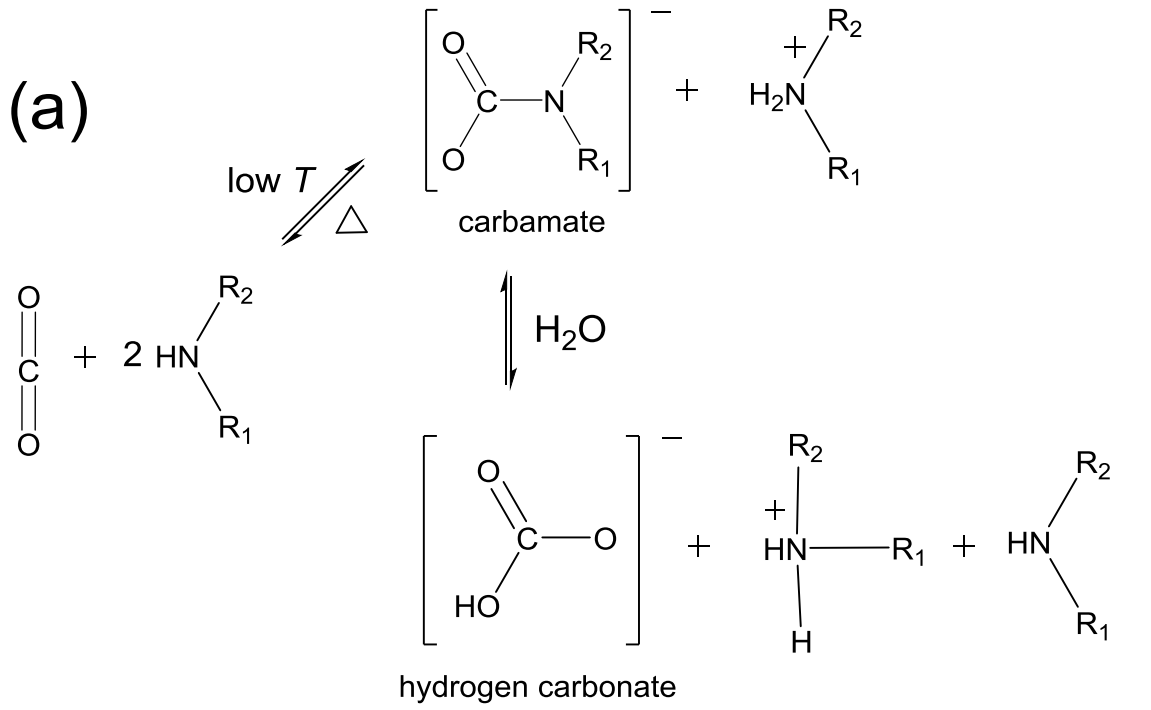

Figure 1.2. General reaction schemes for the chemical absorbtion of CO_2 by (a) primary or secondary and (b) tertiarty amine solution.[1]

1.4 Pore Characterization of Porous Solids

It is worth mentioning that adsorption and absorption are two different uptake processes in nature. While the latter involves trapping the guest molecules in a relatively large space of the bulk of material, the former takes place by interaction of guest molecules on the surface of the adsorbent. As mentioned earlier physisorption defines as weak van der Walls interaction between adsorbate (guest species) and the atoms making up the pore walls of adsorbent (solid). In order to investigate the porous structures of a solid sorbent, a probe gas molecule needs to penetrate into the pores. Employing either nitrogen or argon at cryogenic temperature has been recognized as standard criteria for sorption measurements. However, monoatomic argon molecule has some advantages over diatomic nitrogen molecule. Particularly, quadruple moment of nitrogen molecules might interact with polar surface of a heterogeneous pore. Moreover, performing argon sorption measurement at 87 K (boiling temperature of Ar) compared with nitrogen at 77 K (boiling temperature of N_2) facilitates the equilibrium process and shortens the overall process time. The varying amount of adsorbed gas with respect to relative pressure (P/P_0) is measured by means of a surface area analyzer apparatus. The amount of adsorbed gas (Ar or N_2) per unit of adsorbent at equilibrium is measured against partial pressure of the adsorbate in the gas phase and gives equilibrium adsorption isotherms. The term isotherm is applied because the measurement is carried out at constant temperature. Relative pressure is realized as ratio of absolute pressure (P) to the saturation pressure (P_0) which is the vapor pressure of a pure liquid (around 1 bar for nitrogen or argon at their boiling temperature). Textural properties including specific surface area, total pore volume, pore diameter and pore size distribution can be extracted from N_2 or Ar isotherms.

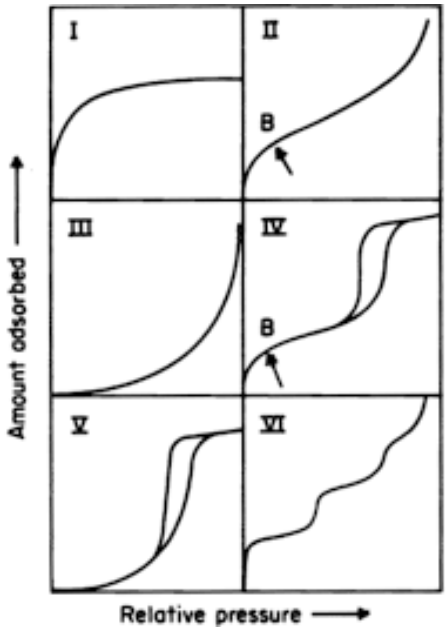

Figure 1.3. Six types of isotherms adopted by AUPAC.[11]

For practical application pores are categorized into three major classes according to their dimensions. 1) Pores with opening greater than 50 nm are designated as "macropores". 2) The term "mesopores" is usually applied for pores with diameters between 2-50 nm. 3) Pores with dimension below 2 nm are identified as "micropores". Due to the significance of micropores in the CO_2 adsorption process, they are further divided into two categories known as ultramicropores (below 0.7 nm) and supermicropores (between 0.7-2 nm). The first systematic attempt to define adsorption isotherms for gas-solid equilibrium was proposed by Brunauer, Deming, Deming, and Teller in 1940.[12] These authors categorized isotherms into five major types. International Union of Pure and Applied Chemistry (IUPAC) as the core of the modern classification of adsorption isotherms adopted this primary classification. Later, Sing *et al.* extended them to six types as demonstrated in Figure 1.3.[11] Type I isotherm, also known as signature of microporous adsorbents,

features a rapid uptake at low pressure area followed by a flat part for the rest of relative pressures. The adsorption of gas molecules is mostly governed by the filling of micropores rather than the external surface area. Type II isotherms are realized for non-porous or macroporous materials and feature a minimal initial slope followed by a gradual increase of uptake with respect to relative pressure. Unrestricted adsorption takes place through monolayer-multilayer formation. The knee point or point B takes place when a monolayer covers the entire pore wall and hence multilayer formation begins to happen. Type III isotherms are rarely observed and are identified by a convex shape for the entire relative pressure range suggesting lower uptake than types I and II. The strong adsorbate-adsorbate interaction is responsible for hindering adsorbate-adsorbent interaction or gas uptake. Type IV is recognized by a hysteresis loop, which occur because of capillary condensation in mesoporous solids. Type V features pore condensation and hysteresis as well as a convex shape and weak interaction between gas-solid in the beginning. Type VI isotherms represent step-shape multilayer adsorption which is indicative of more than one type of sorption site.

Surface area is considered the most important parameter for general evaluation of porous solids for many applications. However, surface area is not a universal concept and its calculated values highly depend upon the method, assumptions and probe molecules. There are many equations proposed to fit the various experimental isotherms among which the Brunauer-Emmett-Teller (BET) theory has been widely accepted for surface area evaluation.[13] BET surface area derived from BET theory is determined based on multilayer formation of adosrbate at the surface of adsorbent. The Langmuir theory which was proposed before BET, determines surface area by the amount of gas adsorbed as a monolayer at the interface of adsorbate/adsorbent.[14]

Aside from surface area, other features of textural property of a porous solid can be determined from gas sorption isotherms. For instance, the total pore volume is calculated from the

amount of vapor adsorbed at a relative pressure close to unity. An assumption has to be made here that the pores filled with liquid adsorbate. Pore size distribution (PSD) can be calculated by applying simulation methods such as Density Functional Theory (DFT) and Monte Carlo (MC) to isotherms. The pore size distribution of micropores and mesopores obtained by simulation models are more reliable than data provided by macroscopic observation such as Dubinin-Radushkevich (D-R), Barrett-Joyner-Halenda (BJH), and Horvath-Kawazoe (HK), which are based on some thermodynamic assumptions. The dominant pore diameter is realized by derivative part of PSD curves while the volume of certain pore sizes (for example pores below 2 nm) is identified by cumulative branch. It is also suggested to use CO_2 as adsorbate gas and derived isotherms at 273 K for assessing ultramicropores.[15] At very low pressures ($10^{-3} – 10^{-7}$ bar), N_2 and Ar molecules at cryogenic temperatures are not able to penetrate into narrow pores and yield unrealistic data. The adsorption of CO_2 at 273 K occurs faster and gives much more reliable information about pore size and distribution of ultramicropores. In general, there is no definite method to evaluate the textural properties and each method is based on a particular theory and some assumptions.

1.5 Solid CO_2 Adsorbing Materials

1.5.1 Metal-Organic Frameworks. A diverse family of metal-organic framework (MOFs) has been formed by reticular synthesis, which creates strong bonds between inorganic (metal clusters) and organic units (ligands). Their surface area, pore size, chemical functionalities and geometry can be easily manipulated by varying their organic and inorganic constituents.[16] Although, MOFs features very high CO_2 uptake at high pressures due to their exceptionally high surface area, their capture capacity performance at very low partial pressure of flue gas is somewhat poor.[17-19] Additionally, the hydrophilic nature of MOFs due to the existence of cation sites limits their application in the vicinity of water vapor.

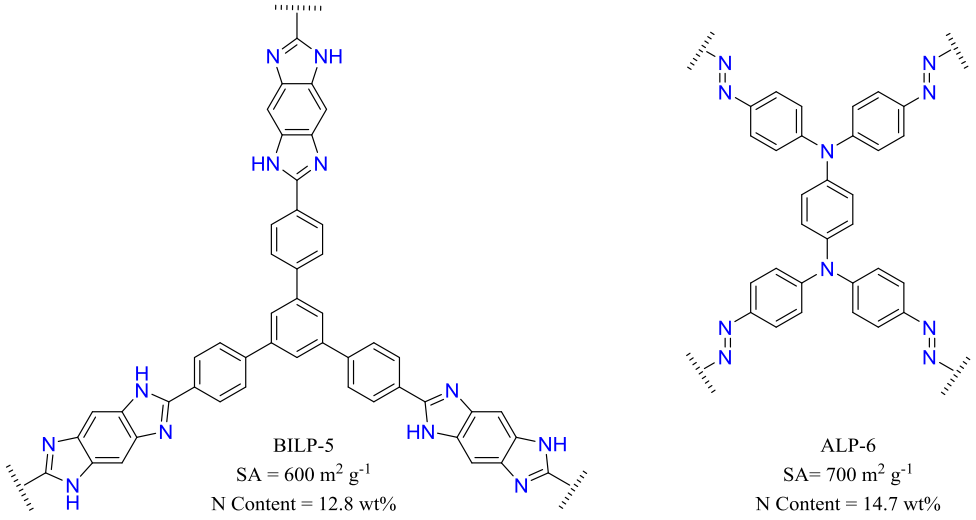

Figure 1.4. Two representative nitrogen rich polymers. ALP-6 (right) and BILP-5 (left)

1.5.2 Porous Organic Polymers. To circumvent moisture sensitivity of MOFs, significant efforts have been devoted to identifying materials that do not contain hydrophilic cation centers. Accordingly, a variety of porous organic polymers (POPs) were synthesized by condensation of two organic constituents or self-condensation of one organic moiety. Recently, POPs as potential CO_2 adsorbent have received enormous interest due to fascinating properties such as high surface area, low density (C, H, N, O are defined as main elements), controllable porous parameters and precise integration of building units into periodic two or three-dimensional structures. In particular, POPs with intrinsic microporosity and basic functional groups show excellent performance in selective CO_2 adsorption. Accordingly, a series of benzimidazole-linked polymers (BILPs) with CO_2 capture capacity as high as 5.12 mmol g^{-1} (at 273 K / 1 bar) and CO_2/N_2 selectivity as high as 63 (at 273 K) was introduced for the first time by El-Kaderi's group.[20-22] In addition to the effect of microporosity achieved by synthetic method, the high CO_2 uptake and selectivity are originated

from strong interactions of the polarizable CO_2 molecules through hydrogen bonding and/or dipole-quadrupole interactions that utilize the protonated and proton-free nitrogen sites of imidazole rings, respectively. Similarly, El-Kaderi's group introduced a new family of azo-linked polymers (ALPs) synthesized via copper (I)-catalyzed self-condensation of aniline-like organic building block as CO_2 adsorbents.[23-24] The highest CO_2 capture capacity and CO_2 over N_2 selectivity of 5.37 mmol g^{-1} and 60 was obtained for ALPs adsorbent, respectively. Scalability and using organic solvents remain two major challenges for application of POPs in industry. Figure 1.4 depicts two representative polymers from ALP and BILP families.

1.5.3 Zeolites and Mesoporous Silicas. Zeolites are a class of crystalline porous aluminosilicate materials, which can occur either naturally or synthetically in the laboratory. They have uniform pore sizes of 0.5-1.2 nm, which forms networks of interconnecting channels or cages for trapping the gas molecules. Most of the moderate surface area and microporous zeolites have shown a promising CO_2 capture capability at room temperature such as zeolite 13X.[25] The CO_2 physisorption on zeolites takes place through ion–dipole interaction or strongly bound carbonate species by bi-coordination.[26] Despite promising CO_2 uptake, the low selective adsorption over other gases (N_2, CH_4 and H_2O) and easy saturation with water vapor from flue gas hinder their application. Additionally, their CO_2 capture performance deteriorates upon increasing the temperature above 30 °C. A great deal of research has been dedicated to enhance CO_2 selective adsorption of zeolites by mechanism such as impregnation/grafting amine, composition and structure modification and cationic exchange.[27-28]

Silica materials display high surface area, large pore volume and manageable range of pore diameters (> 2 nm). In this regard, they are mostly employed as support for adding amine rather than directly as CO_2 adsorbent. [29] Since supports comprise more than 90% of the final cost of CO_2

adsorbents preparation and they are not commercially available, studies for using commercially available, porous and cost-effective silica support attracted a lot of attention.

1.5.4 Activated Carbon. The term activated carbon is correlated to a class of materials with well-developed porous structure, and hence a large capacity for hosting chemicals from gases and liquids. Activated carbon stands out among solid CO_2 sorbents due to the combination of attractive features such as low-cost and availability, chemical stability, high surface area, tunable pore structure and low energy requirement for regeneration. However, most of the activated carbons present moderate CO_2 capture capacity below 3 mmol g^{-1} (at 298 K and 1 bar) which is not comparable with the high uptake values obtained by amine solutions. Moreover, pristine activated carbons are not appropriate for selective adsorption of CO_2 molecules. Nevertheless, their capture capacity and selectivity can be further increased with two major strategies. Tuning the porous structure (such as narrowing down the pore size distribution) seems to be an effective solution to increase the adsorption especially in the low pressure region. Screening of numerous MOFs and porous carbons reveals that narrow pore size (4-8 Å) will expedite CO_2 adsorption owing to overlapping of potential fields of the opposite pore walls and hence strengthening the interaction with CO_2 molecules.[30-31] This strategy for the first time was applied to a porous polymer network (PPN-6) through grafting by sulfonic acid and lithium salt. The results showed that the selectivity of CO_2 over N_2 can reach an exceptionally large value of 414 under ambient condition.[32] In order to obtain carbons with narrower pore size, embedding an extra carbon source to the pores of a carbonaceous polymer and subsequent heat treatment was recently reported. For example, pre-introducing of furfuryl alcohol (FA) into the pores of porous aromatic framework (PAF) followed by thermolysis at 900 °C managed to yield high CO_2 uptake of 4.1 mmol g^{-1} at 295 K / 1 bar

condition.[33] In general, carbons produced through this modification method hold great promise for post combustion capture.

The second strategy refers to modification of the surface chemistry of carbons. CO_2 molecules are slightly acidic due to the electron deficient center on carbon atoms. Therefore, increasing the basicity of the carbon surface will benefit CO_2 adsorption through Lewis acid-base interaction. As a result, a large amount of research has been directed to incorporate basic heteroatoms (mostly nitrogen and oxygen) into the carbon framework structure. In the following section, we will investigate the most widely adopted approaches to incorporate nitrogen and other heteroatom into the framework of carbon. This provides a clue for studies that have been done in this dissertation.

1.6 Nitrogen Doping Methods

1.6.1 Post Synthesis Modification. In this approach, the plain activated carbon is thermally treated with an external source of heteroatom. Namely, ammonia or ammonia-air gas mixture (ammoxidation) have been the most common and frequently used source to generate nitrogen doped carbons.[34] In addition to ammonia, other nitrogen rich reagents such as melamine, dicyanodine amine, nitric acid and hydrogen cyanide also can be used to introduce nitrogen into carbon frameworks. Depending on the physical state of the external source, the treatment is carried out either in solid or liquid phase. The amount of nitrogen incorporated is a function of nitrogen source concentration, temperature and time of heat treatment.[35-37] The heat treatment with ammonia at high temperatures not only helps to modify the surface chemistry of carbon but also alters the textural properties. It has been shown that the decomposition of ammonia at high temperature will generate free radicals such as $^{\circ}NH_2$, $^{\circ}NH$, atomic hydrogen and atomic nitrogen. These radicals then attack the carbon precursor and form nitrogen functionalities and also etch the

framework to develop more porosity.[38] However, nitrogen functional groups developed in such a way are often unstable. High cost, multi-step reaction, corrosion and toxicity of external source are other drawbacks of post synthetic treatment.

1.6.2 Template Method. In this approach, a mesoporous molecular sieve such as zeolite 13X, SBA-15 and MCM-48 is employed as a hard template. Initially, two separate nitrogen and carbons sources or a single source of both nitrogen and carbon will be impregnated (in liquid phase) into the pores of hard templates followed by polymerization at a relatively low temperature (<100 °C). The incorporation of nitrogen into the carbon framework takes place by subsequent high temperature carbonization within the pore channels of mesoporous template. These steps can be shortened if gas-phase chemical vapor deposition (CVD) is used instead of liquid impregnation. In CVD method, a carrier gas is used to transfer the carbon precursor to pores of mesoporous template followed by simultaneous polymerization/carbonization at target temperatures. In addition to the simplicity of the CVD method, other heteroatom can also be doped into the carbon owing to versatility of precursors. Lastly, the hard template needs to be dissolved in a strong acid or base to isolate the final nitrogen doped carbon. Sojka *et al*. used pyrrole as a precursor and SBA-15 mesoporous silica matrix as a template to obtain well-organized graphene layers with nitrogen functionalities (4.6-10.6 wt%) on the surface.[39] Ease of polymerization as well as the abundance of both carbon and nitrogen in pyrrole always makes it a fascinating precursor to generate nitrogen doped carbons.[40] Diaminobenzene (DAB) was also successfully used as single source precursor of both carbon and nitrogen by Gao *et al*. to generate highly nitrogen doped (26.5 wt%) mesoporous carbons.[41] Acetonitrile is another single source precursors which successfully transformed to highly graphitic nitrogen doped carbons through CVD method.[42] Incorporation of other heteroatoms such as oxygen is feasible if the oxygen source also impregnated into the pores.

Oxygen and nitrogen co-doped mesoporous carbon was obtained by hydrothermal carbonization of oxygen rich precursors such as sugar and furfuryl alcohol followed by amination in presence of 3-chloropropylamine.[43]

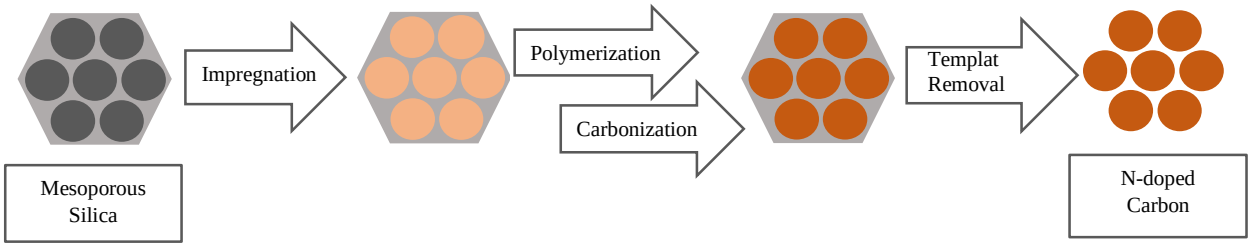

Figure 1.5. Illustration of template synthesis procedure for preparation of nitrogen doped carbon

It can be easily understood that the pore size of the final nitrogen doped carbon relies on templates and can be controlled by varying the template size. Another advantage of this method will be generating more stable nitrogen surface groups with respect to post synthesis heat treatment. However, this method suffers from major drawbacks such as a complex multi-step and time-consuming process. Moreover, the necessity of a strong base or acid for dissolution of the template is realized as a great health concern. The schematic steps of template method to prepare a nitrogen-doped carbon is depicted in Figure 1.5.

1.6.3 Direct Carbonization (Pyrolysis). In this method, development of porosity and nitrogen doping takes place merely through heat treatment of precursor under inert atmosphere. Two separate nitrogen and carbon rich materials or a single source precursor of both elements will be heated to the target temperatures without applying any external agent. The porosity will be generated by formation of some gaseous species and bloating the solid or liquid precursor during carbonization.[44] However, total evaporation and/or decomposition of most of the organic species

limits the selection of suitable precursors for this method. Low-vapor-pressure natural polymers and synthetic polymer can be successfully used for carbonization due to their thermal stability. ZIF-8, a nitrogen rich metal-organic framework, was used as precursor for synthesizing a series of nitrogen decorated carbons with high surface area, CO_2 uptake and selectivity.[45] Kaskel *et al*, obtained a series of nitrogen-doped microporous carbons simply by carbonization of porous imine-linked polymer between 600-800 °C. Retaining noticeable amount of nitrogen (5.6-8.7 wt %) as well as gaining more narrow microporosity during carbonization improved their CO_2 capture performance.[46] Ionic liquids (ILs) which are made up completely cations and anions have been recently employed as a new class of precursors. The carbon-rich nature of ILs as well as their tunable cation-anion combinations, low volatilities, high thermal stabilities and possibility of introducing heteroatoms beyond nitrogen make them ideal candidates for the direct carbonization process.[47] Antonietti *et al.* managed to obtain a vast collection of nitrogen-doped carbons by varying the nitrogen-rich ionic liquids as well as adjusting the thermolysis temperature.[48] In a similar manner to ILs, organic salts also have the potential to be considered as carbonization precursors.[49] Sevilla *et al*. take advantage of co-carbonization of an alkali organic salt and melamine to synthesize a series of nitrogen-doped carbons.[50-51]

1.6.4 Physical Activation. Activation techniques are the most frequently studied methods to produce a vast spectrum of porous carbons. In contrast to the direct carbonization method, a broad range of precursors from biomasses to linear and porous synthetic polymers can be converted to heteroatom-doped carbon by activation approach. In addition, diverse activating agents are employed to tailor the textural properties. Physical activation is regarded as a process of selective gasification of the precursor with carbon dioxide, steam or a mixture of these two gases.[52] The mechanism consists of initial carbonization in an inert atmosphere to eliminate

disorganized carbon or non-carbon atoms on the surface and subsequent pore opening. Further pore widening takes place in the presence of proper oxidizing gas usually at high temperatures (800-1000 °C). The gasification reaction or removal of individual carbon atoms with carbon dioxide gas proceeds as $CO_2 + C \leftrightarrow 2CO$. Physical activation of phenolic resin-based carbon spheres by CO_2 at 850 °C resulted in formation of high surface area spheres with a large fraction of micropores. The remarkable atmospheric CO_2 uptakes values of 4.6 and 8 mmol g^{-1} was obtained on these activated carbon spheres at 298 and 273 K, respectively.[53] Polyacrylonitrile was converted to a nitrogen doped carbon with unprecedented CO_2 capture (11.5 mmol g^{-1} at 273 K and 1 bar), but through a rather complicated two-step physical activation process. The initial heat treatment in air (300 °C) was performed to promote cyclization and aromatization of linear polymer. Then the preheated polymer was converted to carbon by heating under a mixture of argon and carbon dioxide ($Ar:CO_2$, 3:1) up to 1000 °C.[54] We will see in the next section that the same precursor can be transformed to a nitrogen-doped carbon through more efficient chemical activation.

1.6.5 Chemical Activation. The procedure involves mixing precursor(s) with an activating agent (KOH, $ZnCl_2$, H_3PO_4, *etc)* and heating the mixtures to the temperate range of 400-900 °C. The activation mechanism with each chemical is somewhat different. Zinc chloride promotes dehydration by extraction of water from the structure of the carbon molecule while phosphoric acid combines chemically within the structure of the precursor.[55-57] Pore development of carbon framework by potassium hydroxide proceeds as $6KOH + C \leftrightarrow 2K + 3H_2 + 2K_2CO_3$. It is also suggested that at higher activation temperatures the products of K_2CO_3 decomposition (CO_2 and K_2O) further react with carbon and contribute more to the pore formation either through gasification or lattice expansion with metallic potassium.[58] Chemical activation in general is

preferred over physical activation taking into account its superior advantages such as higher yield, higher surface area and pore volume, lower temperature and shorter activation time.

Chemical activation with KOH is well known for introducing micropores into the structure of porous carbon. As a result, by careful selection of a precursor, which is rich in basic heteroatom and subsequent activation, surface chemistry and textural chemistry, can be tuned simultaneously. KOH activation of a single source precursor containing nitrogen and carbon, such as biomasses, commercial and synthetic polymers, has attracted a great deal of attention recently. Biomasses, which are naturally rich in nitrogen and carbon, are the most important candidate due to their sustainability, availability and low-cost. In this regards, biomasses such as yeast,[59] prawn shell,[60] algae[61] and lignocellulosic materials[62] were converted to nitrogen doped carbon with different levels of doping and microposiy through KOH activation. Carbons which are synthesized by KOH activation of commercial polyacrylonitrile features high surface area and nitrogen content of 2231 m^2 g^{-1} and 8 wt%, respectively.[63] In a similar way, polypyrrole was applied as an inexpensive single source of carbon and nitrogen (~ 21-wt% N). The polypyrrole-based activated carbons present high amount of nitrogen groups (up to 10.1 wt% N) and 84% micropores which make them ideal CO_2 sorbent candidates.[40] Porous synthetic polymers with intrinsic nitrogen functionalities such as imine-linked polymers[64], benzimidazole-linked polymers[65] and nitrogen-rich hypercrosslinked porous organic polymers[66] also can be converted to nitrogen doped carbons. Employment of nitrogen rich porous polymers as a single source precursor for chemical activation will further reduce the primary steps such as cleaning, washing, drying, grinding, pre-carbonization and pre-oxidation might be needed for biomasses and commercial linear polymers. In other words, they can be transformed to carbon immediately after synthesis through either physical or solution mixing with KOH.

1.6.6 Other Methods. Hydrothermal treatment of a nitrogen rich carbohydrates biomass derivatives at relatively low temperature (180 °C) is regarded as an effective approach to produce N-doped material.[67] Additionally, hydrothermal treating of natural nitrogen-containing molecules such as amino acids or proteins with glucose or aminated saccharides such as chitosan or glucosamine can produce the nitrogen rich materials up to 8-10 w%.[68] However, this method is just for introducing nitrogen within a carbonaceous scaffold and yields very low surface area (10 m^2g^{-1}). As a result, a subsequent carbonization step at higher temperatures seems to be absolutely necessary when high surface area is needed. The plasma treatment is regarded as a promising technique due to advantages such as presenting a fast, solvent free, simple and controllable procedure. Dielectric-barrier discharge plasma in the presence of nitrogen as career gas was applied to a viscose-based activated carbon fibers (VACFs) to generate nitrogen doping. Despite effective nitrogen modification by plasma, this method just imposes the changes on the surface of carbon materials and leads to slight decrease in the surface area and pore volume.[69]

1.7 Non CCS Applications of Nitrogen Doped Carbons

1.7.1 Separation and Purification. In general, nitrogen and oxygen functionalities on the surface of porous carbon increase the basicity of activated carbon with electron delocalization. Consequently, the adsorption of polar species such as for formaldehyde,[70] NO_2,[71] SO_2,[72] H_2S[73] and water vapor[74] on nitrogen surface group is of great interest for purification purposes. It has been shown that toxic heavy metal ions such as Cr^{3+}, Zn^{2+}, Ni^{2+}, Pb^{2+}, Ag^{+} and Hg^{2+} can be removed from water by basic functional groups *via* coordination mechanisms.[75]

1.7.2 Energy Storage Applications. Carbon dioxide capture and separation is just a short-term solution to reduce the greenhouse effect and mitigate global warming to some extent. In fact, the ultimate goal is the discovery and application of green, renewable and sustainable sources of

energy instead of fossil fuels. Over the course of the last decade supercapacitors as energy storage devices have gained tremendous amount of interest due to high energy density, simple principles, long cycle life, long-term operation stability, low level of heating and high rate capability.[76-77]

Supercapacitors consist of two electrodes immersed in an electrolyte (KOH or H_2SO_4 typically) and separated by a membrane that allows ion transportation (not permeable for electrons) and prevents short circuit at the same time. According to their charge storage mechanism, supercapacitors mainly fall into two main categories: 1) Electric Double Layer Capacitors (EDLC) and 2) pseudocapacitor. The former takes advantage of charge separation upon applying voltage and stores the charge electrostatically at the interface of electrode/electrolyte while the latter store energy by redox reaction (charge transfer) between electrode and electrolyte. Upon applying voltage, (charged state) ions move and adsorb onto the electrode with a different charge. Once the charge state is completed two layers of adsorbed ions on each electrodes will be formed as is depicted in Figure 1.6.

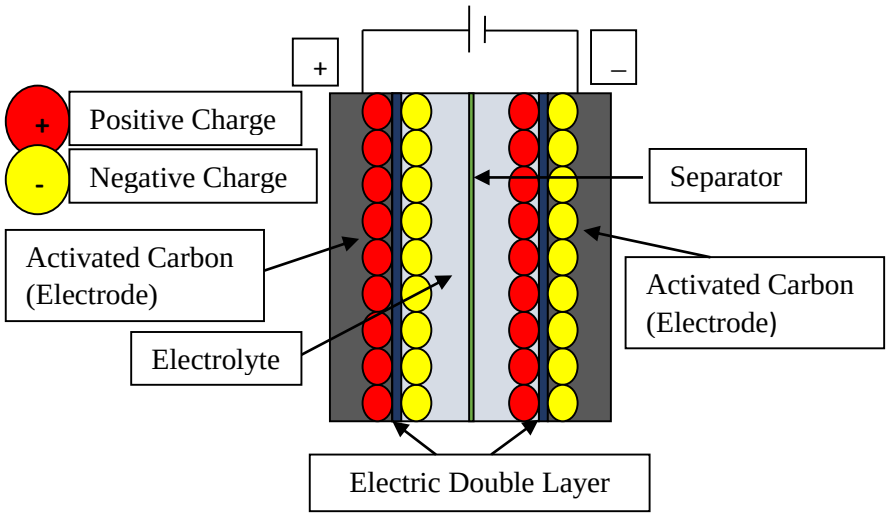

Figure 1.6. Ion absorption mechanism upon applying voltage in EDLCs

Since EDLCs operate by adsorption of electrolyte ions on the surface of electrodes, high surface area conductive material such as pristine activated carbon seems to be a promising electrode material. The capacitive properties of activated carbon can be further enhanced by decorating them with nitrogen heteroatom through inducing a redox reaction effect as well as improving wettability of porous carbons with electrolyte. To further clarify, two collaborative effects make nitrogen doped porous carbons ideal electrode materials: charge separation and storing electrostatically upon applying voltage and redox reaction or charge transfer between electrode and electrolyte. The former will benefit by high porosity of carbon materials and the latter is related to chemical functionalities. In a similar fashion to nitrogen-doped carbons for CO_2 capture, developing and synthesis of nitrogen doped electrode materials has been the subject of numerous research works recently.[78-82]

1.7.3 Catalytic Activity. Activated carbons are considered as ideal supports for catalytic activities. In fact, no other material except carbon exhibits essential features such as high electric conductivity, corrosion resistivity, surface chemistry and low cost for this purpose. Nitrogen-doped porous carbons as heterogeneous catalyst introduce basic sites, which further assists dispersion of catalyst particles, and enhance the interactions with catalyst particles by providing anchoring sites.[83-84] It has been also suggested that nitrogen-doped carbon supports can increase the durability and activity of a Pt catalyst.[85-86]

1.8 Statement of Problem

To this end, we investigated the design, development and strategies toward promising materials for carbon dioxide capture. However, finding a material, which satisfies all the requirements for an ideal adsorbent, is the main challenge. Several significant factors need to be considered when the ultimate goal is utilizing the material and method in practical application such as separation from flue gas. The most important parameters from the material point of view refers to simultaneous high CO_2 uptake and selectivity as well as descent regeneration process. This will be essential especially when we are talking about replacing the efficient chemical absorption on amine solution. Similarly, several concerns regarding synthetic pathways need to be addressed. Namely, reduced steps, cleanliness, scalability and cost of the synthetic approach are as important as selecting a proper material.

To address the challenges that concern the type of materials we decided to design heteroatom-doped activated carbon. Thus, we selected benzimidazole-linked polymer (BILP-5) as a single source precursor of carbon and nitrogen and adopted one-step activation with potassium hydroxide as the synthetic approach. The selection of BILP was based on the presence of nitrogen functionalities in positions that are usually found in nitrogen-doped carbons (pyridine and pyrrolic) and thus requiring less energy input for the transformation of polymer to carbon. Although nitrogen decorated metal organic frameworks (such as ZIFs) and other non-porous nitrogen rich materials have been used frequently as single source precursors, this is the first study on porous organic polymer with nitrogen atoms in imidazole linkages.

In the second study, we deliberately selected azo-linked polymers (ALP-6) as a single source precursor due to the abundance of nitrogen and ease of preparation. Although nitrogen species in ALP-6 are not located in pyridinic and pyrrolic positions as they were BILP-5, the

stability of azo linkage gives it an edge compared to BILP-5. In other words, more nitrogen species are expected to be retained after high temperature heat treatment, which will be advantageous in selective adsorption of CO_2. Chemical activation with potassium hydroxide, chemical activation with zinc chloride and direct carbonization were defined as synthetic pathways. The textural properties as well as CO_2 capture capacity and selectivity of nine different samples prepared by transformation of ALP-6 to carbon were fully characterized.

Although BILP-5 and ALP-6 served as ideal single source precursor and their derived carbon exhibited ultrahigh CO_2 capture capacity and selectivity, they need to be prepared and scaled up upon heat treatment. Using toxic organic solvents such as DMF, THF, pyridine and toluene as well as a low synthesis yield make the scalability of polymer precursors and their derived carbons a major challenge. To address these concerns and achieve comparable uptakes with BILP-5 and ALP-6 derived carbons, we decided to employ molecular benzimidazole as a commercially available and cheap precursor and KOH activation as the synthetic procedure. The acidic nature of NH functional groups in benzimidazole inspired us to use basic KOH as simultaneous stabilizing and activating agent. With these considerations in mind, we successfully synthesized a series of highly heteroatom-doped carbons by simple physical mixing of benizimidazole and subsequent thermal treatment. Textural properties, chemical composition and gas capture performance of resultant carbons were fully investigated. The results of our study represent one of the highest CO_2 capture capacity that has been recorded at the moment of writing this dissertation. Additionally, the solvent-free, scalable, repeatable, straightforward and cost-effective nature of the applied procedure makes it highly promising for practical applications. It is worth noting that the proposed work is the first report on transformation of heterocyclic organic building blocks to highly porous heteroatom doped carbons.

1.9 Organization of Dissertation

Chapter 1 provides a general introduction to carbon dioxide capture and sequestration and promising material and method. The current body of literature on physical adsorption using porous solid sorbents and more specifically nitrogen-doped activated carbons is discussed.

In Chapter 2, the transformation of BILP-5, a particular benzimidazole-linked polymer, to nitrogen doped carbon was discussed. Effect of activation temperature on surface chemistry, atmospheric gas uptake and selectivity and high pressure uptake were investigated.

In Chapter 3, applying three various synthetic pathways of KOH activation, $ZnCl_2$ activation and direct carbonization to ALP-6, a particular azo-linked polymer, was examined. The effect of synthetic strategies on porous parameters, surface chemistry, carbon dioxide capture and selective adsorption was comparatively investigated

In chapter 4, employment of a heterocyclic organic building block as a precursor for chemical activation was evaluated. The mechanism of transformation, heteroatom content and CO_2 capture capacity was discussed.

Chapter 5 concludes the dissertation and provides some prospects for future studies.

1.10 References

1. D'Alessandro, D. M.; Smit, B.; Long, J. R., Carbon Dioxide Capture: Prospects for New Materials. *Angew. Chem., Int. Ed.* **2010**, *49*, 6058-82.

2. Samanta, A.; Zhao, A.; Shimizu, G. K. H.; Sarkar, P.; Gupta, R., Post-Combustion CO_2 Capture Using Solid Sorbents: A Review. *Ind. Eng. Chem. Res.* **2012**, *51*, 1438-1463.

3. Mikkelsen, M.; Jorgensen, M.; Krebs, F. C., The Teraton Challenge. A Review of Fixation and Transformation of Carbon Dioxide. *Energy Environ. Sci.* **2010**, *3*, 43-81.

4. Lee, S.-Y.; Park, S.-J., A Review on Solid Adsorbents for Carbon Dioxide Capture. *J. Ind. Eng. Chem.* **2015**, *23*, 1-11.

5. Haszeldine, R. S., Carbon Capture and Storage: How Green Can Black Be? *Science* **2009**, *325*, 1647-1652.

6. Aaron, D.; Tsouris, C., Separation of CO_2 from Flue Gas: A Review. *Sep. Sci. Technol.* **2005**, *40*, 321-348.

7. Lee, K. B.; Sircar, S., Removal and Recovery of Compressed CO_2 from Flue Gas by a Novel Thermal Swing Chemisorption Process. *AIChE J.* **2008**, *54*, 2293-2302.

8. Markewitz, P.; Kuckshinrichs, W.; Leitner, W.; Linssen, J.; Zapp, P.; Bongartz, R.; Schreiber, A.; Muller, T. E., Worldwide Innovations in the Development of Carbon Capture Technologies and the Utilization of CO_2. *Energy Environ. Sci.* **2012**, *5*, 7281-7305.

9. Rochelle, G. T., Amine Scrubbing for CO_2 Capture. *Science* **2009**, *325*, 1652-4.

10. Kim, D. Y.; Lee, H. M.; Min, S. K.; Cho, Y.; Hwang, I.-C.; Han, K.; Kim, J. Y.; Kim, K. S., CO_2 Capturing Mechanism in Aqueous Ammonia: NH_3-Driven Decomposition−Recombination Pathway. *J. Phys. Chem. Lett.* **2011**, *2*, 689-694.

11. Sing, K. S. W.; Everett, D. H.; Haul, R. A. W.; Moscou, L.; Pierotti, R. A.; Rouquerol, J.; Siemieniewska, T., Reporting Physisorption Data for Gas/Solid Systems. In *Handbook of Heterogeneous Catalysis*, Wiley-VCH Verlag GmbH & Co. KGaA: 2008.

12. Brunauer, S.; Deming, L. S.; Deming, W. E.; Teller, E., On a Theory of the Van Der Waals Adsorption of Gases. *J. Am. Chem. Soc.* **1940**, *62*, 1723-1732.

13. Brunauer, S.; Emmett, P. H.; Teller, E., Adsorption of Gases in Multimolecular Layers. *J. Am. Chem. Soc.* **1938**, *60*, 309-319.

14. Langmuir, I., The Constitution and Fundamental Properties of Solids and Liquids. Part I. Solids. *J. Am. Chem. Soc.* **1916**, *38*, 2221-2295.

15. Ravikovitch, P. I.; Vishnyakov, A.; Russo, R.; Neimark, A. V., Unified Approach to Pore Size Characterization of Microporous Carbonaceous Materials from N_2, Ar, and CO_2 Adsorption Isotherms. *Langmuir* **2000**, *16*, 2311-2320.

16. Furukawa, H.; Cordova, K. E.; O'Keeffe, M.; Yaghi, O. M., The Chemistry and Applications of Metal-Organic Frameworks. *Science* **2013**, *341*, 1230444.

17. Millward, A. R.; Yaghi, O. M., Metal−Organic Frameworks with Exceptionally High Capacity for Storage of Carbon Dioxide at Room Temperature. *J. Am. Chem. Soc.* **2005**, *127*, 17998-17999.

18. Sumida, K.; Rogow, D. L.; Mason, J. A.; McDonald, T. M.; Bloch, E. D.; Herm, Z. R.; Bae, T.-H.; Long, J. R., Carbon Dioxide Capture in Metal–Organic Frameworks. *Chem. Rev.* **2012**, *112*, 724-781.

19. Xiang, S.; He, Y.; Zhang, Z.; Wu, H.; Zhou, W.; Krishna, R.; Chen, B., Microporous Metal-Organic Framework with Potential for Carbon Dioxide Capture at Ambient Conditions. *Nat. Commun.* **2012**, *3*, 954.

20. Rabbani, M. G.; El-Kaderi, H. M., Template-Free Synthesis of a Highly Porous Benzimidazole-Linked Polymer for CO_2 Capture and H_2 Storage. *Chem. Mater.* **2011**, *23*, 1650-1653.

21. Rabbani, M. G.; El-Kaderi, H. M., Synthesis and Characterization of Porous Benzimidazole-Linked Polymers and their Performance in Small Gas Storage and Selective Uptake. *Chem. Mater.* **2012**, *24*, 1511-1517.

22. Rabbani, M. G.; Reich, T. E.; Kassab, R. M.; Jackson, K. T.; El-Kaderi, H. M., High CO_2 Uptake and Selectivity by Triptycene-Derived Benzimidazole-Linked Polymers. *Chem. Commun.* **2012**, *48*, 1141-1143.

23. Arab, P.; Rabbani, M. G.; Sekizkardes, A. K.; İslamoğlu, T.; El-Kaderi, H. M., Copper(I)-Catalyzed Synthesis of Nanoporous Azo-Linked Polymers: Impact of Textural Properties on Gas Storage and Selective Carbon Dioxide Capture. *Chem. Mater.* **2014**, *26*, 1385-1392.

24. Arab, P.; Parrish, E.; Islamoglu, T.; El-Kaderi, H. M., Synthesis and Evaluation of Porous Azo-Linked Polymers for Carbon Dioxide Capture and Separation. *J. Mater. Chem. A* **2015**, *3*, 20586-20594.

25. Su, F.; Lu, C., CO_2 Capture from Gas Stream by Zeolite 13X Using a Dual-Column Temperature/Vacuum Swing Adsorption. *Energy Environ. Sci.* **2012**, *5*, 9021-9027.

26. Wang, Q.; Luo, J.; Zhong, Z.; Borgna, A., CO_2 Capture by Solid Adsorbents and their Applications: Current Status and New Trends. *Energy Environ. Sci.* **2011**, *4*, 42-55.

27. Jadhav, P. D.; Chatti, R. V.; Biniwale, R. B.; Labhsetwar, N. K.; Devotta, S.; Rayalu, S. S., Monoethanol Amine Modified Zeolite 13X for CO_2 Adsorption at Different Temperatures. *Energy Fuels* **2007**, *21*, 3555-3559.

28. Lozinska, M. M.; Mangano, E.; Mowat, J. P. S.; Shepherd, A. M.; Howe, R. F.; Thompson, S. P.; Parker, J. E.; Brandani, S.; Wright, P. A., Understanding Carbon Dioxide Adsorption on Univalent Cation Forms of the Flexible Zeolite Rho at Conditions Relevant to Carbon Capture from Flue Gases. *J. Am. Chem. Soc.* **2012**, *134*, 17628-17642.

29. Xu, X.; Song, C.; Andresen, J. M.; Miller, B. G.; Scaroni, A. W., Novel Polyethylenimine-Modified Mesoporous Molecular Sieve of MCM-41 Type as High-Capacity Adsorbent for CO_2 Capture. *Energy Fuels* **2002**, *16*, 1463-1469.

30. Nugent, P.; Belmabkhout, Y.; Burd, S. D.; Cairns, A. J.; Luebke, R.; Forrest, K.; Pham, T.; Ma, S.; Space, B.; Wojtas, L.; Eddaoudi, M.; Zaworotko, M. J., *Nature* **2013**, *495*, 80-84.

31. Zhang, Z.; Zhou, J.; Xing, W.; Xue, Q.; Yan, Z.; Zhuo, S.; Qiao, S. Z., Critical Role of Small Micropores in High CO_2 Uptake. *Phys. Chem. Chem. Phys.* **2013**, *15*, 2523-2529.

32. Lu, W.; Yuan, D.; Sculley, J.; Zhao, D.; Krishna, R.; Zhou, H.-C., Sulfonate-Grafted Porous Polymer Networks for Preferential CO_2 Adsorption at Low Pressure. *J. Am. Chem. Soc.* **2011**, *133*, 18126-18129.

33. Zhang, Y.; Li, B.; Williams, K.; Gao, W.-Y.; Ma, S., A New Microporous Carbon Material Synthesized via Thermolysis of a Porous Aromatic Framework Embedded with an Extra Carbon Source for Low-Pressure CO_2 Uptake. *Chem. Commun.* **2013**, *49*, 10269-10271.

34. Plaza, M. G.; Rubiera, F.; Pis, J. J.; Pevida, C., Ammoxidation of Carbon Materials for CO_2 Capture. *Appl. Surf. Sci.* **2010**, *256*, 6843-6849.

35. Jansen, R. J. J.; van Bekkum, H., Amination and Ammoxidation of Activated Carbons. *Carbon* **1994**, *32*, 1507-1516.

36. Pietrzak, R.; Wachowska, H.; Nowicki, P.; Babeł, K., Preparation of Modified Active Carbon from Brown Coal by Ammoxidation. *Fuel Process. Technol.* **2007**, *88*, 409-415.

37. Vinke, P.; van der Eijk, M.; Verbree, M.; Voskamp, A. F.; van Bekkum, H., Modification of the Surfaces of a Gasactivated Carbon and a Chemically Activated Carbon with Nitric Acid, Hypochlorite, and Ammonia. *Carbon* **1994**, *32*, 675-686.

38. Stöhr, B.; Boehm, H. P.; Schlögl, R., Enhancement of the Catalytic Activity of Activated Carbons in Oxidation Reactions by Thermal Treatment with Ammonia or Hydrogen Cyanide and Observation of a Superoxide Species as a Possible Intermediate. *Carbon* **1991**, *29*, 707-720.

39. Lezanska, M.; Pietrzyk, P.; Sojka, Z., Investigations into the Structure of Nitrogen-Containing CMK-3 and OCM-0.75 Carbon Replicas and the Nature of Surface Functional Groups by Spectroscopic and Sorption Techniques. *J. Phys. Chem. C* **2010**, *114*, 1208-1216.

40. Sevilla, M.; Valle-Vigón, P.; Fuertes, A. B., N-Doped Polypyrrole-Based Porous Carbons for CO_2 Capture. *Adv. Funct. Mater.* **2011**, *21*, 2781-2787.

41. Liu, N.; Yin, L.; Wang, C.; Zhang, L.; Lun, N.; Xiang, D.; Qi, Y.; Gao, R., Adjusting the Texture and Nitrogen Content of Ordered Mesoporous Nitrogen-Doped Carbon Materials Prepared Using SBA-15 Silica as a Template. *Carbon* **2010**, *48*, 3579-3591.

42. Xia, Y.; Mokaya, R., Generalized and Facile Synthesis Approach to N-Doped Highly Graphitic Mesoporous Carbon Materials. *Chem. Mater.* **2005**, *17*, 1553-1560.

43. Titirici, M.-M.; Thomas, A.; Antonietti, M., Aminated Hydrophilic Ordered Mesoporous Carbons. *J. Mater. Chem.* **2007**, *17*, 3412-3418.

44. Chen, G.; Wang, X.; Li, J.; Hou, W.; Zhou, Y.; Wang, J., Direct Carbonization of Cyanopyridinium Crystalline Dicationic Salts into Nitrogen-Enriched Ultra-Microporous Carbons toward Excellent CO_2 Adsorption. *ACS Appl. Mater. Interfaces* **2015**, *7*, 18508-18518.

45. Aijaz, A.; Fujiwara, N.; Xu, Q., From Metal–Organic Framework to Nitrogen-Decorated Nanoporous Carbons: High CO_2 Uptake and Efficient Catalytic Oxygen Reduction. *J. Am. Chem. Soc.* **2014**, *136*, 6790-6793.

46. Wang, J.; Senkovska, I.; Oschatz, M.; Lohe, M. R.; Borchardt, L.; Heerwig, A.; Liu, Q.; Kaskel, S., Imine-Linked Polymer-Derived Nitrogen-Doped Microporous Carbons with Excellent CO_2 Capture Properties. *ACS Appl. Mater. Interfaces* **2013**, *5*, 3160-3167.

47. Zhang, S.; Dokko, K.; Watanabe, M., Carbon Materialization of Ionic Liquids: From Solvents to Materials. *Mater. Horiz.* **2015**, *2*, 168-197.

48. Paraknowitsch, J. P.; Zhang, J.; Su, D.; Thomas, A.; Antonietti, M., Ionic Liquids as Precursors for Nitrogen-Doped Graphitic Carbon. *Adv. Mater.* **2010**, *22*, 87-92.

49. Adeniran, B.; Masika, E.; Mokaya, R., A Family of Microporous Carbons Prepared via a Simple Metal Salt Carbonization Route with High Selectivity for Exceptional Gravimetric and Volumetric Post-Combustion CO_2 Capture. *J. Mater. Chem. A* **2014**, *2*, 14696-14710.

50. Sevilla, M.; Fuertes, A. B., A General and Facile Synthesis Strategy Towards Highly Porous Carbons: Carbonization of Organic Salts. *J. Mater. Chem. A* **2013**, *1*, 13738-13741.

51. Fuertes, A. B.; Ferrero, G. A.; Sevilla, M., One-Pot Synthesis of Microporous Carbons Highly Enriched in Nitrogen and their Electrochemical Performance. *J. Mater. Chem. A* **2014**, *2*, 14439-14448.

52. Valix, M.; Cheung, W. H.; McKay, G., Preparation of Activated Carbon Using Low Temperature Carbonisation and Physical Activation of High Ash Raw Bagasse for Acid Dye Adsorption. *Chemosphere* **2004**, *56*, 493-501.

53. Wickramaratne, N. P.; Jaroniec, M., Activated Carbon Spheres for CO_2 Adsorption. *ACS Appl. Mater. Interfaces* **2013**, *5*, 1849-1855.

54. Nandi, M.; Okada, K.; Dutta, A.; Bhaumik, A.; Maruyama, J.; Derks, D.; Uyama, H., Unprecedented CO_2 Uptake over Highly Porous N-Doped Activated Carbon Monoliths Prepared by Physical Activation. *Chem. Commun.* **2012**, *48*, 10283-10285.

55. Rodríguez-Reinoso, F.; Molina-Sabio, M., Activated Carbons from Lignocellulosic Materials by Chemical and/or Physical Activation: An Overview. *Carbon* **1992**, *30*, 1111-1118.

56. Molina-Sabio, M.; Rodríguez-Reinoso, F., Role of Chemical Activation in the Development of Carbon Porosity. *Colloids Surf., A* **2004**, *241*, 15-25.

57. Suárez-García, F.; Martínez-Alonso, A.; Tascón, J. M. D., Activated Carbon Fibers from Nomex by Chemical Activation with Phosphoric Acid. *Carbon* **2004**, *42*, 1419-1426.

58. Lillo-Ródenas, M. A.; Cazorla-Amorós, D.; Linares-Solano, A., Understanding Chemical Reactions between Carbons and NaOH and KOH: An Insight into the Chemical Activation Mechanism. *Carbon* **2003**, *41*, 267-275.

59. Shen, W.; He, Y.; Zhang, S.; Li, J.; Fan, W., Yeast-Based Microporous Carbon Materials for Carbon Dioxide Capture. *ChemSusChem* **2012**, *5*, 1274-9.

60. White, R. J.; Antonietti, M.; Titirici, M.-M., Naturally Inspired Nitrogen Doped Porous Carbon. *J. Mater. Chem.* **2009**, *19*, 8645-8650.

61. Sevilla, M.; Falco, C.; Titirici, M.-M.; Fuertes, A. B., High-Performance CO_2 Sorbents from Algae. *RSC Adv.* **2012**, *2*, 12792-12797.

62. Plaza, M. G.; García, S.; Rubiera, F.; Pis, J. J.; Pevida, C., Evaluation of Ammonia Modified and Conventionally Activated Biomass Based Carbons as CO_2 Adsorbents in Postcombustion Conditions. *Sep. Purif. Technol.* **2011**, *80*, 96-104.

63. Shen, W.; Zhang, S.; He, Y.; Li, J.; Fan, W., Hierarchical Porous Polyacrylonitrile-Based Activated Carbon Fibers for CO_2 Capture. *J. Mater. Chem.* **2011**, *21*, 14036-14040.

64. Wang, J.; Senkovska, I.; Oschatz, M.; Lohe, M. R.; Borchardt, L.; Heerwig, A.; Liu, Q.; Kaskel, S., Highly Porous Nitrogen-Doped Polyimine-Based Carbons with Adjustable Microstructures for CO_2 Capture. *J. Mater. Chem. A* **2013**, *1*, 10951-10961.

65. Ashourirad, B.; Sekizkardes, A. K.; Altarawneh, S.; El-Kaderi, H. M., Exceptional Gas Adsorption Properties by Nitrogen-Doped Porous Carbons Derived from Benzimidazole-Linked Polymers. *Chem. Mater.* **2015**, *27*, 1349-1358.

66. Yang, X.; Yu, M.; Zhao, Y.; Zhang, C.; Wang, X.; Jiang, J.-X., Remarkable Gas Adsorption by Carbonized Nitrogen-Rich Hypercrosslinked Porous Organic Polymers. *J. Mater. Chem. A* **2014**, *2*, 15139-15145.

67. Zhao, L.; Baccile, N.; Gross, S.; Zhang, Y.; Wei, W.; Sun, Y.; Antonietti, M.; Titirici, M.-M., Sustainable Nitrogen-Doped Carbonaceous Materials from Biomass Derivatives. *Carbon* **2010**, *48*, 3778-3787.

68. Baccile, N.; Laurent, G.; Coelho, C.; Babonneau, F.; Zhao, L.; Titirici, M.-M., Structural Insights on Nitrogen-Containing Hydrothermal Carbon Using Solid-State Magic Angle Spinning 13C and 15N Nuclear Magnetic Resonance. *J. Phys. Chem. C* **2011**, *115*, 8976-8982.

69. Huang, H.-C.; Ye, D.-Q.; Huang, B.-C., Nitrogen Plasma Modification of Viscose-Based Activated Carbon Fibers. *Surf. Coat. Technol.* **2007**, *201*, 9533-9540.

70. Carter, E. M.; Katz, L. E.; Speitel, G. E.; Ramirez, D., Gas-Phase Formaldehyde Adsorption Isotherm Studies on Activated Carbon: Correlations of Adsorption Capacity to Surface Functional Group Density. *Environ. Sci. Technol.* **2011**, *45*, 6498-6503.

71. Nowicki, P.; Pietrzak, R., Effect of Ammoxidation of Activated Carbons Obtained from Sub-Bituminous Coal on Their NO_2 Sorption Capacity under Dry Conditions. *Chem. Eng. J.* **2011**, *166*, 1039-1043.

72. Grzyb, B.; Albiniak, A.; Broniek, E.; Furdin, G.; Marêché, J. F.; Bégin, D., SO_2 Adsorptive Properties of Activated Carbons Prepared from Polyacrylonitrile and Its Blends with Coal-Tar Pitch. *Microporous Mesoporous Mater.* **2009**, *118*, 163-168.

73. Seredych, M.; Bandosz, T. J., Adsorption of Hydrogen Sulfide on Graphite Derived Materials Modified by Incorporation of Nitrogen. *Mater. Chem. Phys.* **2009**, *113*, 946-952.

74. Hou, P.-X.; Orikasa, H.; Yamazaki, T.; Matsuoka, K.; Tomita, A.; Setoyama, N.; Fukushima, Y.; Kyotani, T., Synthesis of Nitrogen-Containing Microporous Carbon with a Highly Ordered Structure and Effect of Nitrogen Doping on H_2O Adsorption. *Chem. Mater.* **2005**, *17*, 5187-5193.

75. Xiao, B.; Thomas, K. M., Adsorption of Aqueous Metal Ions on Oxygen and Nitrogen Functionalized Nanoporous Activated Carbons. *Langmuir* **2005**, *21*, 3892-3902.

76. Candelaria, S. L.; Shao, Y.; Zhou, W.; Li, X.; Xiao, J.; Zhang, J.-G.; Wang, Y.; Liu, J.; Li, J.; Cao, G., Nanostructured Carbon for Energy Storage and Conversion. *Nano Energy* **2012**, *1*, 195-220.

77. Zhu, Y.; Murali, S.; Stoller, M. D.; Ganesh, K. J.; Cai, W.; Ferreira, P. J.; Pirkle, A.; Wallace, R. M.; Cychosz, K. A.; Thommes, M.; Su, D.; Stach, E. A.; Ruoff, R. S., Carbon-Based Supercapacitors Produced by Activation of Graphene. *Science* **2011**, *332*, 1537-1541.

78. Song, Y.; Zhou, D.; Wang, Y.; Wang, C.; Xia, Y., Preparation of Nitrogen-Containing Mesoporous Carbons and Their Application in Supercapacitors. *New J. Chem.* **2013**, *37*, 1768-1775.

79. Xu, B.; Duan, H.; Chu, M.; Cao, G.; Yang, Y., Facile Synthesis of Nitrogen-Doped Porous Carbon for Supercapacitors. *J. Mater. Chem. A* **2013**, *1*, 4565-4570.

80. Chen, L.-F.; Zhang, X.-D.; Liang, H.-W.; Kong, M.; Guan, Q.-F.; Chen, P.; Wu, Z.-Y.; Yu, S.-H., Synthesis of Nitrogen-Doped Porous Carbon Nanofibers as an Efficient Electrode Material for Supercapacitors. *ACS Nano* **2012**, *6*, 7092-7102.

81. Hou, L.; Lian, L.; Li, D.; Pang, G.; Li, J.; Zhang, X.; Xiong, S.; Yuan, C., Mesoporous N-Containing Carbon Nanosheets Towards High-Performance Electrochemical Capacitors. *Carbon* **2013**, *64*, 141-149.

82. Wei, J.; Zhou, D.; Sun, Z.; Deng, Y.; Xia, Y.; Zhao, D., A Controllable Synthesis of Rich Nitrogen-Doped Ordered Mesoporous Carbon for CO_2 Capture and Supercapacitors. *Adv. Funct. Mater.* **2013**, *23*, 2322-2328.

83. Shao, Y.; Sui, J.; Yin, G.; Gao, Y., Nitrogen-Doped Carbon Nanostructures and their Composites as Catalytic Materials for Proton Exchange Membrane Fuel Cell. *Appl. Catal., B* **2008**, *79*, 89-99.

84. Imran Jafri, R.; Rajalakshmi, N.; Ramaprabhu, S., Nitrogen Doped Graphene Nanoplatelets as Catalyst Support for Oxygen Reduction Reaction in Proton Exchange Membrane Fuel Cell. *J. Mater. Chem.* **2010**, *20*, 7114-7117.

85. Shao, Y.; Yin, G.; Gao, Y., Understanding and Approaches for the Durability Issues of Pt-Based Catalysts for Pem Fuel Cell. *J. Power Sources* **2007**, *171*, 558-566.

86. Lepró, X.; Terrés, E.; Vega-Cantú, Y.; Rodríguez-Macías, F. J.; Muramatsu, H.; Kim, Y. A.; Hayahsi, T.; Endo, M.; Torres R, M.; Terrones, M., Efficient Anchorage of Pt Clusters on N-Doped Carbon Nanotubes and their Catalytic Activity. *Chem. Phys. Lett.* **2008**, *463*, 124-129.

Chapter 2: Exceptional Gas Adsorption Properties by Nitrogen-Doped Porous Carbons Derived from Benzimidazole-Linked Polymers

2.1 Introduction

Porous carbons exhibit multifaceted desirable features such as high thermal and chemical stability, tunable textural properties, lightweight and metal-free framework and ease of regeneration.[1-2] In addition to these properties, the chemical and electronic nature of porous carbons can be tuned by integrating heteroatoms (i.e. N, B, P, S)[3] to access a wide range of applications including heterogeneous catalysis, energy storage, and gas storage and separation, among others. Incorporation of nitrogen atoms Lewis-basic properties has been suggested to simultaneously enhance CO_2 capture capacity and selectivity of plain carbons through Lewis acid-base interactions.[4-7] Employing a single source precursor including both nitrogen and carbon to generate N-doped carbon has been the subject of many research works recently.[8-11]

In this study, we demonstrate successful transformation of benzimidazole-linked polymers (BILPs) as single source precursors to highly porous N-doped carbons (CPCs). Controlled KOH activation of polymers led to a series of N-doped CPCs that feature variable N-content, porosity, and CO_2 capture properties as a function of thermolysis temperature. Notably, the N sites within the imidazole rings of BILPs are intrinsically located in pyrrolic/pyridinc positions typically found in N-doped carbons. Therefore, the chemical and physical transformations of BILPs into N-doped CPCs are thermodynamically favored and allow considerable reduction in energy consumption during carbonization stages.

2.2 Experimental

2.2.1 Materials and Methods. All starting materials and solvents were obtained from commercial sources and used without further purification, unless otherwise mentioned. KOH (99%) was purchased from Alfa Aesar. THF was dried by distillation over Na/benzophenone. BILP-5 was synthesized according to published methods.[4-5] Elemental microanalyses were performed at the Midwest Microlab, LLC. To obtain Scanning Electron Microscopy (SEM) images, each sample was dispersed onto a sticky carbon surface attached to a flat aluminum sample holder. Then, the sample was coated with platinum at a pressure of 1×10^{-5} mbar in a nitrogen atmosphere for 90 s before imaging. SEM images were taken on a Hitachi SU-70 Scanning Electron Microscope. TEM images were recorded on a JEOL 2010 apparatus operated at an accelerating voltage of 200 kV. Samples were dispersed in ethanol and then drop cast onto a 200 mesh carbon-coated copper grid. Powder X-ray diffraction data were collected on a Panalytical X'pert pro multipurpose diffractometer (MPD). Samples were mounted on a sample holder and measured using Cu Kα. X-ray photoelectron spectroscopy (XPS) analysis was performed on a ThermoFisher ESCALAB 250 spectrometer employing Al Kα (1486.68 eV) X-ray source equipped with a hemispherical analyzer. Atmospheric gas (N_2, CO_2 and CH_4) sorption measurements were carried out on a Quantachrome Autosorb iQ volumetric analyzer using UHP grade adsorbates. Prior to the adsorption analyses the samples were degassed at 200 °C for 12 h. The specific BET (Brunauer−Emmett−Teller) surface areas were calculated considering analysis requirements for microporous materials. BET assistant on Quantachrome V.3.0 software was used to correct 0.05-0.30 classical range of P/P_o and find the appropriate pressure range based on "consistency criteria" for microporous materials.[12-13] The specific surface area, pore volume, and

pore size distribution (PSD) from the N_2 isotherms (77 K) were obtained by applying the quench solid density functional theory (QSDFT) on adsorption branch and assuming slit-like geometry on carbon material kernel. Moreover, microporous textural properties were investigated using CO_2 adsorption isotherms (273 K) and applying nonlocal density functional theory (NLDFT) under similar assumptions. High pressure gas sorption measurements were performed using VTI-HPVA-100 volumetric analyzer. High pressure total gas uptakes were calculated by reported literature methods and NIST Thermochemical Properties of Fluid Systems were applied for the calculations.[14-16]

2.2.2 Synthesis of CPCs. Samples of BILP-5 were dispersed and dried at 130 °C overnight in a static oven to increase the interfacial contact area with activation agent KOH. Activated BILP-5 precursors were thoroughly mixed with KOH in an agate with KOH/BILP-5 weight ratio of 2:1 after which the mixture was transferred to tube furnace (MTF-wire wound single zone) for carbonization and activation. Simultaneous chemical activation and decomposition of nitrogen-rich polymer was carried out under a flow of Ar (99.9%) in a temperature range of 550 to 800 °C (heating rate: 3 °C/min and holding time: 3 h). After cooling to room temperature, the samples were thoroughly washed with 1.0 M HCl several times to remove any inorganic salts, followed by washing with 1.0 M NaOH to neutralize acid and then large amount of distilled water until neutral pH was obtained. During acid and base treatment the carbons were soaked for at least two hours to dissolve inorganic salts, metallic potassium, and other unreacted potassium compounds. The chemically activated porous carbons were denoted CPC-T, wherein T represents the activation temperature.

2.2.3 Virial Method Calculation for Isosteric Heats of Adsorption. The virial equation was used to determine the binding affinity and isosteric heats of adsorption. The virial equation[17] can be expressed as:

$$\ln\left(\frac{N}{P}\right) = A_0 N^0 + A_1 N^1 + A_2 N^2 + \text{.....} \qquad \textbf{(I)}$$

In this equation N is defined as the amount adsorbed at pressure P. A_0, A_1, etc. are virial coefficients in the equation. A_0 coefficient is related to adsorbate-adsorbent interactions, A_1, on the other hand represents adsorbate-adsorbate interactions. The other coefficients such as A_2, etc. can be disregarded at the low surface coverage. A virial-type expression in the following form can also be used to fit the experimental isotherm data for a given material at different temperatures.[18]

$$\ln(P) = \ln(N) + \frac{1}{T}\sum_{i=0}^{m} a_i N^i + \sum_{i=0}^{n} b_i N^i \qquad \textbf{(II)}$$

Similar to the first equation, N expresses the amount adsorbed at pressure P, where T is the temperature, a_i and b_i are temperature independent empirical parameters, and m and n determine the number of terms required to adequately describe the isotherm. Then, coefficients a_0 through a_m are applied to the equation (II) to calculate the isosteric heats of adsorption as function of uptake, where R is the universal gas constant (8.314 J K^{-1} mol^{-1})

$$Q_{st} = -R\sum_{i=0}^{m} a_i N^i \qquad \textbf{(III)}$$

The zero-coverage isosteric heats of adsorption is given by :

$$Q_{st} = -Ra_0 \qquad \textbf{(IV)}$$

2.3 Results and Discussion

2.3.1 Synthetic and Characterization Aspects. The synthesis route of CPCs is depicted in Figure 2.1 while Figure 2.2 shows the SEM and TEM images of CPCs. As shown in SEM images 2.2 (A-C), all CPCs exhibit a network morphology composed of irregular particles (~300 nm). The degree of deviation from BILP-5 spherical morphology (Figure 2.3) is more pronounced at elevated activation temperatures. It has been reported that most of activated carbons lose their spherical morphology under harsh activation conditions (activator/precursor >2).[19] However, maintaining spherical morphology under mild activation conditions or direct pyrolysis of spherical precursors is conceivable.[20-22] The TEM image of high temperature activated sample, CPC-800, does not show any ordered domains consistent with its amorphous nature. The amorphous nature of CPCs was further supported by PXRD studies that revealed no diffraction peaks as shown in Figure 2.4. The nitrogen content of CPCs obtained by elemental analysis evidently decreases with respect to activation temperature (Table 2.1). Nevertheless, CPC-550 retains a considerable amount of nitrogen (~8 wt%) surpassing the nitrogen content of many recently reported N-doped porous carbon materials.[19, 23-25]

2.3.2 Textural Properties. The specific surface area, pore volume, and pore size distribution of CPCs were comparatively characterized by means of nitrogen (77 K) and carbon dioxide (273 K) adsorption isotherms for micro/mesopores and ultramicropores, respectively. The nitrogen sorption isotherms of all CPCs and BILP-5 are presented in Figure 2.5 A and Figure 2.6. The isotherms of CPCs show a rapid nitrogen uptake at very low pressure region (P/P_o<0.01) followed by a plateau for most of the pressure range, suggesting that micropores are dominant in

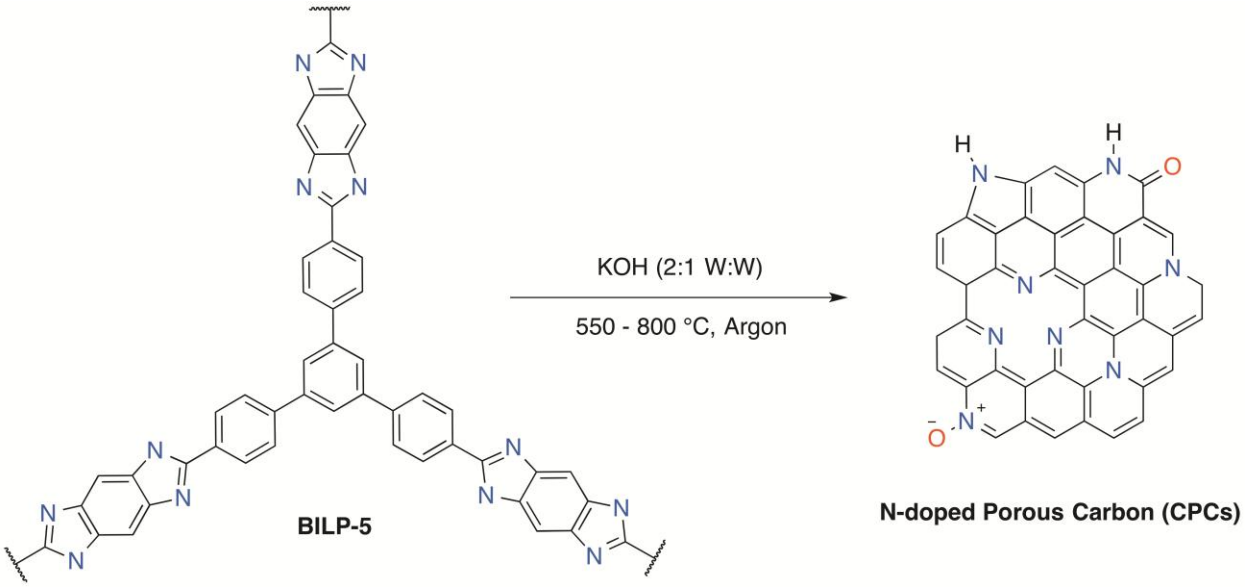

Figure 2.1. Synthesis of N-doped porous carbons.

the samples. For all prepared carbons, the knee between the very low pressure region and the flat plateau of nitrogen isotherms shifts to higher values as the activation temperature rises, which is likely due to narrow mesopores formation. The pore size distribution and cumulative pore volume of CPCs were probed by applying QSDFT and NLDFT on their N_2 (77 K) and CO_2 (273 K) isotherms, respectively. It is worth noting that the QSDFT model is superior for materials with surface chemical heterogeneity when nitrogen or argon are used to probe porosity.[26] Furthermore, the use of the CO_2 isotherm at 273 K proved to be very beneficial in analyzing sub-nanometer micropore distribution more accurately. In fact, the high kinetic energy of CO_2 at 273 K enables it to diffuse into narrower pores.[27] Pore size distributions are given in Figure 2.5 (B) and Figure 2.7. For CPC-550, the PSD is mainly centered at 0.7 nm indicating the presence of dominant micropores. However, the appearance of a small peak at 2.2 nm for CPC-600 is related to the formation of narrow mesopores apart from pre-existed micropores. As the activation temperature

increases, the mesopore peaks shift to higher values of 2.3 nm, 2.5 nm and 3.1 nm for carbons activated at 650, 700 and 800 °C, respectively. Due to the highly microporous nature of prepared carbons, their sub-nanometer pore size distribution is also presented in Figures 2.5 (C) and Figure 2.8. For most of the activated carbons, the fine micropores are distributed around 0.35 and 0.85 nm. Therefore, CPCs show a variety of pore size distributions from purely fine micropores to a hierarchy of micro and narrow mesopores (2-4 nm).

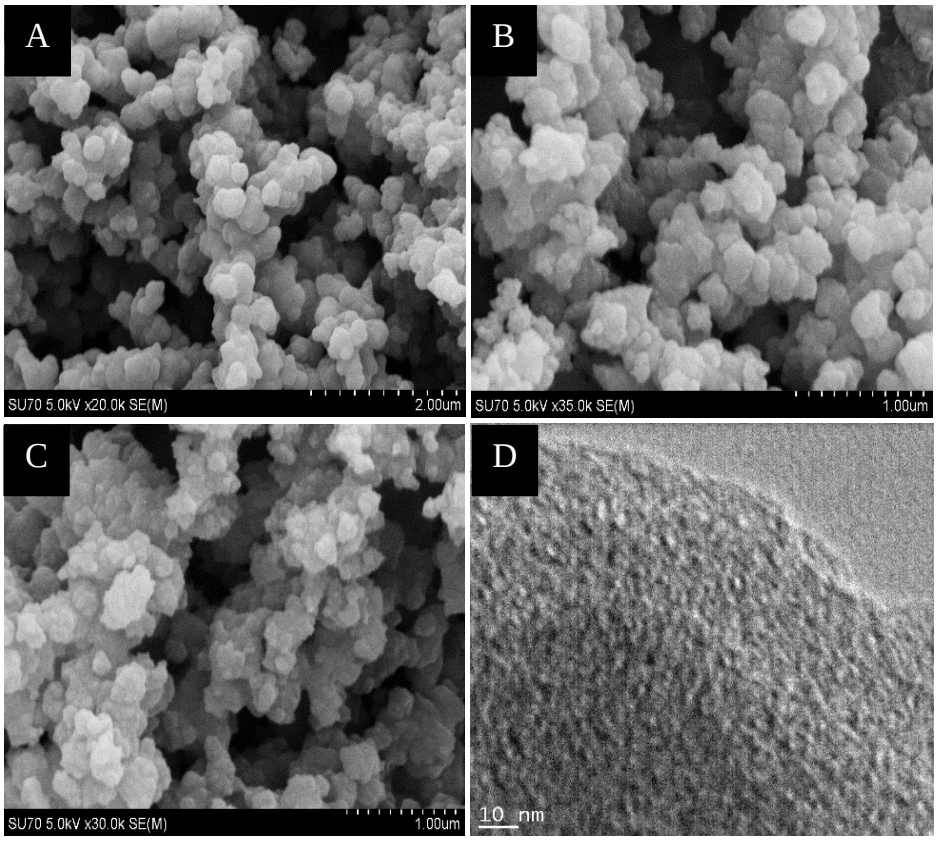

Figure 2.2. Scanning Electron Microscopy (SEM) images of (A) CPC-600, (B) CPC-700, and (C) CPC-800 and (D) Transmission Electron Microscopy (TEM) image of CPC-800.

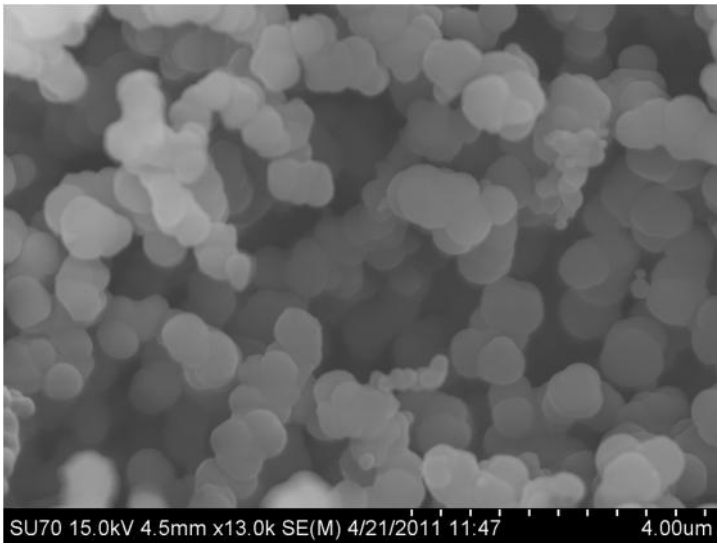

Figure 2.3. SEM image of spherical aggregates in BILP-5 precursor.

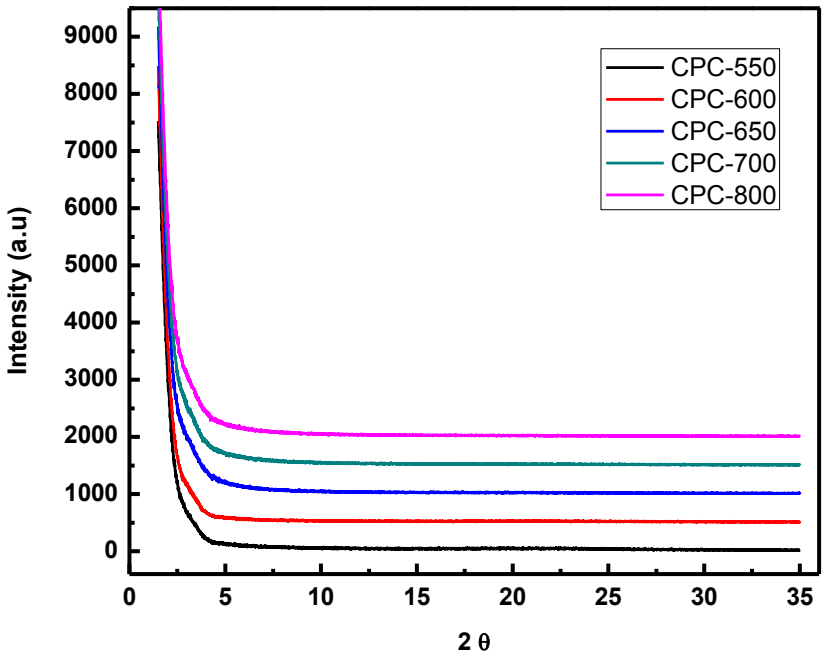

Figure 2.4. XRD pattern of prepared CPCs.

Table 2.1. CHN elemental analysis of BILP-5 and prepared CPCs

Sample	Chemical Composition (wt%)		
	C	N	H
BILP-5	72.67	12.64	4.47
CPC-550	60.62	7.88	2.05
CPC-600	59.00	6.34	2.04
CPC-650	64.84	5.38	1.41
CPC-700	74.29	4.22	1.11
CPC-800	76.56	1	1.17

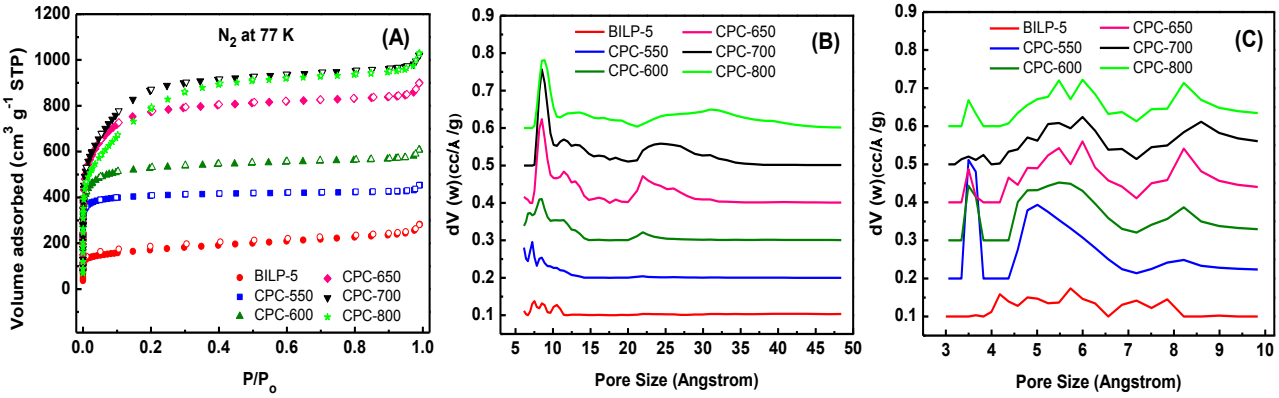

Figure 2.5. (A) Nitrogen isotherms at 77 K, pore size distribution from (B) QSDFT using N_2 at 77 K and (C) from NLDFT using CO_2 at 273 K. (All PSD curves are offset vertically in steps of 0.1 for clarity purpose.)

The specific BET surface areas from nitrogen isotherms were calculated with respect to the consistency criteria for microporous materials as discussed in the experimental section (Figure 2.9) and summarized in Table 2.2. Pore volumes were also determined from nitrogen and CO_2 adsorption isotherms using NLDFT method. Generally, the surface area and pore volume increase with activation temperature until 700 °C and after that decrease due to over activation.[28] The specific surface area and pore volume increase significantly from 626 $m^2 g^{-1}$ (BILP-5) to 3241 $m^2 g^{-1}$ (CPC-700) and from 0.39 $cm^3 g^{-1}$ (BILP-5) to 1.51 $cm^3 g^{-1}$ (CPC-700), respectively (Table 2.2). The lower surface area and pore volume obtained for CPC-800 are probably related to the destruction of pore structures formed at previous steps. Porous structure development during the activation process takes place through chemical reactions between KOH and the carbon framework ($6KOH + C = 2K + 3H_2 + 2K_2CO_3$). As a result, the yield of chemically activated carbons is notably lower than porous carbons obtained by direct pyrolysis. In general, the yield of activated carbons decreases by increasing the activation parameters (temperature and activator to precursor ratio). The yield of CPCs decreases from 47% to 13% by increasing the activation temperature from 550 °C to 800 °C implying more carbon was eliminated during activation process. It was also suggested that at higher activation temperatures, the products of K_2CO_3 decomposition (CO_2 and K_2O) further react with carbon and contribute more to pore formation either through gasification or lattice expansion with metallic potassium.[29] In fact, two activation pathways can be recognized for porosity formation: Low temperature activation (or low KOH/precursor) leads to initiation of pore formation followed by deepening of pores while high temperature activation results in widening of the pores generated during previous steps of activation. Depth activation contributes more micropores while width activation adds some mesopores to the system since the total micropores volume is not decreasing.[26]

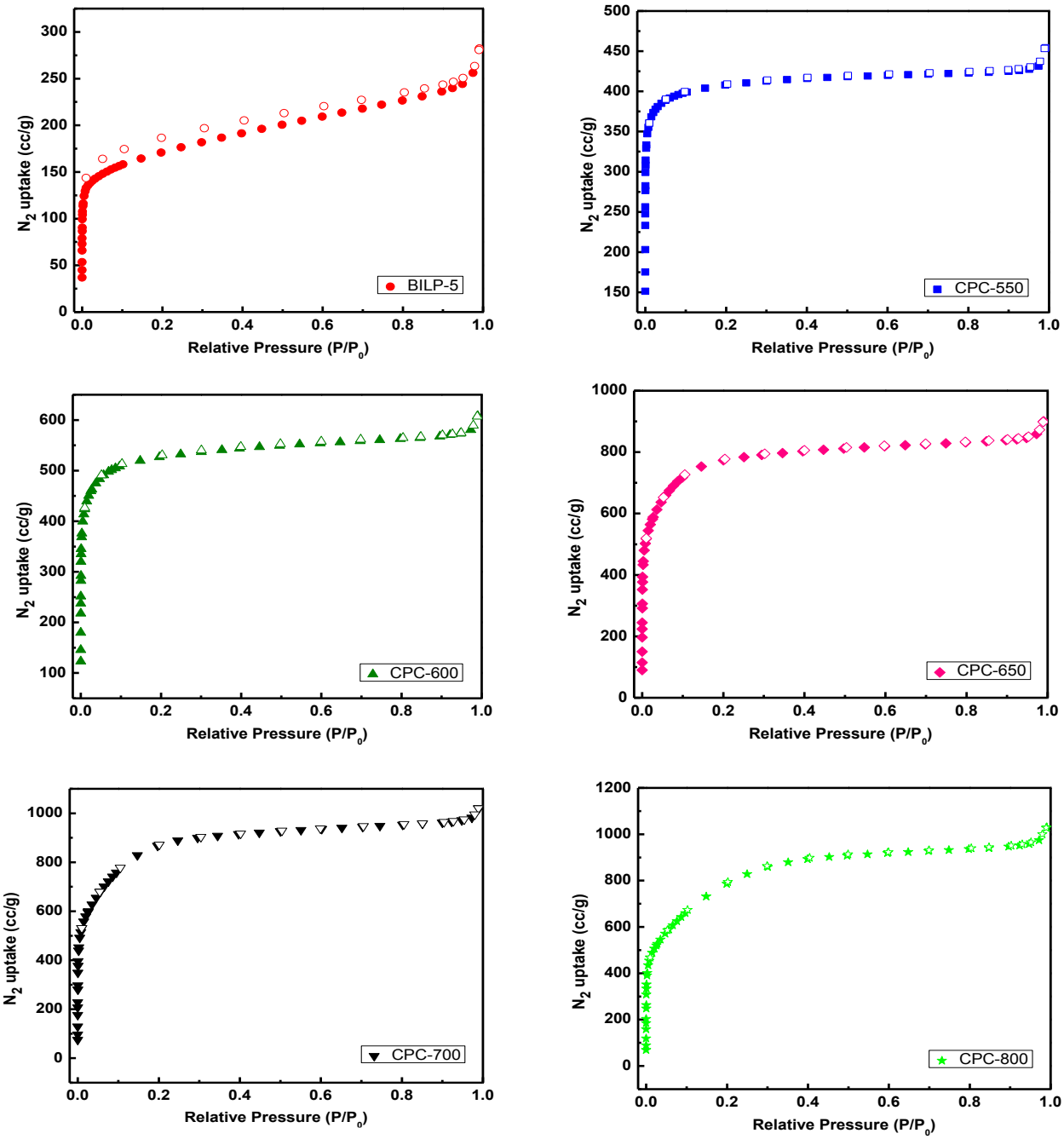

Figure 2.6. N_2 adsorption isotherms for BILP-5 and prepared CPCs measured at 77 K.

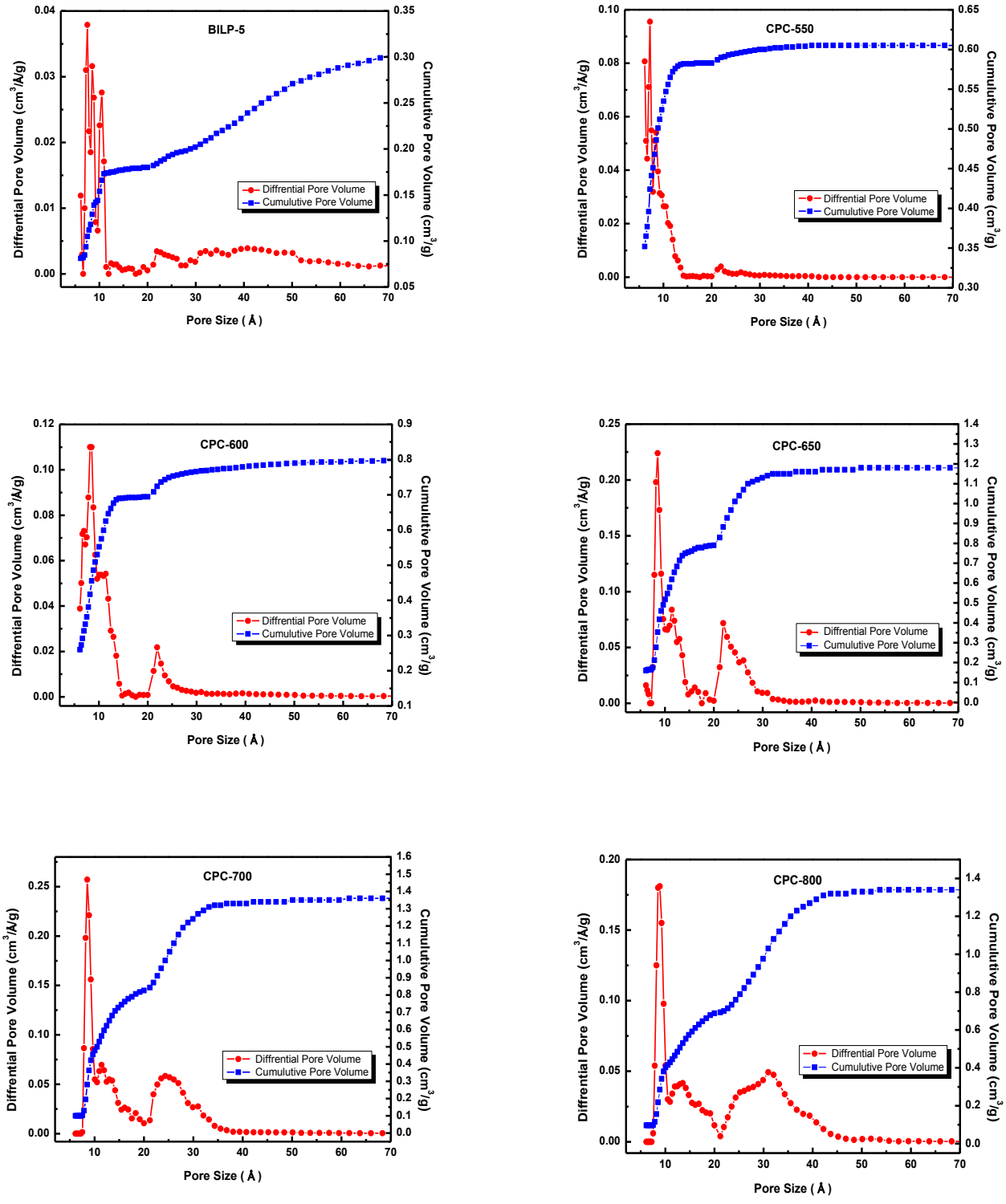

Figure 2.7. Pore size distribution and cumulative pore volume of BILP-5 and prepared CPCs from N_2 sorption isotherms at 77 K, using QSDFT method and assuming slit pore model.

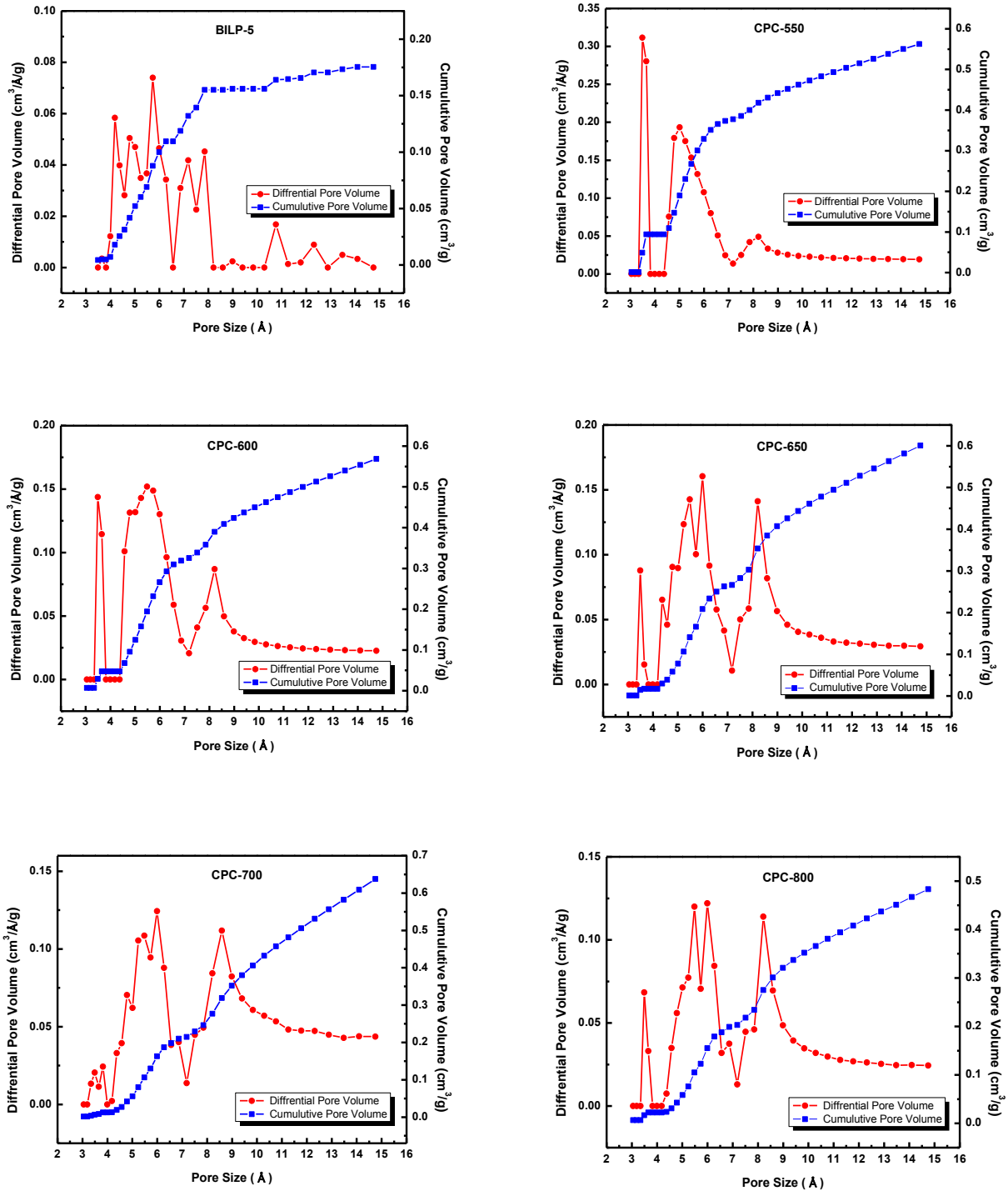

Figure 2.8. Pore size distribution and cumulative pore volume of BILP-5 and prepared CPCs from CO_2 sorption isotherms at 273 K, using NLDFT method and assuming slit pore model.

Table 2.2. Textural Properties of BILP-5 and CPCs.

Sample	S_{BET} [a] / $m^2 g^{-1}$	S_{Mic} [b] / $m^2 g^{-1}$	V_{Mic} [b] / $cm^3 g^{-1}$	V_{Tot} [c] / $cm^3 g^{-1}$	$V_{Mic,DFT}$ [d] / $cm^3 g^{-1}$	$V_{Tot,DFT}$ [d] / $cm^3 g^{-1}$	V_0 [e] / $cm^3 g^{-1}$	D_{Pore} [d] / nm	Yield %	N wt%
BILP-5	626	384	0.17	0.39	0.18 (55)	0.33	0.12	0.8	-	12.64
CPC-550	1630	1540	0.59	0.66	0.58 (97)	0.61	0.35	0.7	47	7.88
CPC-600	2059	1872	0.74	0.89	0.70 (88)	0.80	0.31	0.9	43	6.34
CPC-650	2967	2641	1.06	1.31	0.80 (67)	1.19	0.28	0.9/2.2	38	5.38
CPC-700	3242	2729	1.13	1.51	0.83 (61)	1.36	0.24	0.9/2.5	36	4.22
CPC-800	2872	1704	0.73	1.49	0.69 (51)	1.35	0.22	0.9/3.1	13	1.00

[a]Calculated in the partial pressure range which gives the best linear fitting. [b]Evaluated by the *t*-plot method. [c]Total pore volume at P/P_o = 0.95. [d]Determined by cumulative pore volume and maxima of the PSD assuming slit-shaped pores and QSDFT model; the values in parentheses are the percentage of micropores volume relative to total pore volume. [e]Pore volume of ultramicropores (<0.7 nm) obtained from CO_2 adsorption data at 273 K.

It is worth mentioning that the presence of initial microprosity in BILP-5 is not necessary for micropores formation in activated carbons. According to above-stated mechanisms, KOH activation is well known for introducing micropores to even linear polymers such as polypyrrole[8] and polyaniline[30] or non-porous biomasses.[19] In all cases, carbonization of precursor occurs through simultaneous decomposition and rearrangement of structure as temperature increases. However, considering the fact that decomposition of BILP-5 and dehydration of KOH both take place at 400 °C, that portion of initial micropores which has not completely collapsed might accelerate formation of new micropore. Moreover, gradual increase of temperature adds mesopores to system while micropore volume is still increasing. A similar phenomenon was reported by Kuhn *et al.*[31] where simultaneous polymerization/carbonization was performed by heat

treatment of nitrile monomer and zinc chloride mixture. Also it is reported that retaining some of the initial porosity during heat treatment of a sulfur rich polymer helps to further develop porous structure of the final S-doped carbon by elevating the temperature.[32]

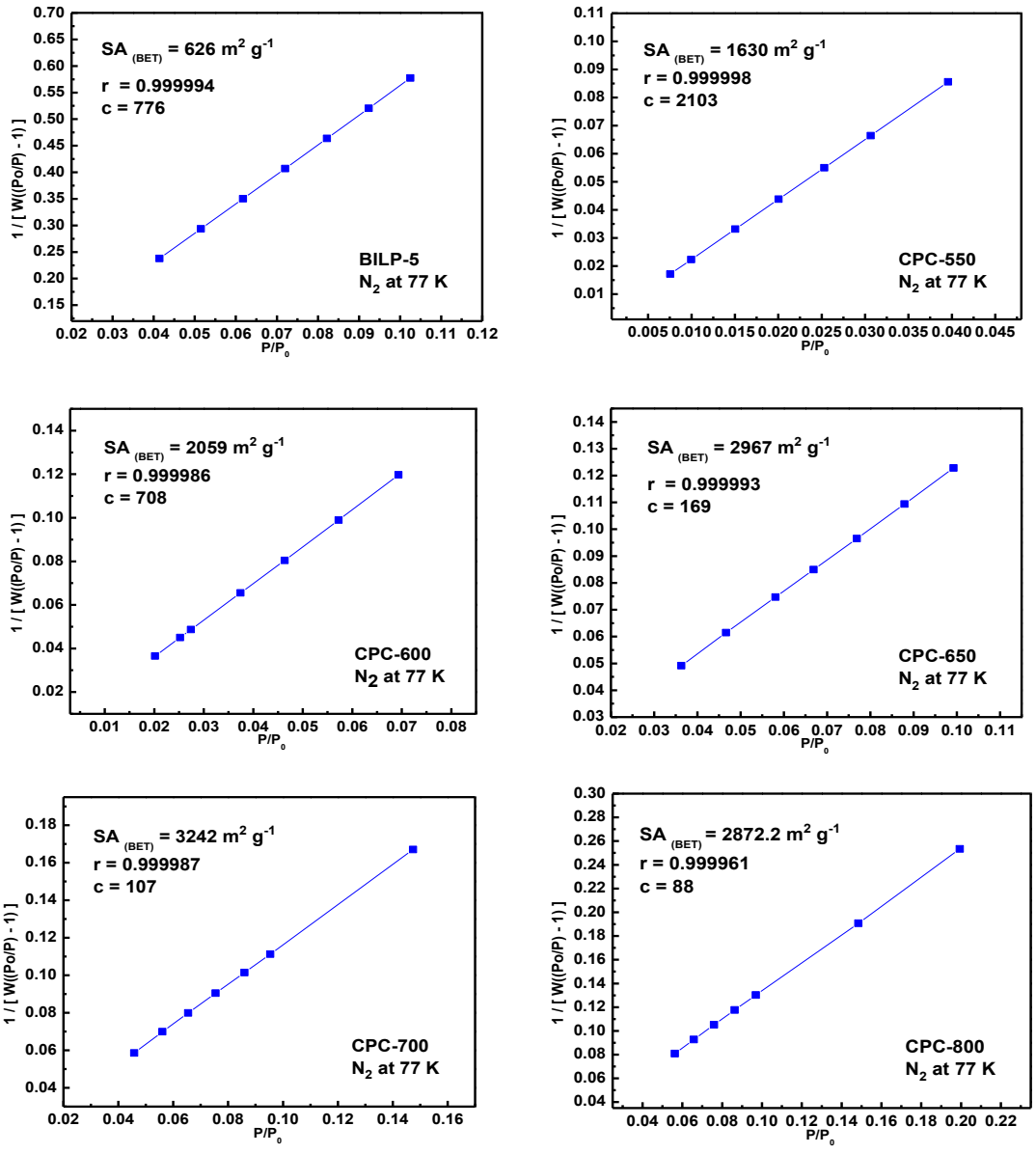

Figure 2.9. BET plots for BILP-5 and prepaid CPCs calculated from the N_2 adsorption isotherms at 77 K. (W = Weight of gas adsorbed at P/P_0, r = Correlation coefficient, c = C constant.)

Micropore volumes of activated carbons were calculated by two methods: *t*-plot and corresponding cumulative pore volume of pore size distribution using DFT method. Since the *t*-plot method uses a relative pressure range of 0.2-0.4 to calculate micropores volume, the values might deviate from the real value especially for mesoporous CPCs (2-4 nm) prepared at high temperatures. As a result, the values obtained by DFT method would be more reliable. The ratio of $V_{Mic,DFT}$/ $V_{Tot,DFT}$ can be considered as a degree of microporosity in CPCs and BILP-5. As shown in Table 2.2, the fraction of micropores can reach up to 97% of total porosity for CPC-550 and decreases at elevated temperatures, but still dominants for all CPCs. It has been reported for many carbon-based sorbents that portion of micropores, which are smaller than 0.7 nm (ultramicropores), has more pronounced effect on gas adsorption properties at ambient pressure compared to wider micropores or total pore volume.[33-35] As a result, the volume of ultramicropores was also calculated by CO_2 adsorption isotherms at 273 K. Interestingly, the amount of ultramicropores drops with increasing the activation temperature at the expense of converting some of ultramicropores to supermicropores (0.7-2 nm) or narrow mesopores (2-4 nm).

X-ray photoelectron spectroscopy (XPS) study not only confirms the successful doping of nitrogen into the frameworks of CPCs but also reveals important information about evolution of nitrogen functional groups during CPCs formation. Thus, the N 1s core level spectra of BILP-5 and all CPCs are presented in Figure 2.10 after peak fitting and deconvolution. The activated carbon prepared at 800 °C retains only 1 wt% of nitrogen and unlike other specimens, its N 1s spectrum cannot be deconvoluted due to the high noise/signal ratio. As presented in Figure 2.10. (A), nitrogen atoms can be found within four different environments in CPCs: pyridinic (N-6, 398.6 eV), pyrrolic/pyridonic (N-5, 400.3 eV), quaternary (N-Q, 401.3 eV), and pyridine-N-oxide (N-X, 403.1-406.1 eV). As expected from its molecular structure, BILP-5 exhibits two peaks at

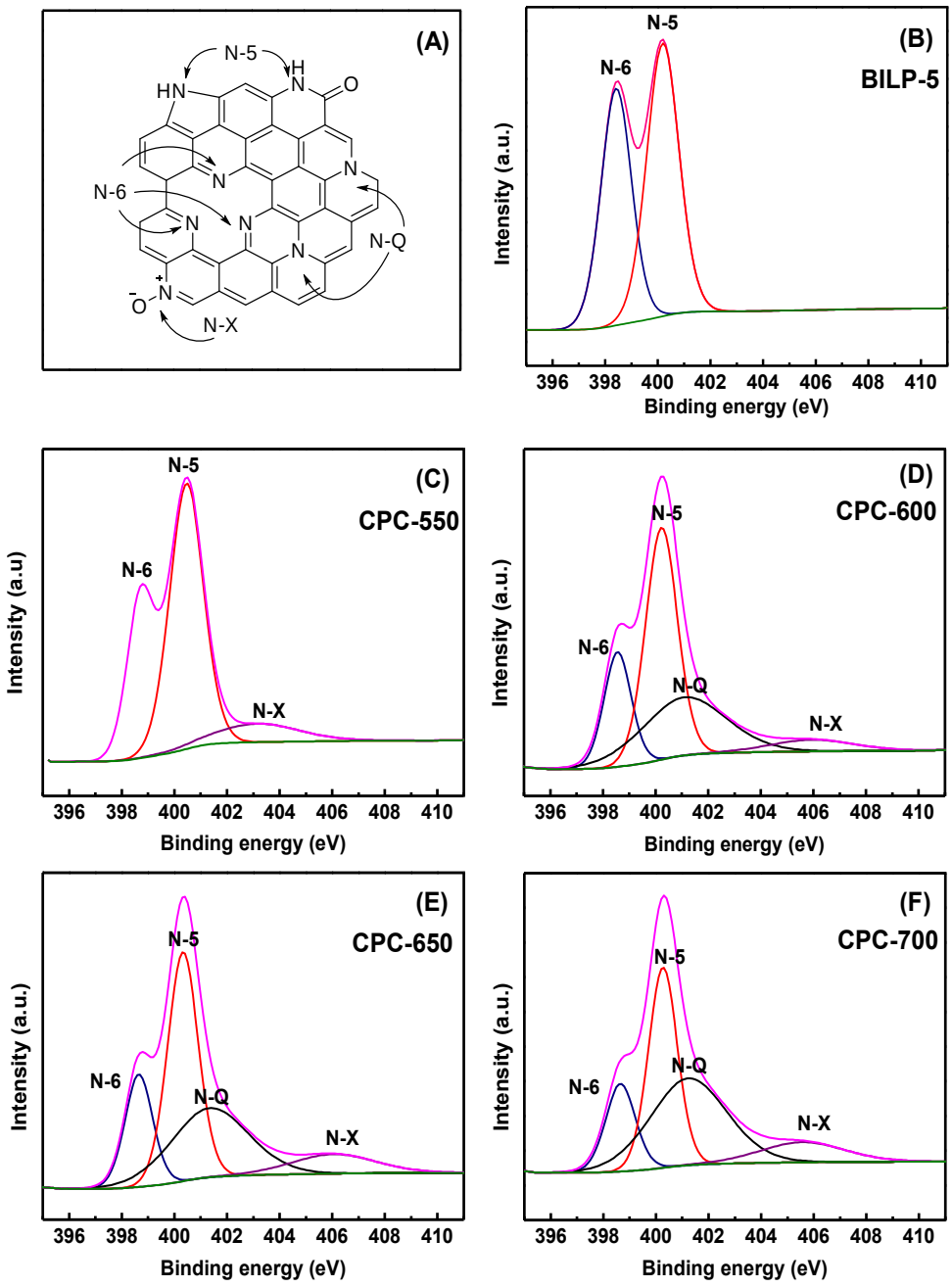

Figure 2.10. Schematic representation for possible nitrogen functionalities of (A) CPCs and deconvoluted N1s spectra of (B) BILP-5, (C) CPC-550, (D) CPC-600, (E) CPC-650 and (F) CPC-700.

398.4 eV and 400.1 eV. The former is assigned to non-protonated pyridinic whereas the latter is attributed to protonated pyrrolic nitrogen atoms both located primarily in the imidazole ring.[36] The derived CPCs contain new nitrogen species indicating chemical transformation of BILP-5 into N-rich carbons. For BILP-5 activated at 550 °C another peak around 403.1 eV appears which can be attributed to N-oxides of pyridine-N. This may result from partial oxidation of pyridinic nitrogen during activation or exposure to ambient air after activation. For CPCs prepared at 600, 650, and 700 °C, a new peak located at 401.2 eV can be clearly distinguished apart from three peaks observed in CPC-550 (N-5, N-6 and N-X). The fourth peak corresponds to the most stable nitrogen form under the current activation conditions often termed quaternary or graphitic nitrogen (N-Q). It is worth mentioning that another type of nitrogen named pyridonic might accompany pyrrolic nitrogen. Since both pyrrolic and pyridonic takes place at same binding energy, they are not distinguishable by XPS. However, taking into consideration the oxidizing environment, temperature of activation and presence of imidazole ring in BILP-5, it is likely to have a hybrid of both pyrrolic and pyridonic (N-5) in the prepared CPCs.

2.3.3 Low Pressure Gas Storage Studies. As stated above, nitrogen doped porous carbons are excellent candidates for CO_2 adsorption.[9, 28, 37-38] Therefore, the CO_2 capture performance of CPCs was investigated at 273 K, 298 K, and 313 K at ambient pressure as well as at 298 K/0.15 bar (CO_2 partial pressure in flue gas) as summarized in Table 2.3. CO_2 adsorption isotherms at different temperatures are also shown in Figure 2.11 (A) and Figures 2.12 (A-B). Knowing that increasing the activation temperature can dramatically change the textural and chemical properties of CPCs, we investigated the effect of these parameters on CO_2 capture. It was observed that the CO_2 adsorption capacity of CPCs decreases as the activation temperature increases. Very

interestingly, at 1.0 bar CPC-550 exhibits the highest CO_2 uptake (367 mg g^{-1}, 8.3 mmol g^{-1}) and (256 mg g^{-1}, 5.8 mmol g^{-1}) at 273 K and 298 K, respectively. Furthermore, CPC-550 displays a high uptake of 94 mg g^{-1} (2.1 mmol g^{-1}) at 0.15 bar / 298 K. To the best of our knowledge, the obtained values for CO_2 capture capacity especially at room temperature, are among the highest uptakes reported to date for different type of porous carbons (Table 2.4). However the uptake of CO_2 at 273 K/1bar is lower than chemically activated petroleum pitch carbon (380 mg g^{-1}, 8.6 mmol g^{-1})[7] and physically activated polyacrylonitrile (507 mg g^{-1}, 11.5 mmol g^{-1}).[39] It has been well documented that microporosity plays a key role in CO_2 adsorption of various activated carbons. However, for the current CPCs, high microporous surface area, pore volume, and apparent surface area obtained for materials prepared at high activation temperatures, led to a drop in CO_2 adsorption. Our observation is consistent with recent studies on a series of activated carbons that showed enhanced CO_2 uptake for samples having micropores below 0.7 nm.[30, 40-41] Given the kinetic size of CO_2 (3.3 Å), CO_2 adsorption inside these pores takes place by micropore filling instead of layer by layer adsorption. According to Table 2.2, the CO_2 uptake has a good correlation with the volume of ultramicropores as well as the nitrogen-doping level of CPCs.

Table 2.3. Gas Uptakes in mg g^{-1} (mmol g^{-1}), Isosteric Heats of Adsorption in kJ mol^{-1}, and Selectivity (CO_2/N_2 and CO_2/CH_4) mol mol^{-1} at 273 K (298 K) for BILP-5 and CPCs.

	CO_2					CH_4			Selectivity	
	0.15 bar	1.0 bar				1.0 bar				
Sample	298 K	273 K	298 K	313 K	Q_{st}	273 K	298 K	Q_{st}	CO_2/N_2	CO_2/CH_4
BILP-5	25 (0.6)	128 (2.9)	87 (2.0)	53 (1.2)	28.5	15 (0.9)	10 (0.5)	14.6	95 (36)	10 (6)
CPC-550	94 (2.1)	367 (8.3)	256 (5.8)	189 (4.3)	35.3	43 (2.7)	27 (1.7)	21.0	65 (59)	13 (12)
CPC-600	59 (1.3)	331 (7.5)	207 (4.7)	147 (3.3)	30.8	37 (2.3)	24 (1.5)	18.5	48 (26)	10 (6)
CPC-650	40 (0.9)	297 (6.8)	176 (4.0)	117 (2.7)	24.4	35 (2.2)	21 (1.3)	19.5	24 (17)	6 (5)
CPC-700	30 (0.7)	257 (5.9)	147 (3.3)	102 (2.3)	24.2	34 (2.1)	22 (1.4)	16.2	16 (12)	4 (3)
CPC-800	31 (0.7)	236 (5.4)	137 (3.1)	88 (2.0)	27.9	32 (2.0)	20 (1.2)	18.5	19 (15)	5 (4)

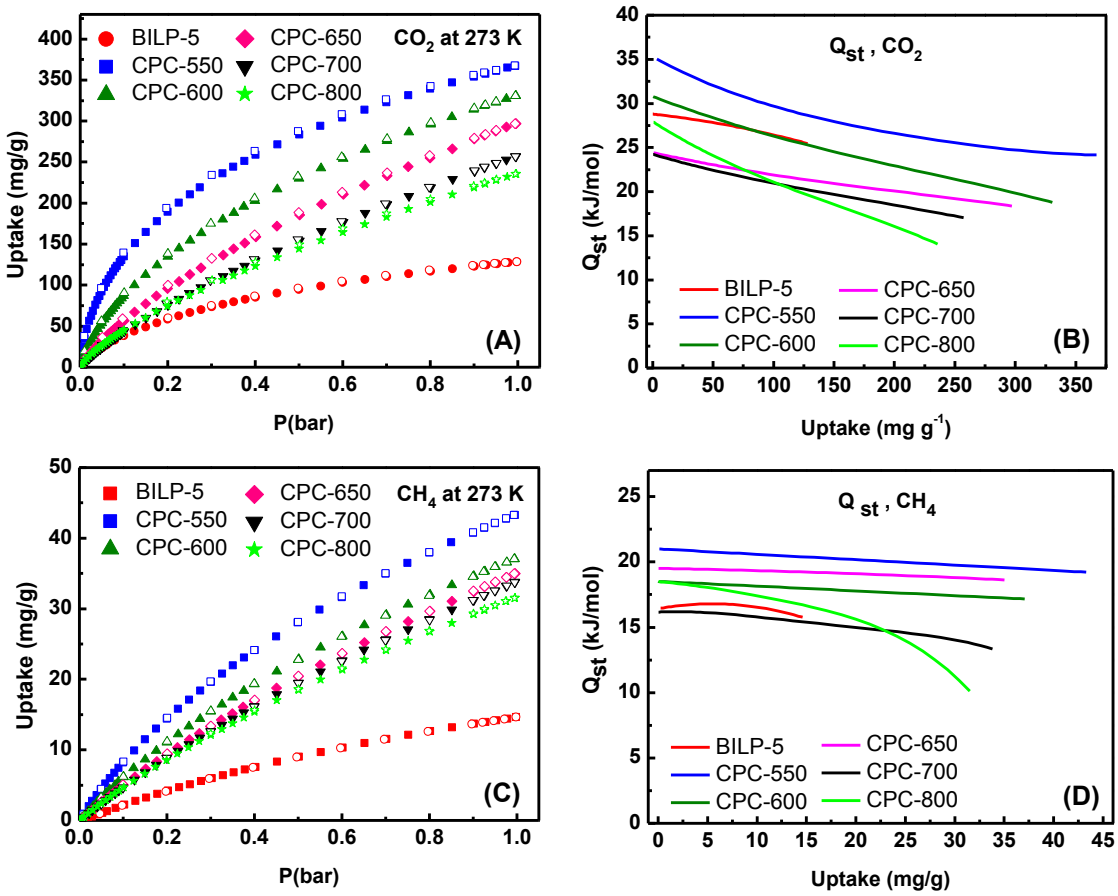

Figure 2.11. Gas uptake isotherms of (A) CO_2 and (B) CH_4 at 273 K and 1.0 bar, isosteric heat of adsorption of (C) CO_2 and (D) CH_4 for BILP-5 and all CPCs.

To investigate CPCs/CO_2 surface interactions, isosteric heats of adsorption (Q_{st}) were calculated by the virial method using CO_2 adsorption isotherms collected at 273 K and 298 K.[42] The Q_{st} values as a function of CO_2 loading increase with nitrogen content. These values range between 24-35.3 kJ mol^{-1} and are comparable with those of N-doped polypyrrole-based porous carbon (19-32 kJ mol^{-1}),[19] spherical nitrogen-containing microporous carbon (25-31 kJ mol^{-1})[22] and polyaniline-based porous carbon (21-35 kJ mol^{-1}).[30] The relatively high Q_{st} value for CPC-

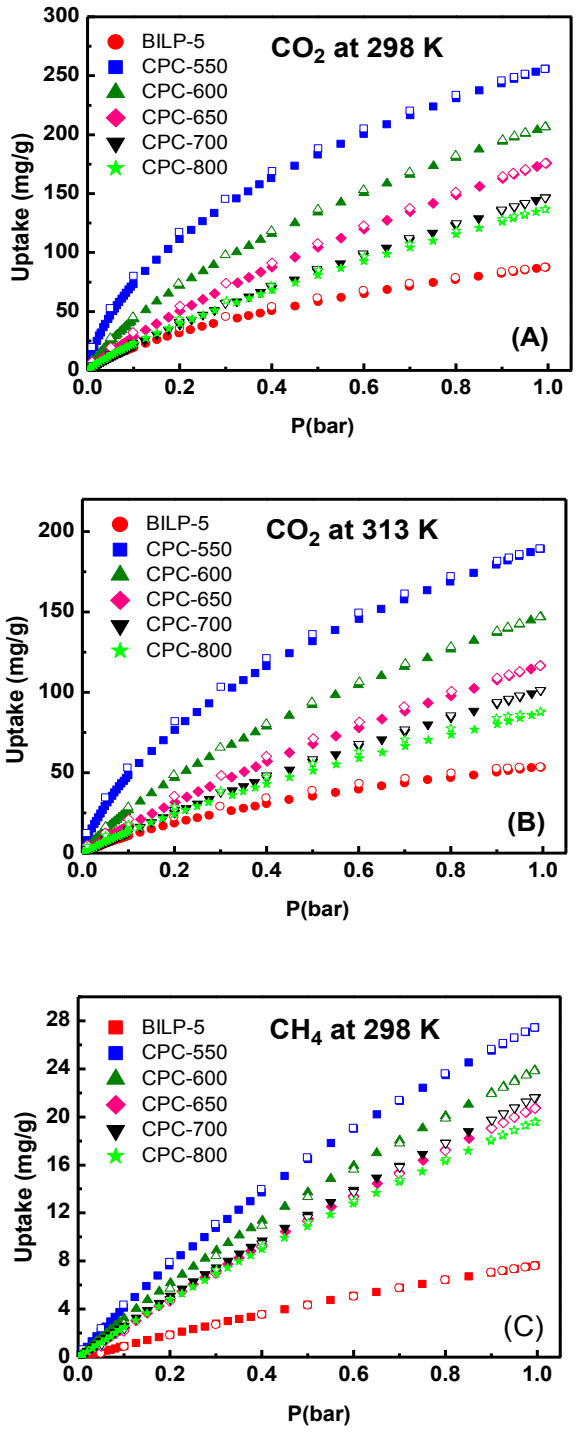

Figure 2.12. Gas sorption capacities of (A) CO_2 at 298 K, (B) CO_2 at 313 K and (C) CH_4 at 298 K for BILP-5 and prepared CPCs at 1 bar.

Table 2.4. CO_2 capture capacity, Heat of adsorption and N-level of the most recent porous carbons

Sorbent	CO_2 Uptake in mmol g^{-1}			Q_{st} / kJ mol^{-1}	N/ wt%	Sample Name and ref
	298 K, 0.15 bar	298 K, 1 bar	273 K, 1 bar			
BILP-5 derived carbon by KOH activation	2.1	5.8	8.3	35.3	7.9	CPC-550 This work
Petroleum pitch derived carbon by KOH activation	N/A	4.2	8.6	N/A	0	VR-5-M [7]
N-doped activated carbon by CO_2 physical activation of PAN	N/A	5.1	11.5	65.2	1.8	ACM-5 [39]
Porous organic polymer derived carbon by KOH activation	N/A	3.71 (1.13 bar)	6.51 (1.13 bar)	25	2.36	FCDTPA-K-700 [28]
Carbonized PAF with extra framework	1.35 (295 K)	4.1 (295 K)	N/A	27.0	0	PAF-1/C-900 [43]
Terephthalaldehyde/phenylenediamine KOH activated Carbon	N/A	2.8	4.9	28.0	0.86	MPC-700 [44]
Direct carbonized PAF-1	N/A	N/A	4.5	27.8	0	PAF-1-450 [45]
Fungi-based porous carbon	N/A	3.5	5.5	N/A	0	PC-1 [46]
Polyacrylonitrile-derived carbon by KOH activation	N/A	4.4	N/A	N/A	8.1	PAN-PK [9]
KOH activated of polypyrrole functionalized graphite sheet	N/A	4.3 a-NDC6	N/A	N/A	7 (At%)	a-NDC [47]
N-doped algae-derived carbon	N/A	4.5	7.4	25	1.5	AG-2-700 [48]
N-doped polypyrrole based porous carbon	N/A	3.9	6.2	31.5	10.1	CP-2-600 [8]
Poly(acrylonitrile-co-acrylamide) KOH activated carbon	2.1	3.8	6.6	N/A	5.9 (At%)	CSA-700 [49] CSA-800
p-diaminobenzene+ furfural alcohol KOH activated carbon	1.75 (0.2 bar)	4.50	N/A	36.1	12.9	IBN9-NC1-A[38]
Resorcinol-formaldehyde KOH activated carbon	1 (0.1 bar)	3.1	N/A	N/A	1.9	RFL-500 [23]
Phenolic resin-based carbon spheres by CO_2 physical activation	1.42 (0.2 bar)	4.55	8.03	27.7	0	CS-6-CD-4 [21] CS-6-CD-8
Polyimine based carbon by KOH activation	N/A	3.10	5.26	43	4.11	NPC-650 [37]
PAF-1 derived carbon by KOH activation	2.2 (273 K)	N/A	7.2	26	0	K-PAF-1-600 [50]
Sawdust derived carbon by KOH activation	N/A	4.8	6.6	22	0	AS-2-700 [19] AS-2-600
Graphene/polyaniline based carbon by KOH activation	N/A	2.7	5.8	56	4.19	NG7 [25]
Direct carbonized ZIF-8 with extra framework	1.53	3.9	5.1	26	2.7	NC900 [51]

550 at low coverage indicates a very favorable interaction between CO_2 molecules and the chemically heterogeneous surface of the ultrafine pores. The binding affinity of CO_2 drops at higher coverage as the favorable binding sites become less accessible. These moderate heats of adsorption of CPCs provide not only a good affinity for CO_2 capture but also a facile adsorbent regeneration without heating which is vital for large scale CCS processes. To find out the mechanisms of CO_2 adsorption on the surface of CPCs both textural properties and surface chemistry should be taken into account. Three distinct regions can be distinguished in CO_2 adsorption isotherms of CPCs (Figure 2.11 A): Low pressure (<0.2 bar) with a sharp increase in uptake, intermediate pressure (0.2-0.8), and high pressure up to 1.0 bar. As we mentioned above, CO_2 ultramicropores volume filling and interaction with nitrogen functionalities is the common adsorption mechanism in the first stage of CO_2 capture. Adsorption in the intermediate pressure range most likely takes place by filling larger micropores through layer by layer adsorption. The final step involves free volume filling by CO_2 as the pressure reaches 1.0 bar. It can be clearly seen that as the activation temperature increases, the low pressure region shrinks and changes the overall shape of the CO_2 isotherms to a more steady increase with pressure. Notably, all isotherms are far from saturation at 1.0 bar indicating that all CPCs would accommodate more CO_2 upon applying higher pressure.

Methane uptake by CPCs was also investigated to study CO_2/CH_4 separation at low pressure and methane storage at high pressure. As summarized in Table 2.3 and shown in Figure 2.11 (C), activation processes resulted in methane uptake improvement for all CPCs with respect to BILP-5. The general trend of CH_4 adsorption at 1.0 bar is similar to that observed for CO_2 adsorption isotherms; CPC-550 exhibits the best methane uptake among all CPCs storing 2.7 mmol g^{-1} and 1.7 mmol g^{-1} at 273 K and 298 K, respectively. These values are comparable to KOH

activated carbons derived from PAF-1 (2.4 mmol g^{-1} at 273 K and 1.0 bar),[50] and the poly-(vinylidene chloride)-based carbon (1.8 mmol g^{-1} at 298 K and 1bar).[52] Therefore, at atmospheric pressure the surface area of CPCs has minimum contribution to methane uptake. Unlike CO_2, CH_4 has no quadropole moments and much lower polarizability which limit its interaction with the Lewis basic nitrogen functionalities of CPCs.[53] A simulation study on porous carbon using Grand Canonical Ensemble has shown that the optimum pore diameter for adsorption of two layers of methane should be about 0.8 nm.[54] As a result, the very high methane sorption capacity of CPC-550 can be ascribed to its higher ultramicropores volume. The Q_{st} for methane was calculated to be in a range of 16.2 to 21.0 kJ mol^{-1}. The highest was observed for CPC-550 then dropped with higher activation temperatures up to 800 °C when the collapse of large pores, reestablishes the formation of narrower pores relevant to favorable CH_4 interactions.

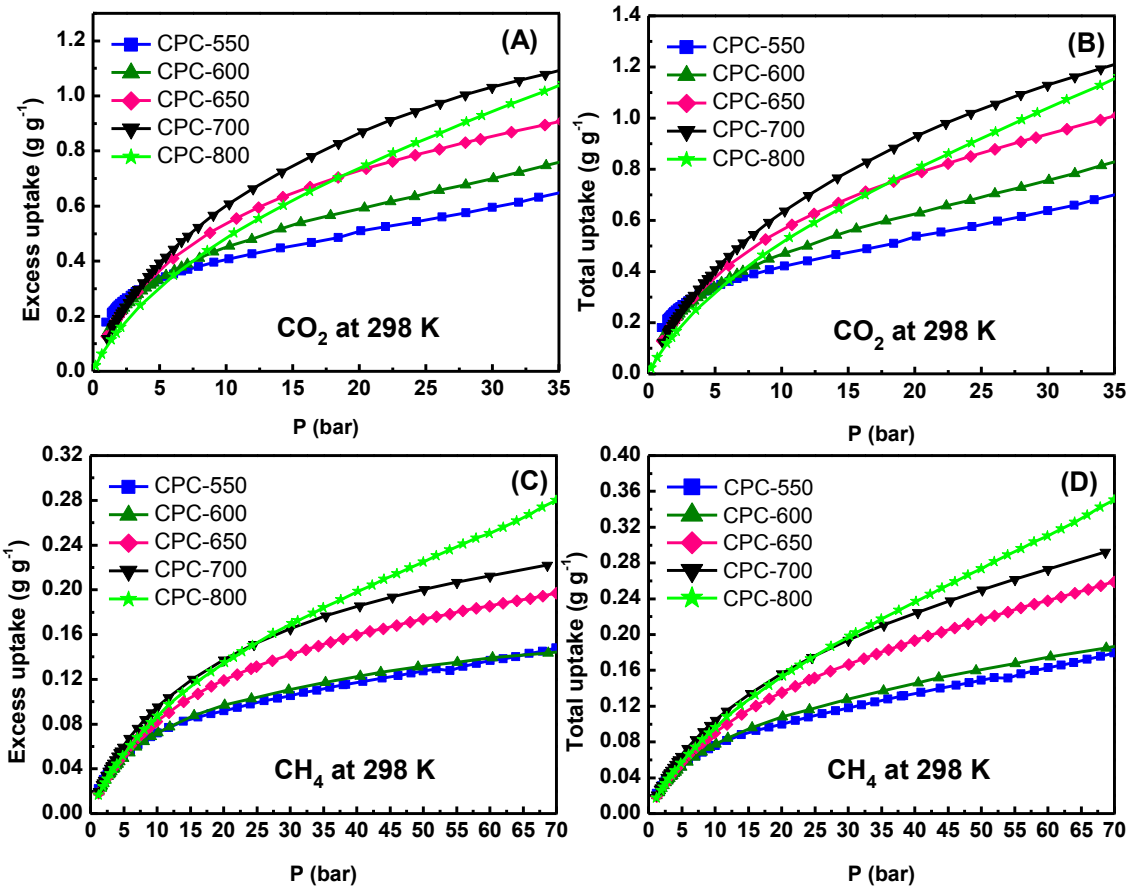

Figure 2.13. CO_2 high pressure (A) excess and (B) total adsorption isotherms and CH_4 high pressure (C) excess and (D) total adsorption isotherms at 298 K in g g^{-1}.

2.3.4 High Pressure Gas Storage Studies. Motivated by the high uptake of CO_2 and CH_4 at ambient pressure, we explored the storage capacity of CPCs at high pressure settings. The CO_2 excess and total adsorption isotherms are depicted in Figure 2.13 (A-B) and Figure 2.14 (A-B), respectively. These results indicate that unlike low pressure uptake, which is mostly governed by ultramicropores, large micropores and narrow mesopores, are the predominant attributes for attaining high storage capacities at elevated pressure. Our findings are in a good agreement with a sorption study on a series of mesophase pitch derived porous carbons reported recently by

Silvestre-Albero *et al.* [55] . More specifically, they discovered while narrow micropores has the major contribution to atmospheric CO_2 uptake, total micropore and small mesopores (2-3 nm) volumes play a key role at high pressure (up to 45 bar) uptake. Similarly, Gogotsi *et al.* [33] analyzed a series of activated carbons and concluded when the pressure is in the range of 1 to 10 bar, the volume of ultramicropores is the major contributor to high CO_2 uptake at 298 K. In contrast, at a pressure higher than 10 bar the uptake is mainly controlled by total pore volume of micro and mesopores as well as the apparent surface area. A similar study on a series of porous carbon indicated that high pressure (>20 bar) CO_2 adsorption increases linearly with BET surface area, pore volume and average pore size.[56] The highest total CO_2 uptake was recorded for CPC-700 (25.7 mmol g^{-1} at 30 bar and 298 K). This value exceeds the CO_2 adoption capacity of graphene oxide derived carbons which show similar pore volume but lower surface area.[56] This amount is also comparable to those of commercialized activated carbons, MAXSORB, having similar textural properties.[57-59] CPC-700 is outperformed by MOF-5 derived carbons due to their exceptionally high pore volume (up to 5.53 cm^3 g^{-1}) and hierarchy of micro, meso and macro pores.[60] A petroleum pitch derived carbon, VR5-4:1, also shows superior CO_2 adsorption capacity under similar condition owing to its higher percentage of large micropores/narrow mesopores.[55] In addition to high CO_2 uptake, the working capacity of an adsorbent is of similar significance. Table 2.5 lists the working capacity of CPCs at 298 K defined as the difference between total adsorption values at 30 bar and 1.0 bar. Not surprisingly, CPC-700 which has the highest uptake at high pressure and low uptake at 1.0 bar shows the best working capacity of ~23 mmol g^{-1}. This value is very comparable to the working capacity of the recently studied MOF-5 derived carbon (24.3 mmol g^{-1})[60] as well as most of the commercially available activated carbons including MAXSORB (21.2-24.5 mmol g^{-1}).[57, 59, 61]

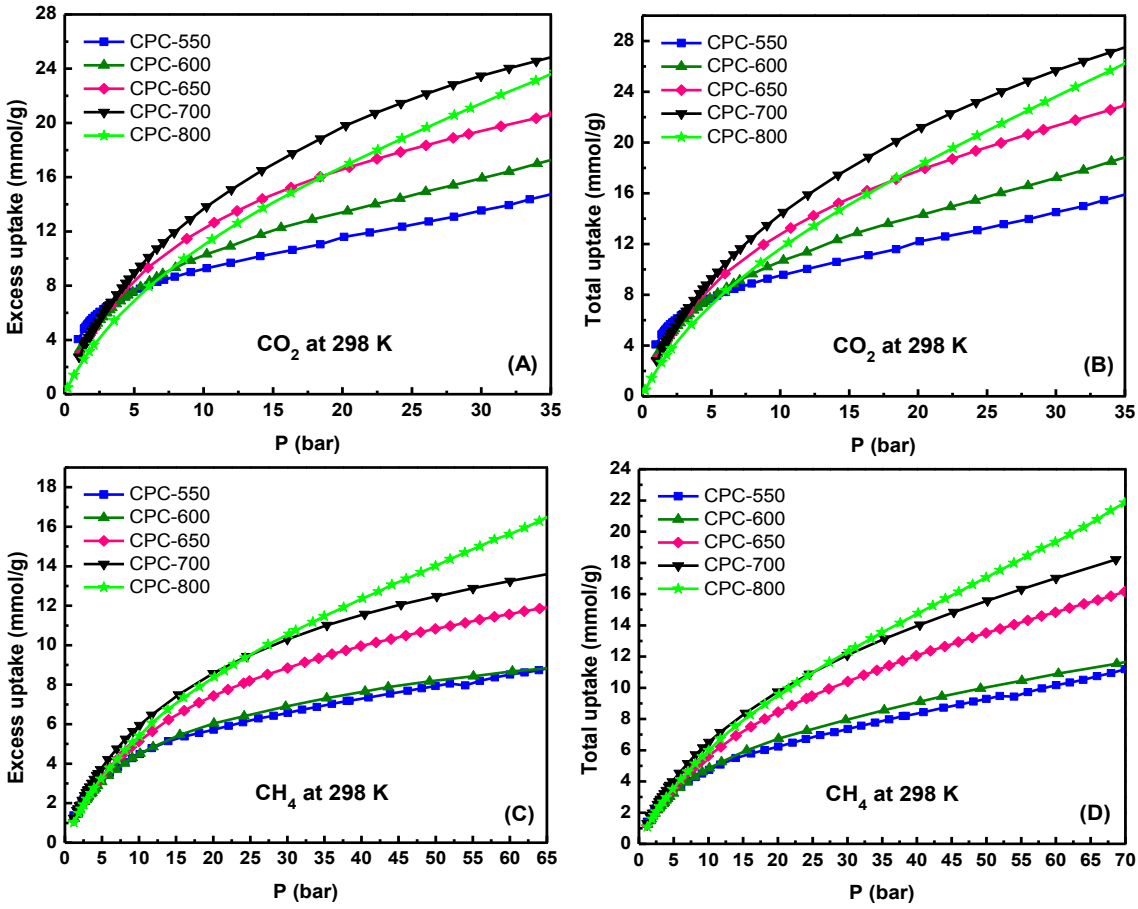

Figure 2.14. CO_2 high pressure (A) excess and (B) total adsorption isotherms and CH_4 high pressure (C) excess and (D) total adsorption isotherms at 298 K in mmol g^{-1}.

To see whether CPCs meet the new DOE target for methane (0.5 g/g), isotherms of CH_4 up to 65 bar at 298 K were collected. The results depicted in Figure 2.13 (C-D) and Figure 2.14 (C-D) and summarized in Table 2.5 indicate that CPC-800 has the highest total storage ability of 20.5 mmol g^{-1} at 65 bar. For methane storage, it has been shown that adsorption on porous carbons at room temperature and high pressures (< 30 bar) is governed by total micropore volume.[61] The improved performance of CPC-800 over CPC-700 (at P > 30 bar), despite its lower surface area, can be related to the presence of hierarchy of meso/micro pores in this sample. The storage capacity

of CPC-800 reaches 66% of the new DOE gravimetric target and is comparable to similar activated carbons derived from a variety of precursors.[50, 52] The deliverable methane capacity, which is defined as the difference between storage and discharge pressures of 65 and 5 bar, respectively, reaches a high value for CPC-800 (0.273 g g^{-1}) due to its low uptake at low pressures and high uptake at high pressures, which makes it promising for practical applications.

Table 2.5 CH_4 and CO_2 High Pressure Uptake Characteristics of CPCs at 298 K.

	CH_4 (65 bar and 298 K)			CO_2 (30 bar and 298 K)		
CPCs	Excess g g^{-1}	Total g g^{-1}	WC g g^{-1}	Excess g g^{-1}	Total g g^{-1}	WC g g^{-1}
CPC-550	0.142	0.171	0.118	0.599	0.648	0.462
CPC-600	0.143	0.182	0.130	0.705	0.763	0.618
CPC-650	0.191	0.249	0.192	0.855	0.939	0.807
CPC-700	0.218	0.284	0.219	1.033	1.131	1.007
CPC-800	0.265	0.330	0.273	0.944	1.040	0.953

The working capacity is defined as the difference in total uptake between 65 to 5 bar for CH_4 and 30 to 1.0 bar for CO_2.

2.3.5 Selective CO_2 Uptake Studies. In addition to their remarkably high CO_2 uptake, CPCs should exhibit facile regenerability and high selectivity for CO_2 over N_2 and CH_4 to be useful under practical conditions. To evaluate recyclability, we have selected CPC-600 and tested it by six continuous CO_2 adsorption/desorption cycles under ambient condition. As shown in Figure 2.15, CPC-600 maintains its initial CO_2 uptake capacity after six cycles, which confirms excellent recyclability of the sample. To evaluate the merit of CPCs for CO_2/N_2 and CO_2/CH_4 separation, single component adsorption isotherms of CO_2, CH_4 and N_2 were collected at 273 K / 298 K and

1.0 bar for all CPCs. Utilizing these isotherms and applying Henry's law constant to their low pressure region, the initial slope ratios for all gases were calculated as summarized in Table 2.3 and Figures 2.16-2.19. Results in Table 2.3 show that the selectivity values of CPCs generally decrease as the activation temperature increases. It is worth mentioning that CPC-550 exhibits comparable selectivity values to BILP-5. However, the general drop in CPCs selectivity is driven by the activation process that leads to nitrogen loss, increase in surface area, and pores enlargement. The larger pores and low nitrogen content reduce CO_2 binding affinity and provide better access for N_2 and CH_4 molecules. For CPC-800, the selectivity values of CO_2 over both N_2 and CH_4 are higher than those of CPC-700 because the former has narrower pores due to partial structure collapse that favor CO_2 uptake. The optimal CO_2/N_2 selectivity value of CPC-550 at ambient temperature (59) is significantly higher than those of recently reported activated carbons such as (benzoxazine-co-resol)-based porous carbons (27.8),[62] N-doped microporous carbons with extra cation framework (33),[38] nitrogen doped hollow carbon nanospheres (29),[63] fungi-based carbons (18.5),[64] polypyrrole-graphene based carbons (34),[47] imine-linked derived porous carbons (12.5)[37] and algae derived carbons (10).[48]

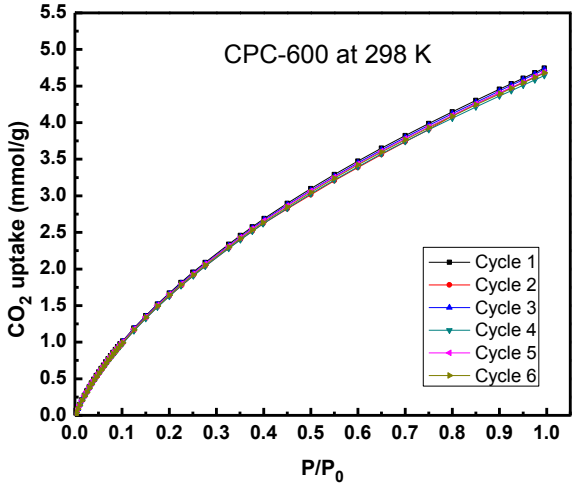

Figure 2.15. CO_2 adsorption isotherms on CPC-600 at 298 K for six repeat runs.

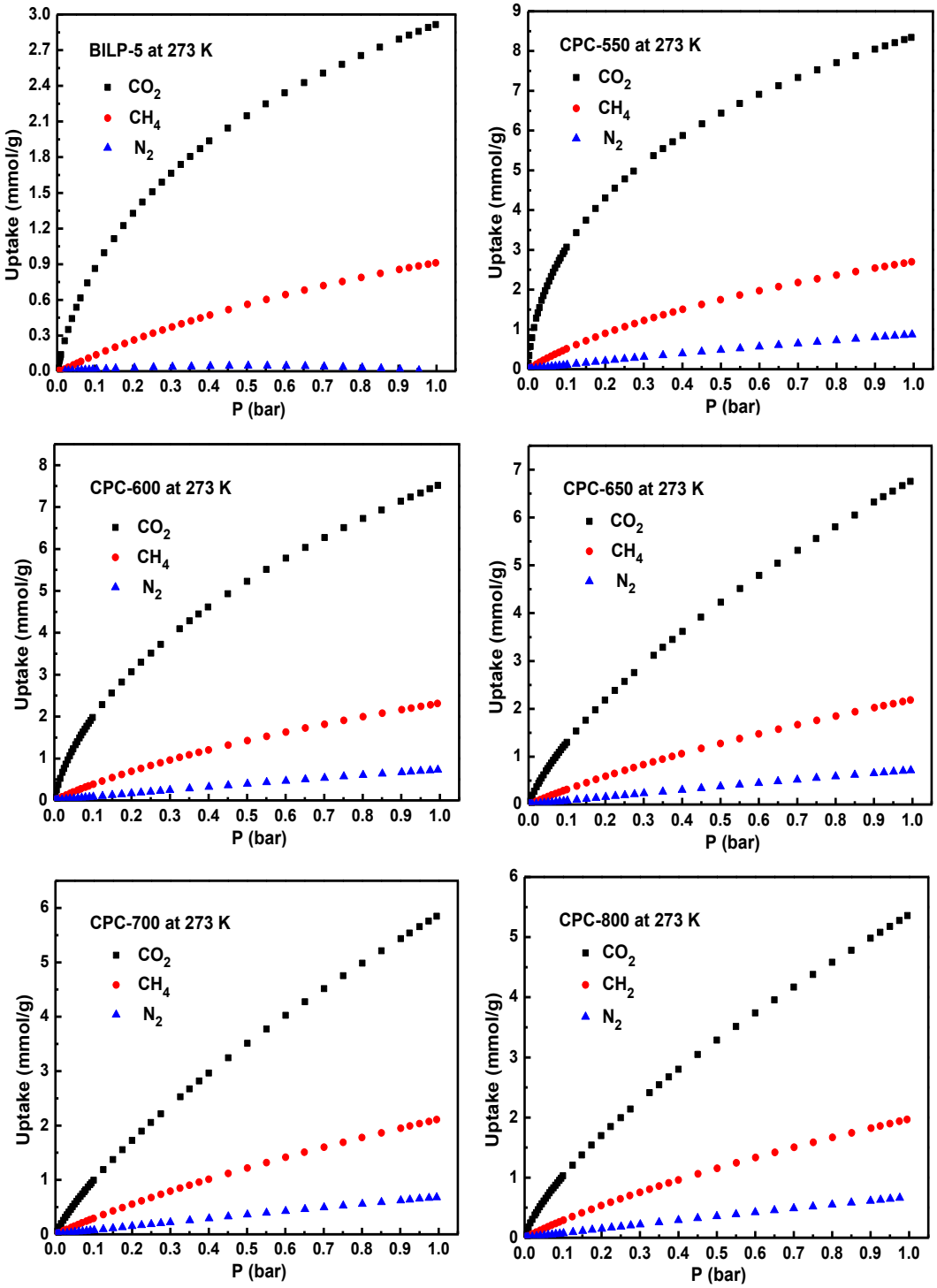

Figure 2.16. Gas sorption capacities for BILP-5 and prepared CPCs at 273 K. CO_2 (black square), CH_4 (red circle) and N_2 (Blue triangle).

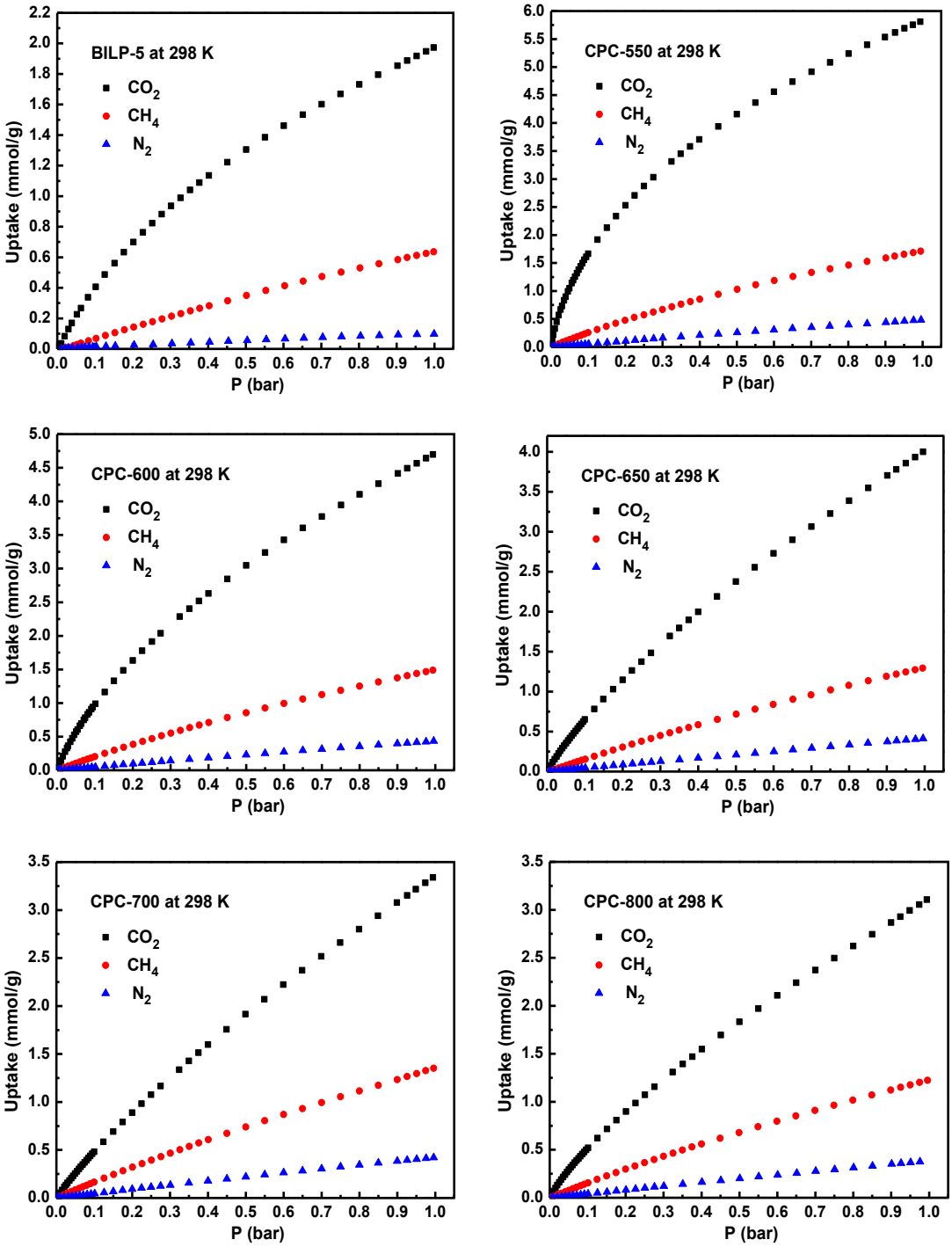

Figure 2.17. Gas sorption capacities for BILP-5 and prepared CPCs at 298 K. CO_2 (black square), CH_4 (red circle) and N_2 (Blue triangle).

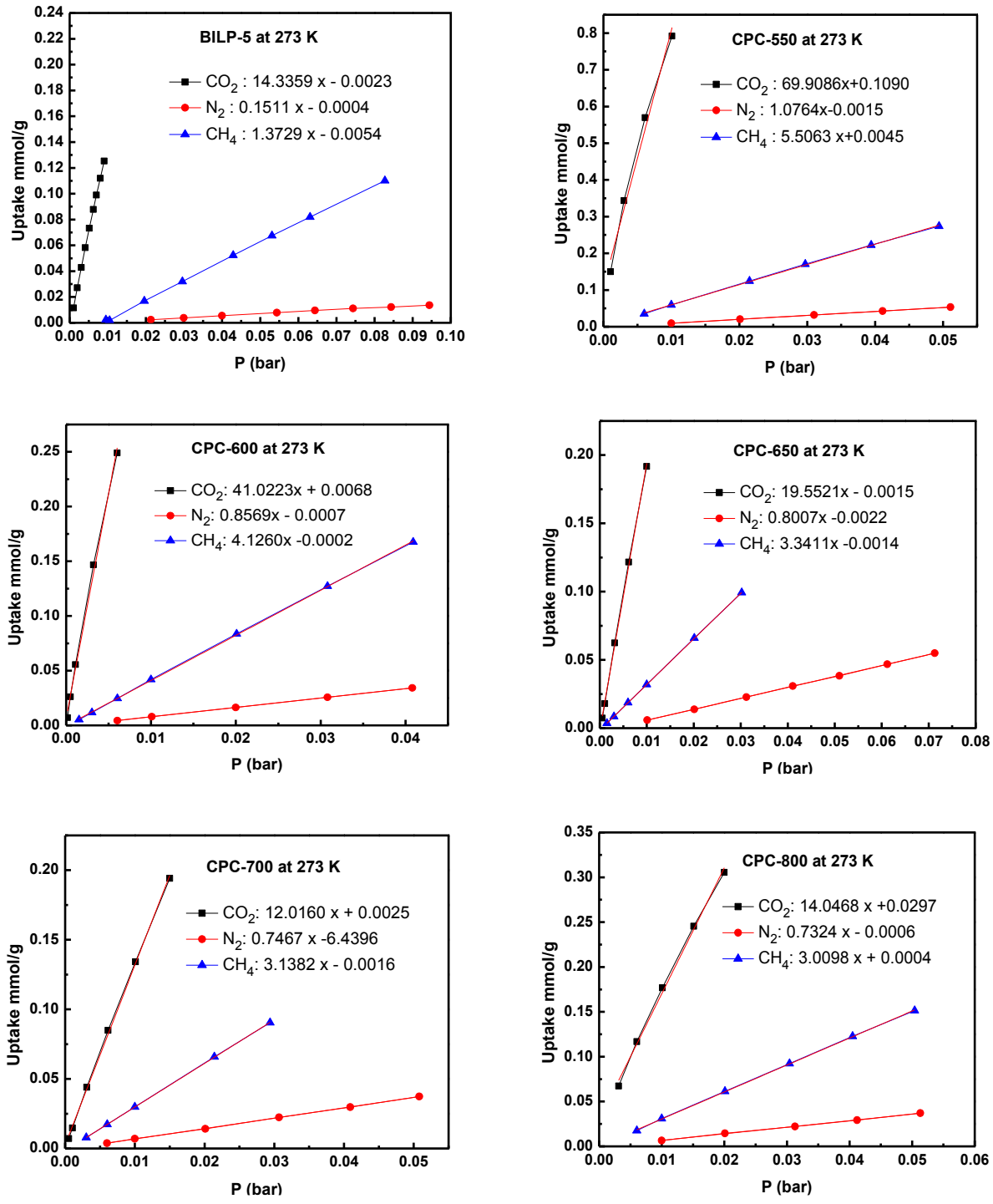

Figure 2.18. Adsorption selectivity of CO_2 over N_2 and CH_4 for BILP-5 and prepared CPCs from obtained by initial slope calculations at 273 K. CO_2 (black), CH_4 (blue) and N_2 (red).

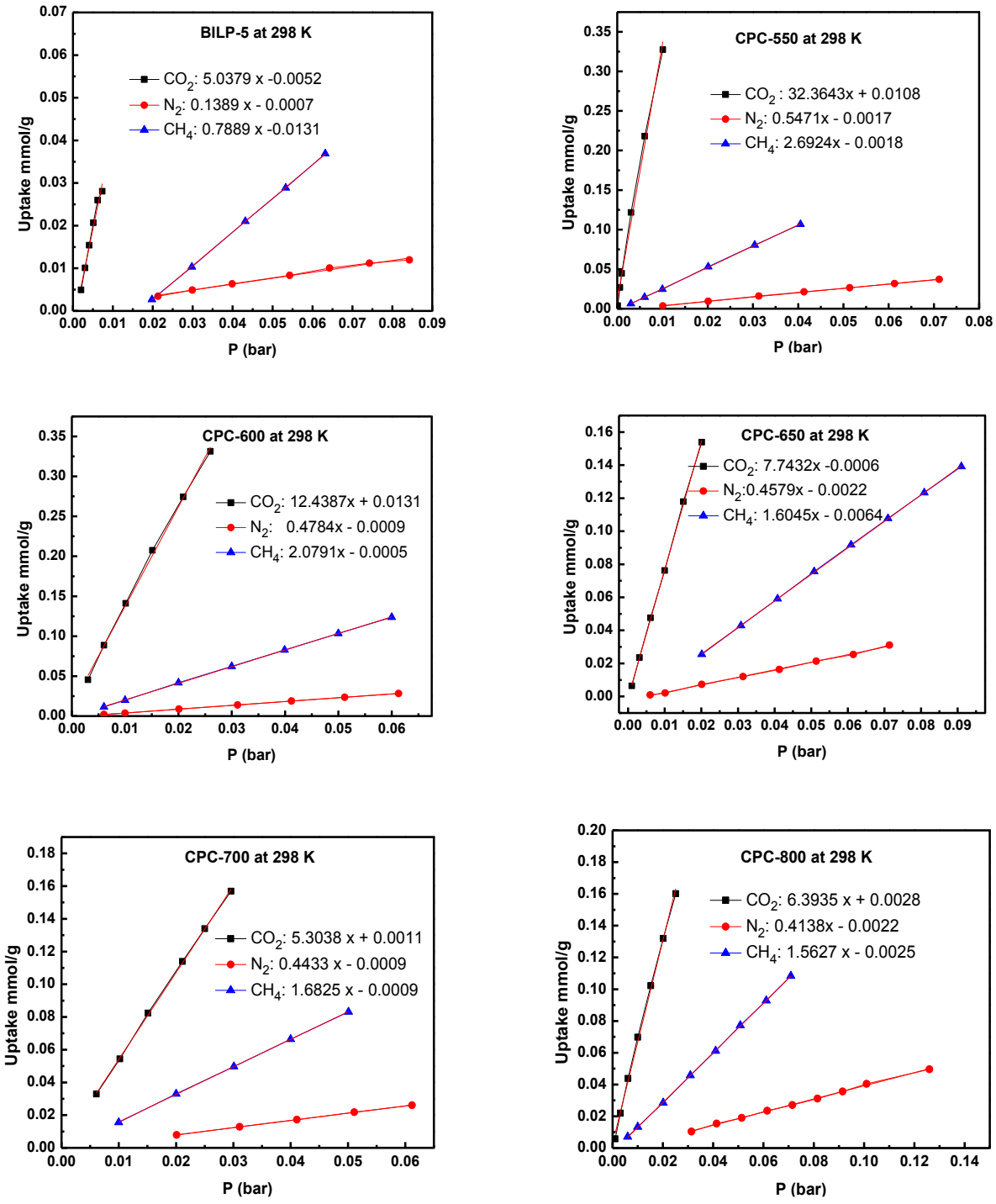

Figure 2.19. Adsorption selectivity of CO_2 over N_2 and CH_4 for BILP-5 and prepared CPCs from obtained by initial slope calculations at 298 K. CO_2 (black), CH_4 (blue) and N_2 (red).

2.4 Conclusion

In conclusion, chemical activation of benzimidazole-linked polymers with KOH followed by thermolysis afforded a series of highly porous and N-doped activated carbons with a wide range of textural properties relevant to gas storage and separation. The unique combination of high nitrogen content and ultramicroporosity in one of the prepared carbons, CPC-550, enabled high CO_2 uptake at 298 K and 1.0 bar (5.8 mmol g^{-1}). The porosity of CPCs increased significantly with activation temperature until 800 °C at which pores collapse seemed to take place. The improved textural properties (surface area and pore volume) led to very high CO_2 and CH_4 uptakes and working capacities at high pressure. In contrast, the enhanced textural properties hamper selective CO_2 separation form N_2 and CH_4 gas mixtures. For practical application of CPCs in CO_2 capture and separation, however, challenges such as reducing the cost and scalability of precursor should be solved.

2.5 References

1. White, R. J.; Budarin, V.; Luque, R.; Clark, J. H.; Macquarrie, D. J., Tuneable Porous Carbonaceous Materials from Renewable Resources. *Chem. Soc. Rev.* **2009**, *38*, 3401-3418.

2. White, R. J.; Antonietti, M.; Titirici, M.-M., Naturally Inspired Nitrogen Doped Porous Carbon. *J. Mater. Chem.* **2009**, *19*, 8645-8650.

3. Paraknowitsch, J. P.; Thomas, A., Doping Carbons Beyond Nitrogen: An Overview of Advanced Heteroatom Doped Carbons with Boron, Sulphur and Phosphorus for Energy Applications. *Energy Environ. Sci.* **2013**, *6*, 2839-2855.

4. Rabbani, M. G.; El-Kaderi, H. M., Template-Free Synthesis of a Highly Porous Benzimidazole-Linked Polymer for CO_2 Capture and H_2 Storage. *Chem. Mater.* **2011**, *23*, 1650-1653.

5. Rabbani, M. G.; El-Kaderi, H. M., Synthesis and Characterization of Porous Benzimidazole-Linked Polymers and Their Performance in Small Gas Storage and Selective Uptake. *Chem. Mater.* **2012**, *24*, 1511-1517.

6. Arab, P.; Rabbani, M. G.; Sekizkardes, A. K.; İslamoğlu, T.; El-Kaderi, H. M., Copper(I)-Catalyzed Synthesis of Nanoporous Azo-Linked Polymers: Impact of Textural Properties on Gas Storage and Selective Carbon Dioxide Capture. *Chem. Mater.* **2014**, *26*, 1385-1392.

7. Wahby, A.; Ramos-Fernández, J. M.; Martínez-Escandell, M.; Sepúlveda-Escribano, A.; Silvestre-Albero, J.; Rodríguez-Reinoso, F., High-Surface-Area Carbon Molecular Sieves for Selective CO_2 Adsorption. *ChemSusChem* **2010**, *3*, 974-981.

8. Sevilla, M.; Valle-Vigón, P.; Fuertes, A. B., N-Doped Polypyrrole-Based Porous Carbons for CO_2 Capture. *Adv. Funct. Mater.* **2011**, *21*, 2781-2787.

9. Shen, W.; Zhang, S.; He, Y.; Li, J.; Fan, W., Hierarchical Porous Polyacrylonitrile-Based Activated Carbon Fibers for CO_2 Capture. *J. Mater. Chem.* **2011**, *21*, 14036-14040.

10. Gadipelli, S.; Guo, Z. X., Tuning of ZIF-Derived Carbon with High Activity, Nitrogen Functionality, and Yield - A Case for Superior CO_2 Capture. *ChemSusChem* **2015**, *8*, 2123-32.

11. Modak, A.; Bhaumik, A., Porous Carbon Derived Via KOH Activation of a Hypercrosslinked Porous Organic Polymer for Efficient CO_2, CH_4, H_2 Adsorptions and High CO_2/N_2 Selectivity. *J. Solid State Chem.* **2015**, *232*, 157-162.

12. Bae, Y.-S.; Yazaydın, A. Ö.; Snurr, R. Q., Evaluation of the BET Method for Determining Surface Areas of MOFs and Zeolites that Contain Ultra-Micropores. *Langmuir* **2010**, *26*, 5475-5483.

13. Walton, K. S.; Snurr, R. Q., Applicability of the BET Method for Determining Surface Areas of Microporous Metal−Organic Frameworks. *J. Am. Chem. Soc.* **2007**, *129*, 8552-8556.

14. Ma, S.; Zhou, H.-C., Gas Storage in Porous Metal-Organic Frameworks for Clean Energy Applications. *Chem. Commun.* **2010**, *46*, 44-53.

15. Furukawa, H.; Miller, M. A.; Yaghi, O. M., Independent Verification of the Saturation Hydrogen Uptake in MOF-177 and Establishment of a Benchmark for Hydrogen Adsorption in Metal-Organic Frameworks. *J. Mater. Chem.* **2007**, *17*, 3197-3204.

16. Rabbani, M. G.; Sekizkardes, A. K.; Kahveci, Z.; Reich, T. E.; Ding, R.; El-Kaderi, H. M., A 2D Mesoporous Imine-Linked Covalent Organic Framework for High Pressure Gas Storage Applications. *Chem. Eur. J.* **2013**, *19*, 3324-3328.

17. Zhao, X.; Villar-Rodil, S.; Fletcher, A. J.; Thomas, K. M., Kinetic Isotope Effect for H_2 and D_2 Quantum Molecular Sieving in Adsorption/Desorption on Porous Carbon Materials. *J. Phys. Chem. B* **2006**, *110*, 9947-9955.

18. Tedds, S.; Walton, A.; Broom, D. P.; Book, D., Characterisation of Porous Hydrogen Storage Materials: Carbons, Zeolites, MOFs and PIMs. *Faraday Discuss.* **2011**, *151*, 75-94.

19. Sevilla, M.; Fuertes, A. B., Sustainable Porous Carbons with a Superior Performance for CO_2 Capture. *Energy Environ. Sci.* **2011**, *4*, 1765-1771.

20. Liu, X.; Zhou, L.; Zhao, Y.; Bian, L.; Feng, X.; Pu, Q., Hollow, Spherical Nitrogen-Rich Porous Carbon Shells Obtained from a Porous Organic Framework for the Supercapacitor. *ACS Appl. Mater. Interfaces* **2013**, *5*, 10280-10287.

21. Wickramaratne, N. P.; Jaroniec, M., Activated Carbon Spheres for CO_2 Adsorption. *ACS Appl. Mater. Interfaces* **2013**, *5*, 1849-1855.

22. Liu, L.; Deng, Q.-F.; Hou, X.-X.; Yuan, Z.-Y., User-friendly Synthesis of Nitrogen-Containing Polymer and Microporous Carbon Spheres for Efficient CO_2 Capture. *J. Mater. Chem.* **2012**, *22*, 15540-15548.

23. Hao, G.-P.; Li, W.-C.; Qian, D.; Lu, A.-H., Rapid Synthesis of Nitrogen-Doped Porous Carbon Monolith for CO_2 Capture. *Adv. Matter.* **2010**, *22*, 853-857.

24. Saleh, M.; Chandra, V.; Kemp, K. C.; Kim, K. S., Synthesis of N-Doped Microporous Carbon via Chemical Activation of Polyindole-Modified Graphene Oxide Sheets for Selective Carbon Dioxide Adsorption. *Nanotechnology* **2013**, *24*, 255702.

25. Kemp, K. C.; Chandra, V.; Saleh, M.; Kim, K. S., Reversible CO_2 Adsorption by an Activated Nitrogen Doped Graphene/Polyaniline Material. *Nanotechnology* **2013**, *24*, 235703.

26. Hu, X.; Radosz, M.; Cychosz, K. A.; Thommes, M., CO_2-Filling Capacity and Selectivity of Carbon Nanopores: Synthesis, Texture, and Pore-Size Distribution from Quenched-Solid Density Functional Theory (QSDFT). *Environ. Sci. Technol.* **2011**, *45*, 7068-7074.

27. Lozano-Castelló, D.; Cazorla-Amorós, D.; Linares-Solano, A., Usefulness of CO_2 Adsorption at 273 K for the Characterization of Porous Carbons. *Carbon* **2004**, *42*, 1233-1242.

28. Yang, X.; Yu, M.; Zhao, Y.; Zhang, C.; Wang, X.; Jiang, J.-X., Remarkable Gas Adsorption by Carbonized Nitrogen-Rich Hypercrosslinked Porous Organic Polymers. *J. Mater. Chem. A* **2014**.

29. Wang, J.; Kaskel, S., KOH Activation of Carbon-Based Materials for Energy Storage. *J. Mater. Chem.* **2012**, *22*, 23710-23725.

30. Zhang, Z.; Zhou, J.; Xing, W.; Xue, Q.; Yan, Z.; Zhuo, S.; Qiao, S. Z., Critical Role of Small Micropores in High CO_2 Uptake. *Phys. Chem. Chem. Phys.* **2013**, *15*, 2523-2529.

31. Kuhn, P.; Forget, A.; Su, D.; Thomas, A.; Antonietti, M., From Microporous Regular Frameworks to Mesoporous Materials with Ultrahigh Surface Area: Dynamic Reorganization of Porous Polymer Networks. *J. Am. Chem. Soc.* **2008**, *130*, 13333-13337.

32. Paraknowitsch, J. P.; Thomas, A.; Schmidt, J., Microporous Sulfur-Doped Carbon from Thienyl-Based Polymer Network Precursors. *Chem. Commun.* **2011**, *47*, 8283-8285.

33. Presser, V.; McDonough, J.; Yeon, S.-H.; Gogotsi, Y., Effect of Pore Size on Carbon Dioxide Sorption by Carbide Derived Carbon. *Energy Environ. Sci.* **2011**, *4*, 3059-3066.

34. Wei, H.; Deng, S.; Hu, B.; Chen, Z.; Wang, B.; Huang, J.; Yu, G., Granular Bamboo-Derived Activated Carbon for High CO_2 Adsorption: The Dominant Role of Narrow Micropores. *ChemSusChem* **2012**, *5*, 2354-2360.

35. Sevilla, M.; Parra, J. B.; Fuertes, A. B., Assessment of the Role of Micropore Size and N-Doping in CO_2 Capture by Porous Carbons. *ACS Appl. Mater. Interfaces* **2013**, *5*, 6360-6368.

36. Hua, M.-Y.; Chen, H.-C.; Tsai, R.-Y.; Lai, C.-S., A Novel Polybenzimidazole-Modified Gold Electrode for the Analytical Determination of Hydrogen Peroxide. *Talanta* **2011**, *85*, 631-637.

37. Wang, J.; Senkovska, I.; Oschatz, M.; Lohe, M. R.; Borchardt, L.; Heerwig, A.; Liu, Q.; Kaskel, S., Highly Porous Nitrogen-Doped Polyimine-based Carbons with Adjustable Microstructures for CO_2 Capture. *J. Mater. Chem. A* **2013**, *1*, 10951-10961.

38. Zhao, Y.; Zhao, L.; Yao, K. X.; Yang, Y.; Zhang, Q.; Han, Y., Novel Porous Carbon Materials with Ultrahigh Nitrogen Contents for Selective CO_2 Capture. *J. Mater. Chem.* **2012**, *22*, 19726-19731.

39. Nandi, M.; Okada, K.; Dutta, A.; Bhaumik, A.; Maruyama, J.; Derks, D.; Uyama, H., Unprecedented CO_2 Uptake over Highly Porous N-Doped Activated Carbon Monoliths Prepared by Physical Activation. *Chem. Commun.* **2012**, *48*, 10283-10285.

40. Pevida, C.; Drage, T. C.; Snape, C. E., Silica-Templated Melamine–Formaldehyde Resin Derived Adsorbents for CO_2 Capture. *Carbon* **2008**, *46*, 1464-1474.

41. Martín, C. F.; Plaza, M. G.; Pis, J. J.; Rubiera, F.; Pevida, C.; Centeno, T. A., On the Limits of CO_2 Capture Capacity of Carbons. *Sep. Purif. Technol.* **2010**, *74*, 225-229.

42. Czepirski, L.; JagieŁŁo, J., Virial-Type Thermal Equation of Gas-Solid Adsorption. *Chem. Eng. Sci.* **1989**, *44*, 797-801.

43. Zhang, Y.; Li, B.; Williams, K.; Gao, W.-Y.; Ma, S., A New Microporous Carbon Material Synthesized via Thermolysis of a Porous Aromatic Framework Embedded with an Extra Carbon Source for Low-Pressure CO_2 Uptake. *Chem. Commun.* **2013**, *49*, 10269-10271.

44. Wang, J.; Liu, Q., An Efficient One-Step Condensation and Activation Strategy to Synthesize Porous Carbons with Optimal Micropore Sizes for Highly Selective CO_2 Adsorption. *Nanoscale* **2014**, *6*, 4148-4156.

45. Ben, T.; Li, Y.; Zhu, L.; Zhang, D.; Cao, D.; Xiang, Z.; Yao, X.; Qiu, S., Selective Adsorption of Carbon Dioxide by Carbonized Porous Aromatic Framework (PAF). *Energy Environ. Sci.* **2012**, *5*, 8370-8376.

46. Wang, J.; Heerwig, A.; Lohe, M. R.; Oschatz, M.; Borchardt, L.; Kaskel, S., Fungi-Based Porous Carbons for CO_2 Adsorption and Separation. *J. Mater. Chem.* **2012**, *22*, 13911-13913.

47. Chandra, V.; Yu, S. U.; Kim, S. H.; Yoon, Y. S.; Kim, D. Y.; Kwon, A. H.; Meyyappan, M.; Kim, K. S., Highly Selective CO_2 Capture on N-Doped Carbon Produced by Chemical Activation of Polypyrrole Functionalized Graphene Sheets. *Chem. Commun.* **2012**, *48*, 735-737.

48. Sevilla, M.; Falco, C.; Titirici, M.-M.; Fuertes, A. B., High-Performance CO_2 Sorbents from Algae. *RSC Advances* **2012**, *2*, 12792-12797.

49. Zhu, B.; Li, K.; Liu, J.; Liu, H.; Sun, C.; Snape, C. E.; Guo, Z., Nitrogen-Enriched and Hierarchically Porous Carbon Macro-Spheres - Ideal for Large-Scale CO_2 Capture. *J. Mater. Chem. A* **2014**, *2*, 5481-5489.

50. Li, Y.; Ben, T.; Zhang, B.; Fu, Y.; Qiu, S., Ultrahigh Gas Storage Both at Low and High Pressures in KOH-Activated Carbonized Porous Aromatic Frameworks. *Sci. Rep.* **2013**, *3*. 2420.

51. Aijaz, A.; Fujiwara, N.; Xu, Q., From Metal–Organic Framework to Nitrogen-Decorated Nanoporous Carbons: High CO_2 Uptake and Efficient Catalytic Oxygen Reduction. *J. Am. Chem. Soc.* **2014**, *136*, 6790-6793.

52. Cai, J.; Qi, J.; Yang, C.; Zhao, X., Poly(Vinylidene Chloride)-Based Carbon with Ultrahigh Microporosity and Outstanding Performance for CH_4 and H_2 Storage and CO_2 Capture. *ACS Appl. Mater. Interfaces* **2014**, *6*, 3703-3711.

53. Herm, Z. R.; Krishna, R.; Long, J. R., CO_2/CH_4, CH_4/H_2 and $CO_2/CH_4/H_2$ Separations at High Pressures Using Mg_2(DOBDC). *Microporous Mesoporous Mater.* **2012**, *151*, 481-487.

54. Mosher, K.; He, J.; Liu, Y.; Rupp, E.; Wilcox, J., Molecular Simulation of Methane Adsorption in Micro- and Mesoporous Carbons with Applications to Coal and Gas Shale Systems. *Int. J. Coal Geol.* **2013**, *109–110*, 36-44.

55. Casco, M. E.; Martínez-Escandell, M.; Silvestre-Albero, J.; Rodríguez-Reinoso, F., Effect of the Porous Structure in Carbon Materials for CO_2 Capture at Atmospheric and High-Pressure. *Carbon* **2014**, *67*, 230-235.

56. Srinivas, G.; Burress, J.; Yildirim, T., Graphene Oxide Derived Carbons (GODCs): Synthesis and Gas Adsorption Properties. *Energy Environ. Sci.* **2012**, *5*, 6453-6459.

57. Himeno, S.; Komatsu, T.; Fujita, S., High-Pressure Adsorption Equilibria of Methane and Carbon Dioxide on Several Activated Carbons. *J. Chem. Eng. Data* **2005**, *50*, 369-376.

58. Marco-Lozar, J. P.; Juan-Juan, J.; Suárez-García, F.; Cazorla-Amorós, D.; Linares-Solano, A., MOF-5 and Activated Carbons as Adsorbents for Gas Storage. *Int. J. Hydrogen Energy* **2012**, *37*, 2370-2381.

59. Saha, B. B.; Jribi, S.; Koyama, S.; El-Sharkawy, I. I., Carbon Dioxide Adsorption Isotherms on Activated Carbons. *J. Chem. Eng. Data* **2011**, *56*, 1974-1981.

60. Srinivas, G.; Krungleviciute, V.; Guo, Z.-X.; Yildirim, T., Exceptional CO_2 Capture in a Hierarchically Porous Carbon with Simultaneous High Surface Area and Pore Volume. *Energy Environ. Sci.* **2014**, *7*, 335-342.

61. Marco-Lozar, J. P.; Kunowsky, M.; Suarez-Garcia, F.; Carruthers, J. D.; Linares-Solano, A., Activated Carbon Monoliths for Gas Storage at Room Temperature. *Energy Environ. Sci.* **2012**, *5*, 9833-9842.

62. Hao, G.-P.; Li, W.-C.; Qian, D.; Wang, G.-H.; Zhang, W.-P.; Zhang, T.; Wang, A.-Q.; Schüth, F.; Bongard, H.-J.; Lu, A.-H., Structurally Designed Synthesis of Mechanically Stable Poly(Benzoxazine-Co-Resol)-Based Porous Carbon Monoliths and Their Application as High-Performance CO_2 Capture Sorbents. *J. Am. Chem. Soc.* **2011**, *133*, 11378-11388.

63. Zhou, L.; Shao, Y.; Liu, J.; Ye, Z.; Zhang, H.; Ma, J.; Jia, Y.; Gao, W.; Li, Y., Preparation and Characterization of Magnetic Porous Carbon Microspheres for Removal of Methylene Blue by a Heterogeneous Fenton Reaction. *ACS Appl. Mater. Interfaces* **2014**.

64. Xing, W.; Liu, C.; Zhou, Z.; Zhang, L.; Zhou, J.; Zhuo, S.; Yan, Z.; Gao, H.; Wang, G.; Qiao, S. Z., Superior CO_2 Uptake of N-Doped Activated Carbon through Hydrogen-Bonding Interaction. *Energy Environ. Sci.* **2012**, *5*, 7323-7327.

Chapter 3: From Azo-Linked Polymers to Microporous Heteroatom Doped Carbons: Tailored Chemical and Textural Properties for Gas Separation

3.1 Introduction

Design of task-specific single source precursors (of carbon and desired heteroatom) for generation of high performance nanoporous carbons has been the subject of many research works in recent years.[1-2] Accordingly, various promising single sources of nitrogen and carbon including nitrogen-decorated metal-organic-frameworks (ZIF-8),[3-4] nitrogen containing porous organic polymers (imine-linked, benizimidazole-linked and hypercross-linked polymers),[5-7] ionic liquids[8-10] and biomasses and derivatives[11-12] have been employed. However, the elimination of non-carbon atoms upon carbonization results in low dopant level in final product. This challenge can be addressed by selecting a precursor with intrinsically more robust heteroatom bonds.

In this chapter, we introduce a new series of nitrogen and oxygen co-doped porous carbons by using an azo-linked polymer as precursor. The task-specific ALP-6 precursor consists of high nitrogen content (14.7 wt%) and initial porosity (SA_{BET}= 800 m^2 g^{-1}). Additionally, it is believed that highly stable nitrogen linkage will benefit high doping level of heteroatoms and CO_2 selective adsorption. Direct carbonization, $ZnCl_2$ and KOH activation were applied to obtain three different classes of ALP-6 derived carbons (ALPDCD, ALPDCZ and ALPDCK, respectively). Textural properties, surface chemistry and gas adsorption and selectivity of prepared carbons along with ALP-6 were comparatively investigated.

3.2 Experimental

3.2.1 Preparation of Heteroatom Doped Carbons. The single source precursor, ALP-6, was synthesized through copper (I)-catalyzed oxidative homocoupling of *N*,*N*,*N'*,*N'*-tetrakis (4-aminophenyl)-1,4-phenylenediamine monomer following the procedure we recently reported.[13-14] ALP-6 batches were combined (~ 3.0 g) and outgassed at 120 °C and 150 mTor for 24 h. The first class of porous carbons was synthesized by direct carbonization of ALP-6. In a typical synthesis, 300 mg of outgassed ALP-6 was placed in a ceramic boat then directly heated to the targeted temperatures of 600, 700 and 800 °C with a heating rate of 5 °C /min under ultrahigh purity Ar flow and held for 1 h at the desired temperature. ALP-6 derived carbons synthesized by this procedure were labeled as ALPDC*DT*, where *D* and *T* represent direct pyrolysis and the targeted carbonization temperature, respectively. The second and third classes of porous carbons were synthesized by pyrolysis of ALP-6 after activation with KOH and $ZnCl_2$, respectively. In a typical procedure, 400 mg of activated ALP-6 precursor was thoroughly mixed with 800 mg of KOH or $ZnCl_2$ (2:1 weight ratio of activating agent to polymer). To minimize the effect of water absorption on the surface of activated polymers and reaction with activation agents, this step was carried out under nitrogen inside a glovebox. The uniform powder mixture obtained by physical mixing and grinding was placed in a boat then transferred to a tube furnace and heated up to 500, 600 and 700 °C as discussed above. After cooling to room temperature, the black carbon samples were soaked and washed three times with HCl (1.0 M) to remove unreacted KOH, $ZnCl_2$ or residual salts. Further purification was performed by washing with distilled water and ethanol, respectively. The resulting activated carbons were dried under vacuum at 200 °C for 12 h. These classes of ALP-6 derived carbons were denoted as ALPDC*KT* and APLDC*ZT* in which, *K*, *Z* and

T represent chemical activation by KOH, $ZnCl_2$ and activation temperature, respectively. Synthetic routes of porous carbons are depicted in Figure 3.1.

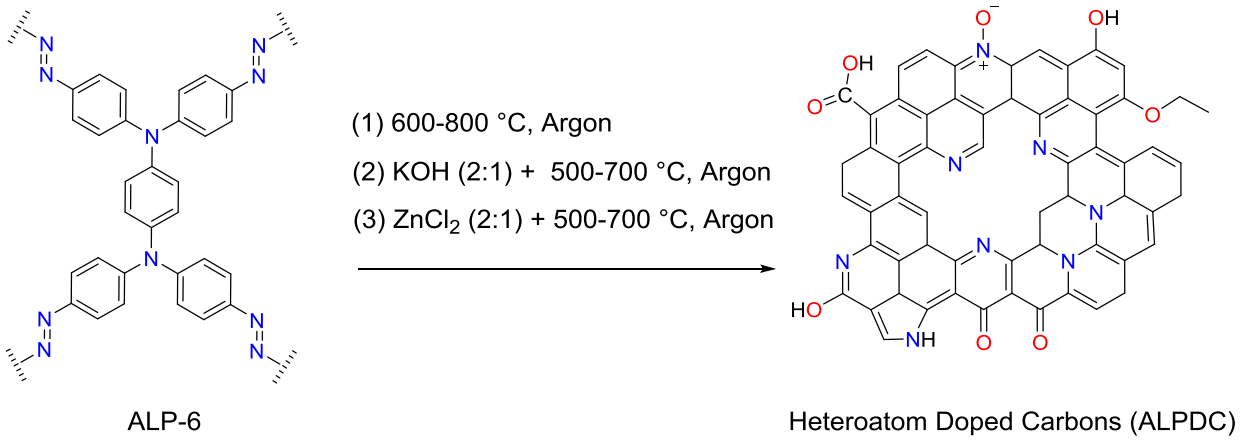

Figure 3.1. Schematic representation of the synthesis of ALP-6 derived carbons.

3.2.2 Measurements and Characterization. Gas adsorption isotherms for N_2 (at 77, 273 and 298 K), CO_2 (at 273 and 298 K) and CH_4 (at 273 and 298 K) were measured on Autosorb-iQ2 volumetric adsorption analyzers (Quantachrome Inc.) using ultrahigh purity grade adsorbates. Before adsorption measurements, each sample was degassed under vacuum for at least 12 h at 200 °C. The specific surface area of the samples was measured using the Brunauer−Emmett−Teller (BET) method. Incremental pore size distributions (PSD) were obtained from adsorption branch of N_2 (at 77 K) isotherms by the QSDFT (Quench Solid Density Functional Theory) method as well as adsorption branch of CO_2 (at 273 K) isotherms by the NLDFT (Non Local Density Functional Theory) method assuming slit-like geometry on carbon material kernel. The volume of micropores (V_{Mic}) was estimated by cumulative pore size distribution curves and corresponding

volume at pore size of 2 nm. As a control, *t*-plot method provided by Quantachrome was also utilized to confirm V_{Mic} obtained by PSD curves. The volume of ultramicropores (V_0) was estimated from CO_2 (273 K) isotherms after adjustment of CO_2 pressure at 273 K. Scanning Electron Microscopy (SEM) images were obtained using Hitachi SU-70 scanning electron microscope. The samples were prepared by dispersing each specimen onto the surface of a sticky carbon attached to a flat aluminum sample holder. Then, the samples were coated with platinum at a pressure of 10^{-5} mbar in a N_2 atmosphere for 60 seconds before SEM imaging. Elemental analyses of carbon, nitrogen, hydrogen, and ash were performed at the Midwest Microlab, LLC. X-ray photoelectron spectroscopy (XPS) analysis was performed on a ThermoFisher ESCALAB 250 spectrometer employing Al Kα (1486.68 eV) X-ray source equipped with a hemispherical analyzer.

3.3 Results and Discussion

3.3.1 Textural Properties. Nitrogen sorption measurements were carried out to investigate the porous nature of ALP-6 derived porous carbons. The BET equation was applied to the N_2 adsorption isotherms to obtain the surface area where the P/P_0 range was chosen by micropore BET assistant software to yield a high R^2 value and a positive line intersect of multi-pint BET fitting (Figure 3.2). To compare the porosity levels, nitrogen isotherms for each class of prepared carbons were stacked along with isotherm of ALP-6 in a separate graph as illustrated in Figures 3.3 (A-C).

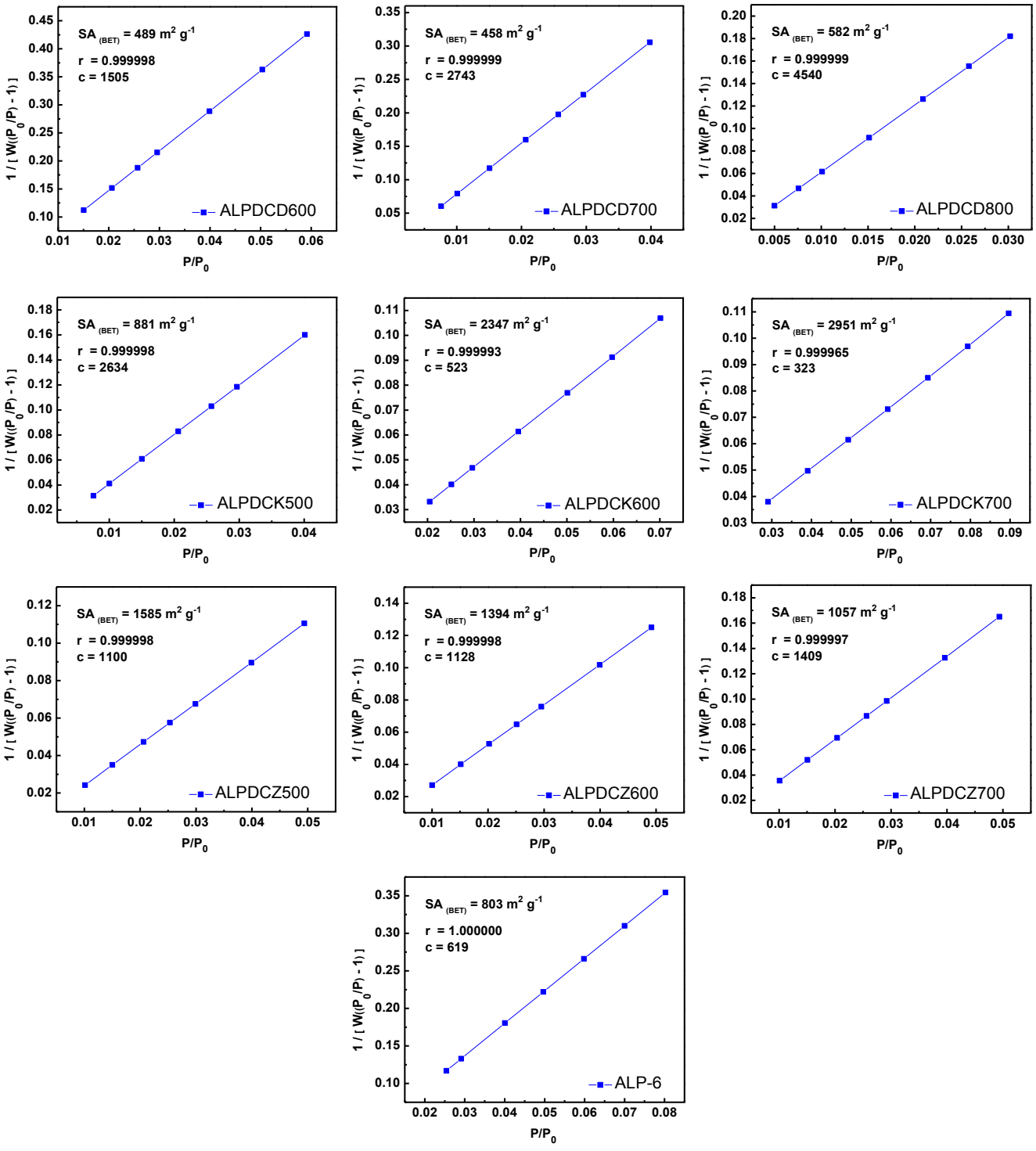

Figure 3.2. BET plots for ALP-6 and its derived carbons calculated from the N_2 adsorption isotherms at 77 K. (W = Weight of gas adsorbed at P/P_0, r = Correlation coefficient, c = C constant).

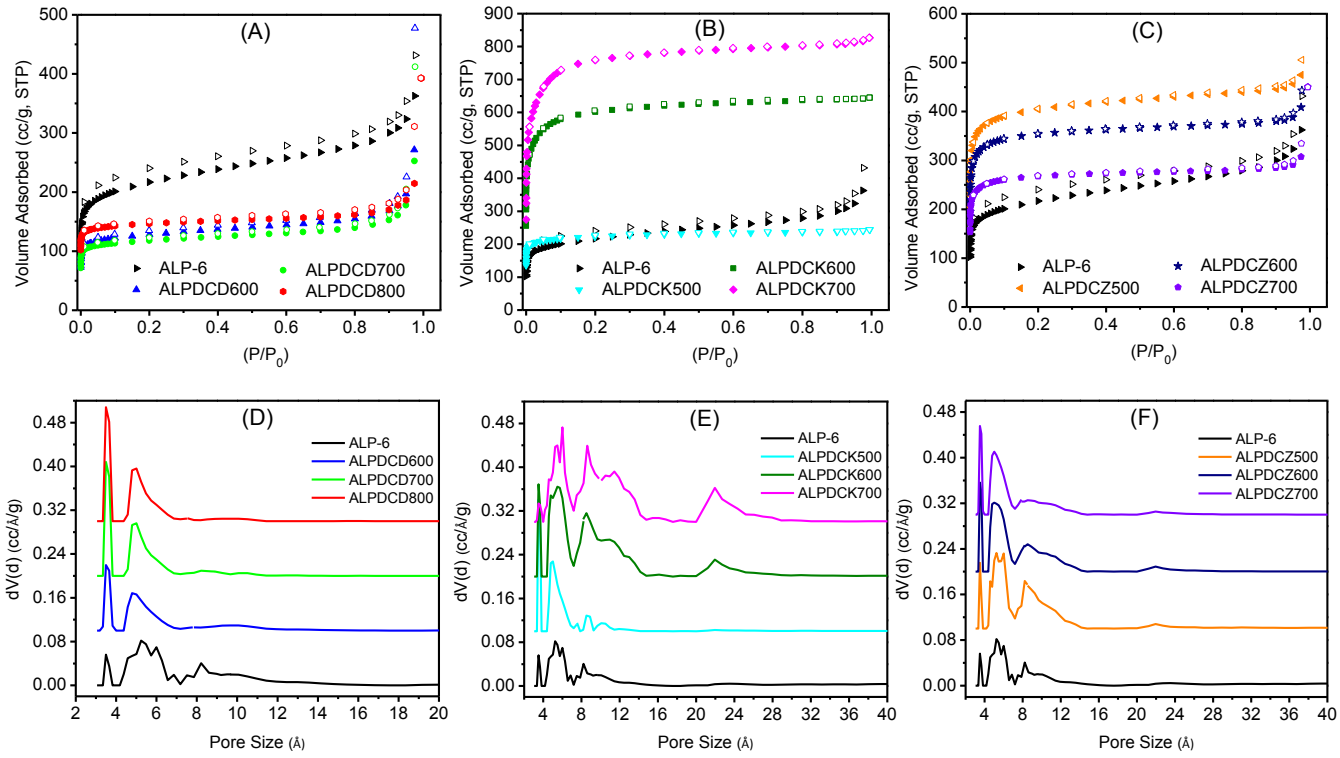

Figure 3.3 (A-C) Nitrogen isotherms at 77 K and (D-F) pore size distributions calculated by DFT method for ALP-6 derived carbons and ALP-6 precursor (All PSD curves are offset vertically in steps of 0.1 for clarity purpose).

Consistent with the most of the porous organic polymers, ALP-6 exhibits type I/IV isotherm with a notable hysteresis loop at P/P_o = 0.2-0.8 that vanishes upon carbonization. According to Figures 3.3 (A-C) direct carbonized samples show lower uptakes with respect to ALP-6, whereas, activated carbons feature enhanced uptakes. The nitrogen adsorption isotherms of all ALP-6 derived carbons can be classified as type I with a sharp uptake at low partial pressure region (P/P_o < 0.01) followed by a plateau for most of the remaining pressure range, which is indicative of microporosity. Compared with the BET surface area of ALP-6 (800 m^2 g^{-1}), the BET

surface areas of ALPDCD600, ALPDCD700 and ALPDCD800 drop to 489, 458 and 582 $m^2 g^{-1}$, respectively. This drop in porosity level is most likely driven by collapse of pores and the lack of activation mechanisms during direct carbonization process. In contrast, the surface areas of KOH activated carbons found to be 881, 2347 and 2952 $m^2 g^{-1}$ for ALPDCK500, ALPDCK600 and ALPDCK700, respectively. The ALPDCK500 sample features almost an identical surface area to the pristine polymer; however, the nature of porosity in these two materials is different. The type I nitrogen isotherm of ALPDCK500 (Figure 3.3 B) as well as the numerical values for micropore and ultramicropore volume (V_{Mic} and V_0 in Table 3.1) clearly indicate that unlike ALP-6 this carbon sample is mainly composed of fine micropores. The significant enhancement of surface area for samples synthesized at higher temperatures (600 and 700 °C) can be correlated to the higher degree of activation achieved by KOH through mechanisms such as etching (by redox reactions), gasification (by evolving gaseous species such as CO and CO_2) and expansion (by metallic potassium) of carbon framework.[15] The use of higher activation temperatures also leads to narrow mesopores formation as evidenced by the broadening of the N_2 isotherms knees at relatively low pressures as well as pore size distribution studies as we discuss below. Similarly, activation of ALP-6 with zinc chloride also led to improved porosity 1585, 1395 and 1057 $m^2 g^{-1}$ for ALPDCZ500, ALPDCZ600 and ALPDCZ700, respectively. It seems that activation by $ZnCl_2$ has the most pronounced effect at 500 °C while increasing the activation temperate to 600 and 700 °C has negative impact on porosity. The mechanism of activation by $ZnCl_2$ differs from that of KOH. While the latter is a strong base, the former is a Lewis acid. In general, KOH activation mechanism is governed by evolution of CO_x or C_xH_y gaseous species due to oxidative environment, whereas, $ZnCl_2$ activation is mainly dictated by dehydration of carbon precursor upon increasing the temperature.[16] $ZnCl_2$ reacts with the precursor after initial dehydration and

inhibits further development in porous structure. As a result, slight degradation of textural properties for carbons activated at temperatures above 500 °C can be realized.[17] Olivares-Marín *et al.* performed a comprehensive study on the $ZnCl_2$ activation parameters (temperature and impregnation ratio) effect on textural properties of prepared carbons using Chery stone as precursor. In a similar trend to our results, they noticed that among five carbons obtained by activation between 400-800 °C, the one prepared at 500 °C presented the highest surface area and micropore volume.[18]

Table 3.1. Textural Properties of ALP-6 Derived Carbons and ALP-6

	Textural properties				
Sample	S_{BET} [a]/ $m^2\ g^{-1}$	V_{Tot} [b]/ $cm^3\ g^{-1}$	V_{Mic} [c] / $cm^3\ g^{-1}$	V_{Mic} [d]/ $cm^3\ g^{-1}$	V_0 [e]/ $cm^3\ g^{-1}$
ALP-6	803	0.50	0.23 (46)	0.23	0.14
ALPDCD600	489	0.31	0.16 (52)	0.16	0.12
ALPDCD700	458	0.28	0.15 (54)	0.15	0.12
ALPDCD800	582	0.29	0.20 (69)	0.20	0.15
ALPDCK500	881	0.37	0.31 (84)	0.32	0.22
ALPDCK600	2347	0.99	0.77 (78)	0.84	0.35
ALPDCK700	2952	1.26	0.90 (71)	1.0	0.30
ALPDCZ500	1585	0.71	0.54 (76)	0.56	0.26
ALPDCZ600	1395	0.60	0.48 (80)	0.50	0.25
ALPDCZ700	1057	0.45	0.37 (82)	0.37	0.21

[a] Calculated in the partial pressure range which gives the best linear fitting. [b] Total pore volume at P/P_o = 0.95. [c] Determined by cumulative pore volume and maxima of the PSD assuming slit-shaped pores and QSDFT model; the values in parentheses are the percentage of micropores volume relative to total pore volume. [d] Evaluated by the *t*-plot method. [e] Pore volume of ultramicropores (<0.7 nm) obtained from CO_2 adsorption data at 273 K.

Pore size distribution (PSD) of ALP-6 and its derived carbons were thoroughly investigated by N_2 (77 K) isotherms and quenched solid density functional theory (QSDFT) model which is widely employed for carbons with heterogeneous pore walls.[19] Moreover, CO_2 isotherms (273 K) and non-local density functional theory (NLDFT) model were employed to assess the distribution of fine micropores where nitrogen molecules diffusion is limited by extremely slow and time consuming kinetic. In other words, higher kinetic energy of the CO_2 molecules at 273 K enables them to penetrate and probe narrower pores than N_2 at 77 K or Ar at 87 K are able to perform. That is to say, the CO_2 isotherm presents more reliable data for distribution of pores below 0.7 while N_2 is more beneficial to evaluate the distribution of larger micropores, mesopores and any possible macropores. Consequently, the overall PSD spectra are achieved by information gathered from both N_2 and CO_2 isotherms and results are depicted in Figure 3.4. In a similar manner to N_2 isotherms, PSD curves for each class of ALP-6 derived carbons together with the ALP-6 parent precursor are stacked and demonstrated in Figures 3.3 D-F.

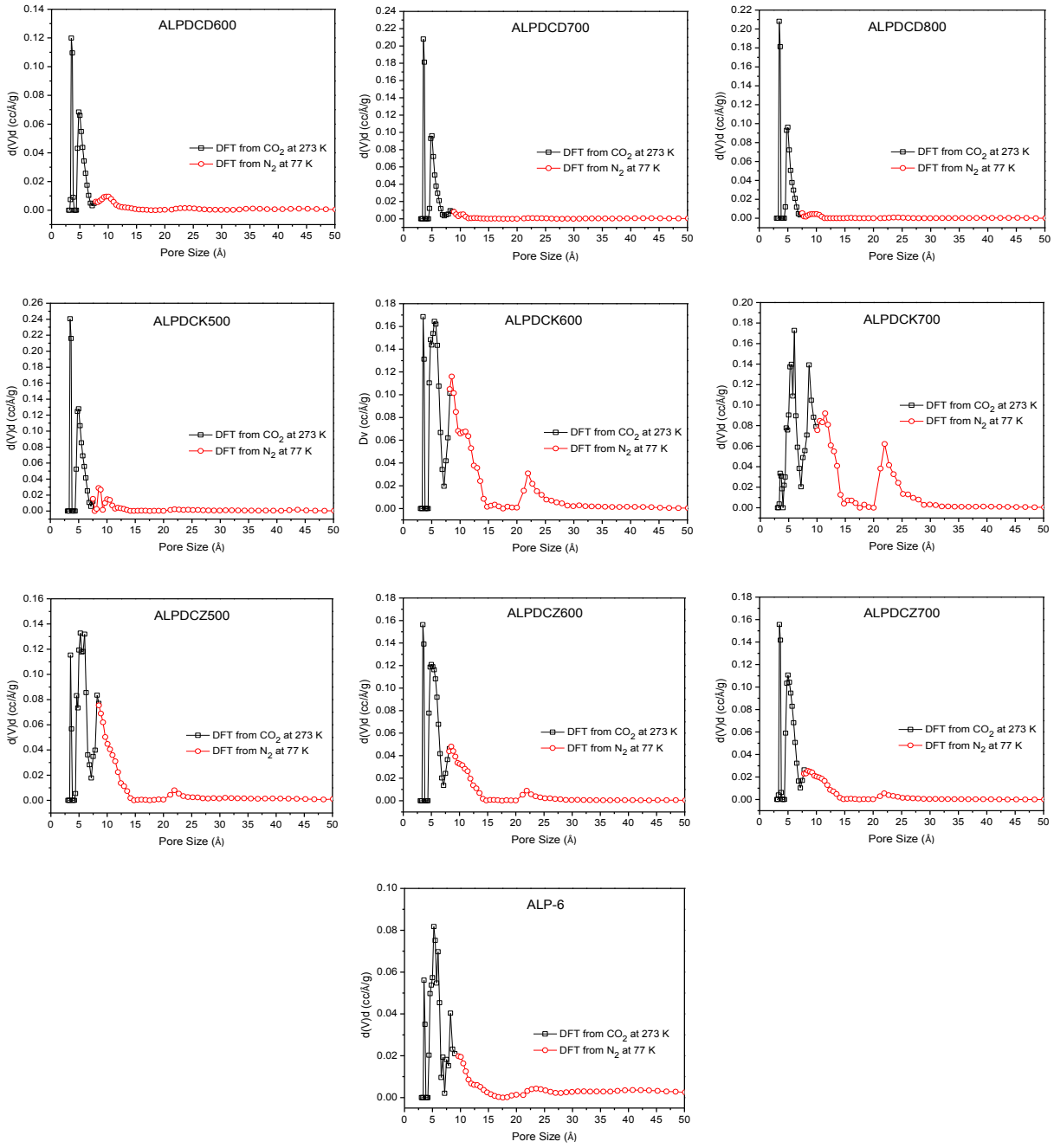

Figure 3.4. Pore size distribution curves for ALP-6 and its derived carbons. Red circles obtained by applying QSDFT model on adsorption branch of N_2 (77 K) isotherms assuming slit shape pores and black squares obtained by applying NLDFT model on adsorption branch of CO_2 (273 K) isotherms assuming slit shape pores.

The pore size distribution of ALPDCDs is predominantly centered around 5 Å in contrast to the randomly distributed pores of ALP-6 all across the micropore size range (< 2 nm). The PSD curves of KOH activated carbons (Figure 3.3 E) indicate that their porosity is made up mostly of micropores. The pore size of low temperature activated ALPDCK500 centers around 5 and 9 Å. Increasing the activation temperature to 600 and 700 °C not only shifts the dominant peaks to slightly higher values, but also adds a small fraction of narrow mesoporosity which distributed around 23-24 Å to the system. The pores of $ZnCl_2$ activated carbons were also realized to distribute around 5 and 9 Å (Figure 3.3 F). A slight reduction in dominant pore size as well as appearance of narrow mesopores around 22 Å were observed upon increasing the activation temperature from 500 to 700 °C.

The pore volume of microporous carbons was extensively studied due to its significance in gas adsorption properties. Accordingly, the total pore volume (V_{Tot}, at $P/P_0 = 0.95$), the micropore volume (V_{Mic}, calculated by DFT and *t*-plot), the ratio of micro to total pore volume (V_{Mic}/V_{Tot}, as a degree of microporosity) and the volume of ultramicropores (V_0, pores below 7 Å) were calculated and summarized in Table 3.1. The total pore volume of merely carbonized samples decreases with respect to ALP-6. However, micropore volume, ultramicropore volume and percentage of microporosity increase by increasing the carbonization temperature and reach to the highest values of 0.20 $cm^3\ g^{-1}$, 0.15 $cm^3\ g^{-1}$ and 69% for ALPDCD800, respectively. Among KOH activated carbons, the ALPDCK500 exhibits lower total pore volume of 0.37 $cm^3\ g^{-1}$ comparing 0.50 $cm^3\ g^{-1}$ of ALP-6 but enhanced micropore and ultramicropore volume. The ALPDCK700 exhibits the highest total and micropore volume of 1.26 $cm^3\ g^{-1}$ and 0.90 $cm^3\ g^{-1}$, respectively, among all studied carbons. Importantly, ALPDCK600 possesses the highest volume of ultramicropores (0.35 $cm^3\ g^{-1}$), which benefits small gas adsorption performance. The degree of

microporosity dropped from 84 to 71% by increasing the activation temperature from 500 to 700 °C due to the mesopores formation. Activation by $ZnCl_2$ led to enhancement in all types of pore volumes compared to ALP-6. As discussed above for surface area studies, the most effective activation mechanism at 500 °C results in the highest values for total, micro and ultramicro pore volume up to 0.71, 0.54 and 0.26 $cm^3\ g^{-1}$, respectively. However, unlike KOH-activation the lack of effective pore formation mechanism at elevated temperatures (600 and 700 °C) results in narrower pores. Therefore, the microporosity level shows slight improvement up to 80 and 82% for ALPDZ600 and ALPDCZ700, respectively.

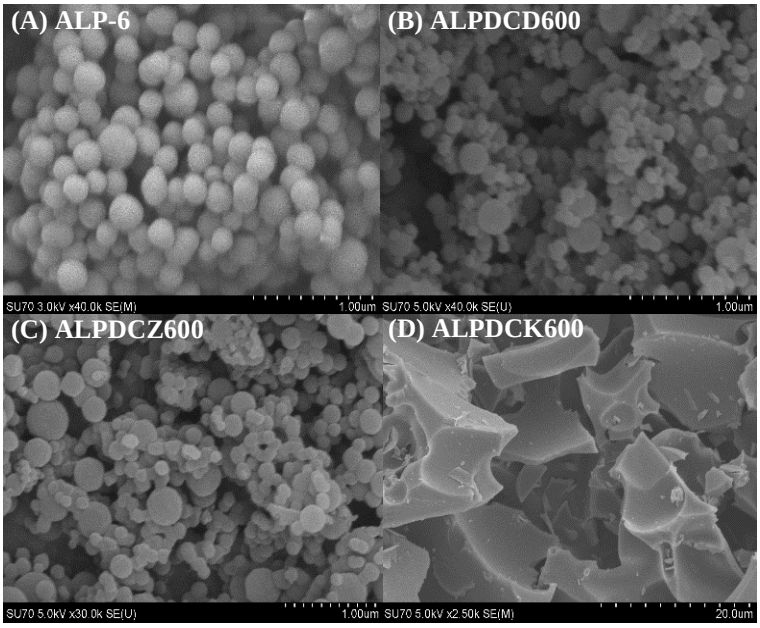

Figure 3.5. Scanning electron microscopy (SEM) images of (A) ALP-6, (B) ALPDCD600, (C) ALPDCK600 and (D) ALPDCZ600.

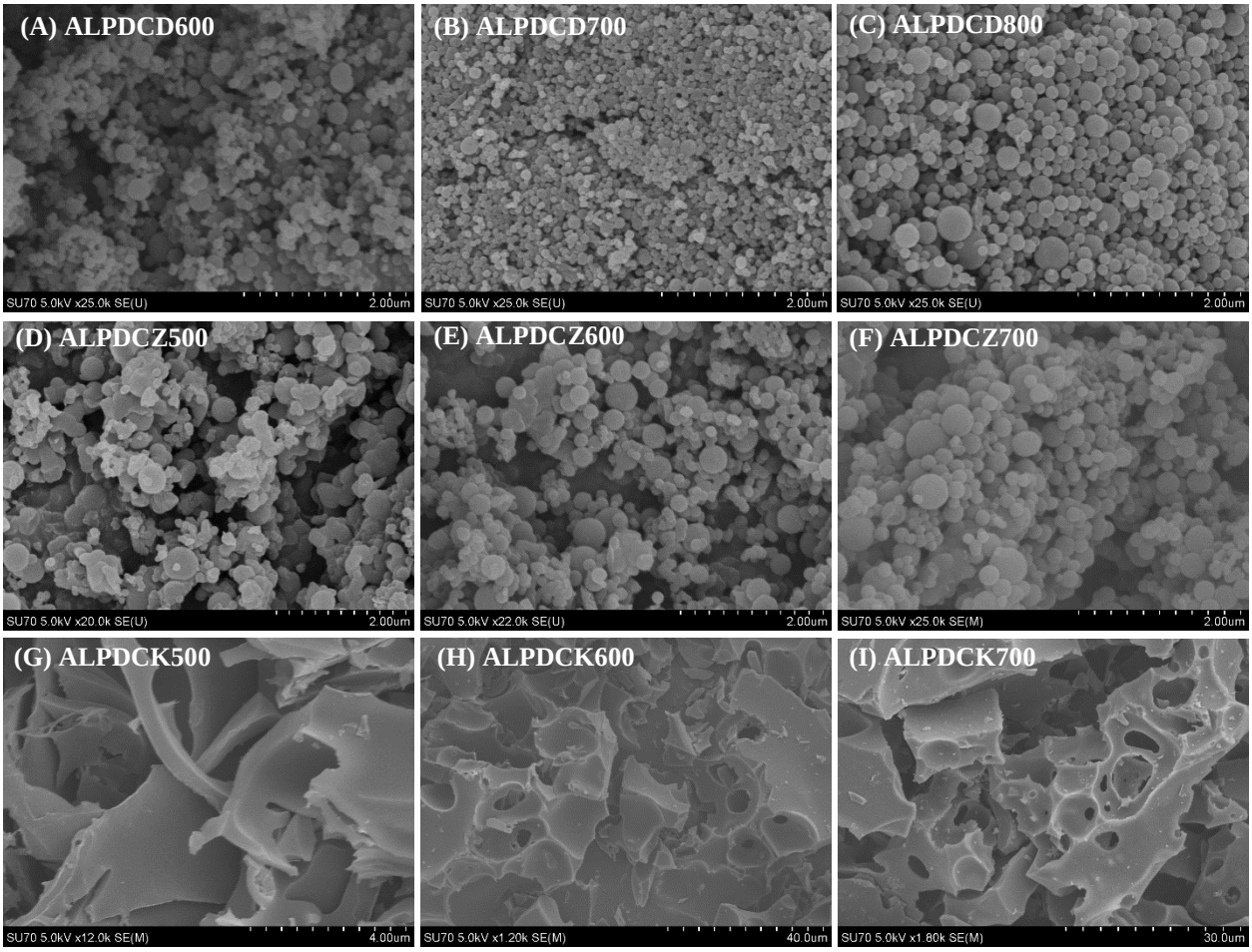

Figure 3.6. Additional SEM images of ALP-6 derived carbons. (A-C) ALPDCDs (D-F) ALPDCZs (G-I) ALPDCKs.

3.3.2 Microstructure and Composition of Carbons. The SEM images of ALP-6 together with one representative sample of each series of carbons (synthesized at 600 °C) are presented in Figure 3.5 for comparison. The ALP-6 precursor displays a spherical morphology. The direct carbonized samples retain the original spherical shape with slight shrinkage in size compared to parent ALP-6. The $ZnCl_2$ activated carbons display somewhat diverse microstructure. The most

effective activation at 500 °C leads to destruction of the most of the primary spheres existed in ALP-6 and converts them to smaller and more irregular-shaped phases. Interestingly, activation at 600 and 700 °C seems to be more effective in maintaining original spherical morphology as ALPDCZ700 is just composed of spherical morphology with reduced particle size (Figures 3.6 D-F). In contrast to ALPDCD and ALPDCZ series, a dramatic morphological change was observed for KOH activated carbons. The activation by KOH results in total destruction of the original spherical morphology and formation of massive irregular-shaped structures at all temperatures. (Figure 3.5 D and Figure 3.6 G-I).

Table 3.2. Elemental Analysis and XPS Data for ALP-6 Derived Carbons and ALP-6

	CHN Elemental Analysis				XPS		
Sample	C wt%	H wt%	N wt%	Ash wt%	C wt%	O wt%	N wt%
ALP-6	69.5	4.2	14.7	-	76.7	10.8	12.5
ALPDCD600	78.7	2.7	14.3	0.5	83.5	4.7	11.8
ALPDCD700	80.3	1.7	12.6	1.2	84.4	6.2	9.4
ALPDCD800	80.0	1.0	8.5	2.5	84.6	8	7.4
ALPDCK500	61.5	2.3	12.1	4.5	72.3	17.9	9.8
ALPDCK600	68.7	1.6	9.3	1.9	74.3	17.2	8.5
ALPDCK700	73.2	1.0	4.7	1.9	79	16.1	4.9
ALPDCZ500	60.0	1.9	11.1	20.2	77.3	11.6	11.2
ALPDCZ600	71.7	1.7	12.6	4.3	79	10.2	10.8
ALPDCZ700	71.4	1.4	13.7	2.5	77.4	11.2	11.4

The chemical composition was evaluated by elemental analysis (EA). The CHN elemental composition (carbon, hydrogen and nitrogen wt%) as well as remaining ash content (wt%) of the studied carbons and parent polymer are provided in Table 3.2. It is clear that both carbonization and activating led to diminution of nitrogen level with respect to ALP-6. The results showed that the nitrogen content in ALPDCD and ALPDCK classes of carbons decreases by increasing the temperature whereas in ALPDCZ series it slightly increases. The latter can be justified by the optimum $ZnCl_2$ activation at 500 °C as it was explained above. Namely, three samples of ALPDCD600, ALPDCK500 and ALPDCZ700 retained the highest nitrogen level (wt %) of 14.3, 12.1 and 13.7, respectively.

To study the oxygen and nitrogen species on the pore walls of ALPDCs, X-ray photoelectron spectroscopy (XPS) was performed. Survey spectra of all ALP-derived carbons as well as ALP-6 distinctly feature three dominant peaks centered at 285.1, 399.9 and 532.7 eV corresponding to the presence of C 1s, N 1s and O 1s, respectively (Figure 3.7). The absence of any other peaks in the full survey pattern clearly confirms the removal of metal traces during acid washing process. The surface concentration of C, N and O are calculated from the corresponding peak areas of XPS spectra and results are summarized in Table 3.2. The percentages of carbon and nitrogen obtained by XPS are in a good agreement with values tested by elemental analysis. It should be taken into account that elemental analysis is carried out in the bulk of carbon material but XPS is a surface sensitive method and values for C, N and O content usually are gathered from the surface of samples. This reveals that the amounts of the surface nitrogen groups are slightly lower than the ones in the bulk materials. Reversely, the relatively higher amounts of carbon and oxygen reported by XPS can be ascribed to the possible adsorption of carbon dioxide and water on the surface of porous carbons. Moreover, the consistent results of XPS and EA reflects the

uniform distribution of heteroatoms into the porous carbon framework. The nature of oxygen and nitrogen functionalities was further investigated by deconvolution of their 1s core level spectra. In general, four nitrogen species as N-6 (pyridinic), N-5 (pyrrolic and/or pyridonic), N-Q (quaternary) and N-X (oxidized) as well as three different components of oxygen groups as O-I (quinone), O-II (phenol and/or ether) and O-III (carboxylic groups and/or water) are mostly recognizable in porous carbons.[20-21] A schematic representation of all possible nitrogen and oxygen species for a typical porous carbons and ALP-6 molecule along with their binding energy has been depicted in Figure 3.8. High resolution deconvoluted N 1s and O 1s spectra of the ALP-6 derived carbons and the ALP-6 are depicted in Figure 3.9 and Figure 3.10, respectively. Clearly, two different types of nitrogen (Amine and Azo) can be distinguished by molecular formula of ALP-6 which are not correlated to any four species found in N-functionalized carbons. Surprisingly, after deconvolution and peak fitting just one single peak at 399.8 eV was recognized (denoted as N-A, hereafter). Interestingly, we found that Amine and Azo nitrogen groups have almost identical N 1s binding energies which well explains their overlapping.[22] It is expected that pristine N-A nitrogen species evolve to N-5/N-6/N-Q/N-X surface groups in the course of heat treatment and activation. Consequently, the ALPDCD class possess all four types of nitrogen and three oxygen surface groups. They also contain the lowest oxygen content, which might be attributed to the adsorption of water, O_2 and CO_2 from ambient. By contrast, the ALPDCK and ALPDCZ classes are lacking quaternary nitrogen (N-Q) and pyrrolic/pyridonic nitrogen (N-5) is dominating. Notably, the chemical activation awards higher amounts of oxygen surface group to the resultant carbons owing to the oxidative and dehydrating effects of KOH and $ZnCl_2$, respectively. It also has been observed that nitrogen functional groups oxidize easily[17, 23] which further supports the presence of N-X type of nitrogen in all studied carbons. For the sake of comparison, nitrogen species of one

representative sample of each class of carbons (ALPDCD600, ALPDCK600, ALPDCZ600) and ALP-6 are also shown in Figure 3.11 together.

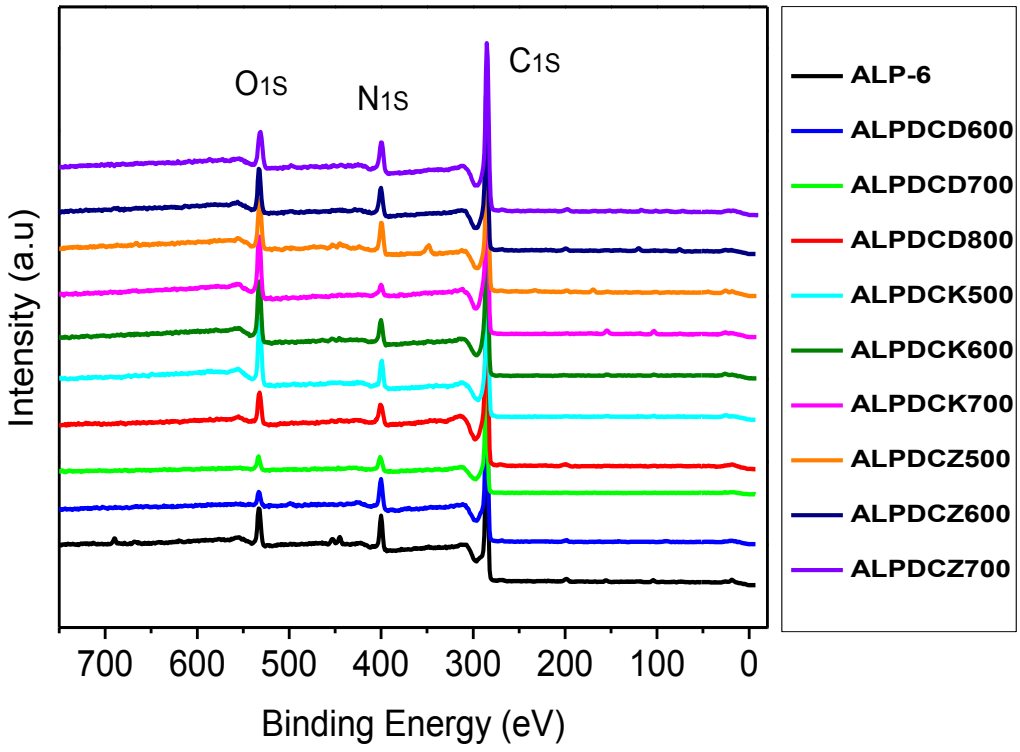

Figure 3.7. X-ray photoelectron spectroscopy (XPS) survey spectra of ALP-6 and its derived carbons.

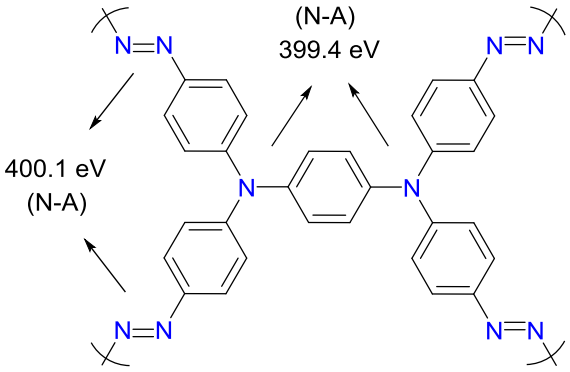

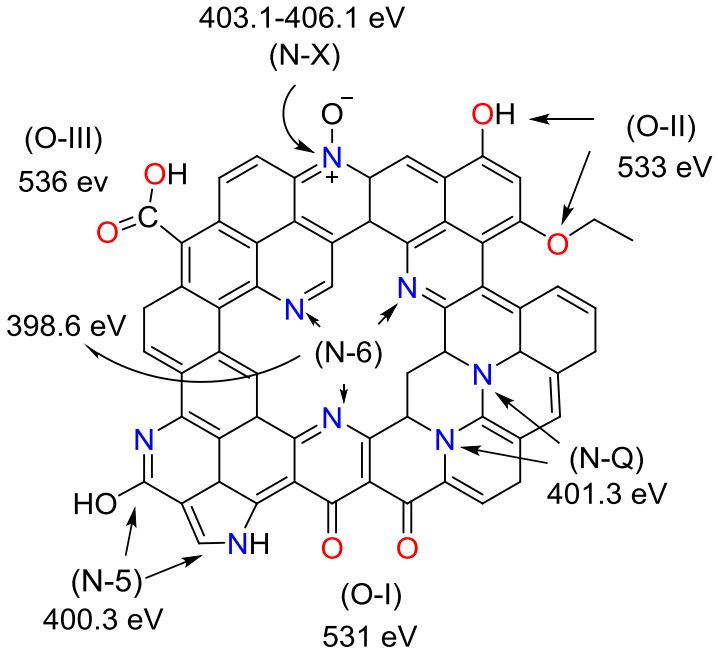

Figure 3.8. The schematic representation of nitrogen species in (A) ALP-6 and (B) nitrogen/oxygen species in a hypothetical porous carbon.

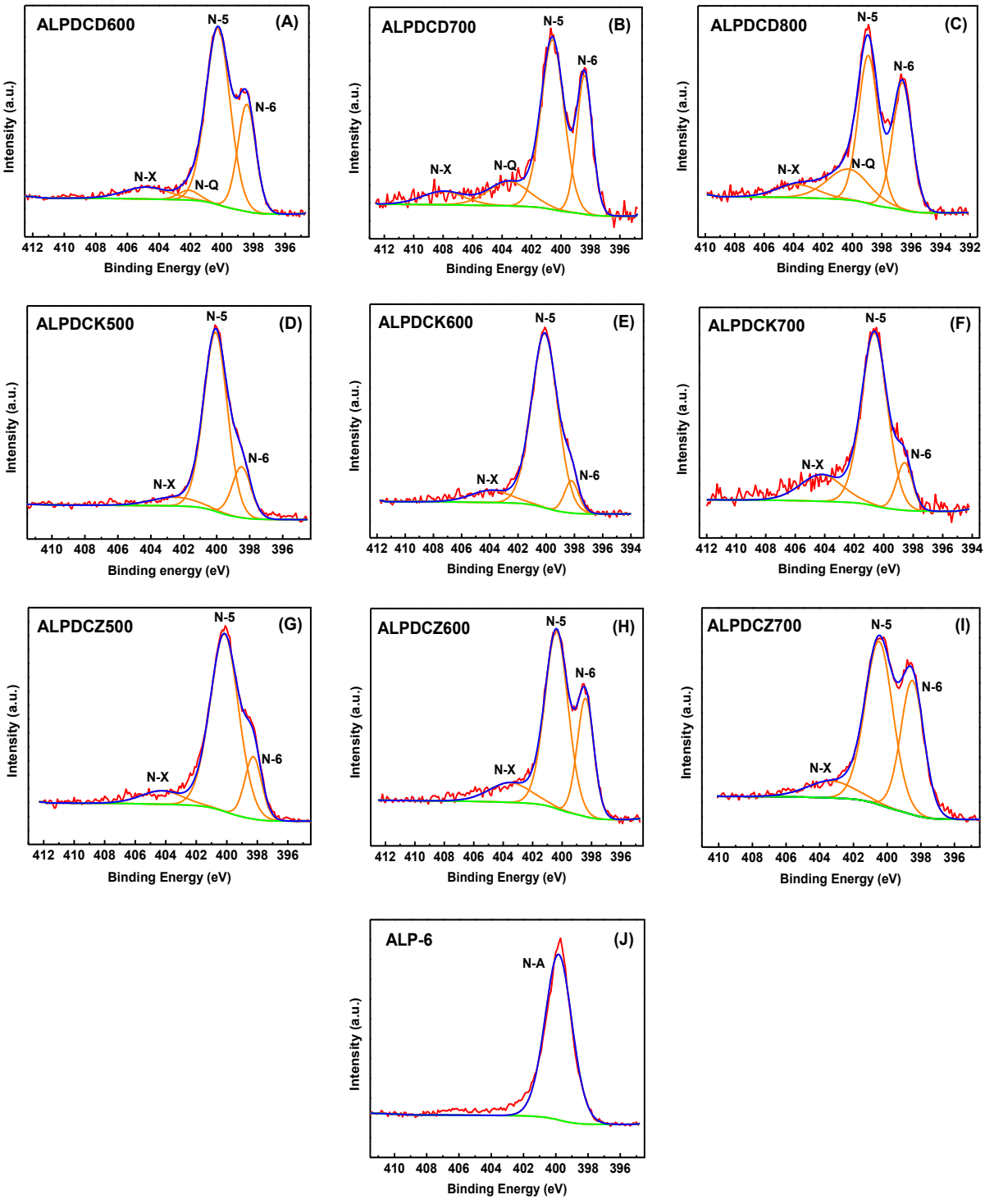

Figure 3.9. High resolution deconvoluted N 1s spectra of (A-C) ALPDCDs, (D-F) ALPDCKs, (G-I) ALPDCZs (G-I) and (J) ALP-6.

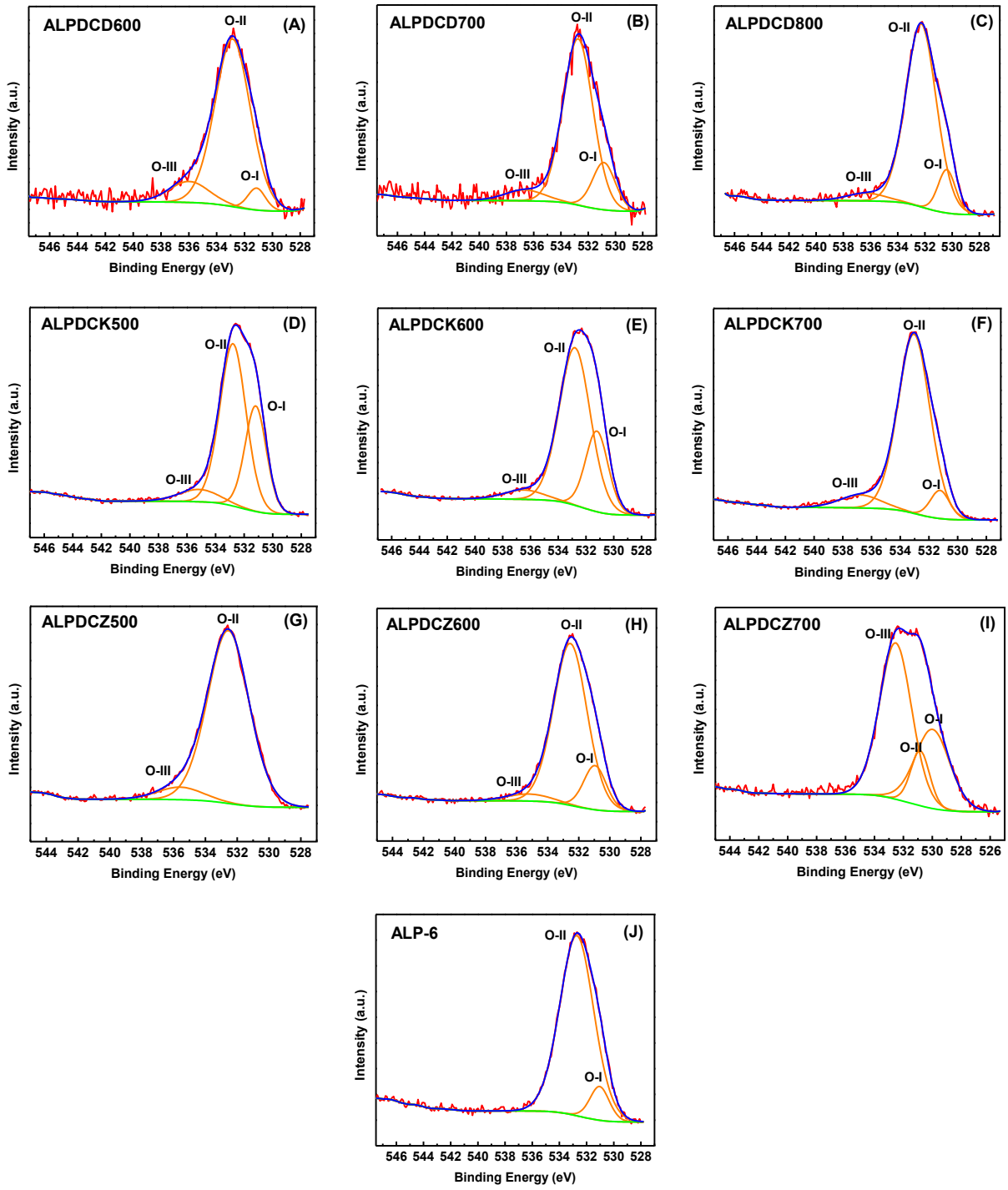

Figure 3.10. High resolution deconvoluted O 1s spectra of (A-C) ALPDCDs, (D-F) ALPDCKs, (G-I) ALPDCZs and (J) ALP-6.

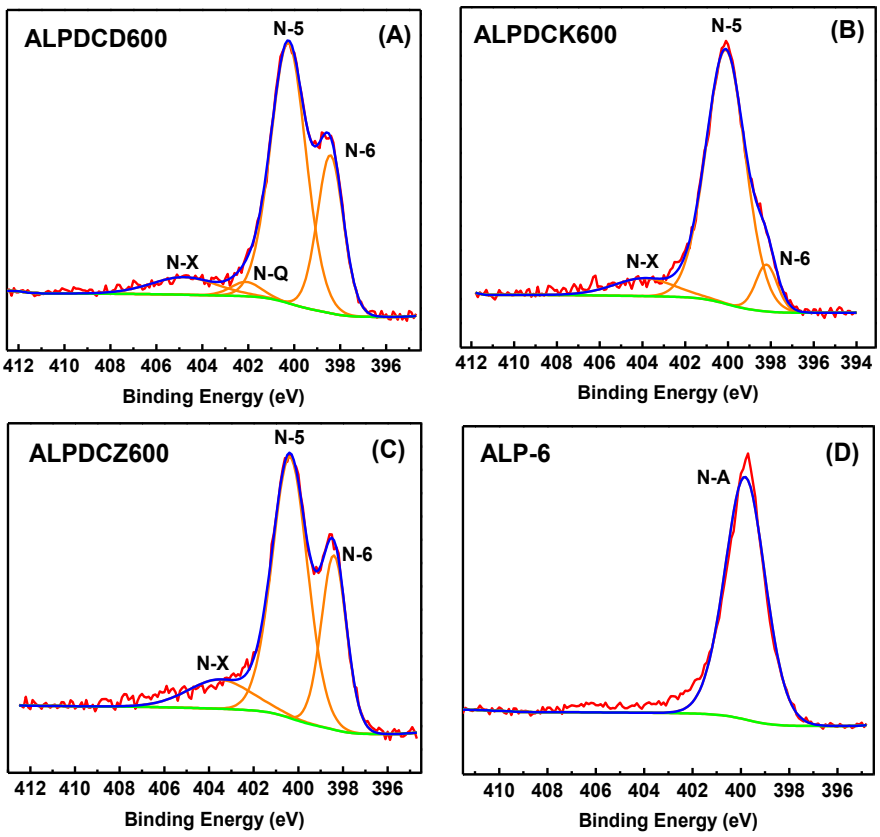

Figure 3.11. High resolution deconvoluted N 1s spectra for (A) ALPDCD600, (B) ALPDCK600, (C) ALPDCZ600 and (D) ALP-6.

3.3.3 CO_2 and CH_4 Capture Performance. Motivated by the large portion of microporosity and high level of basic heteroatoms (O and N) generated during carbonization/activation process, the CO_2 capture performance of ALP-6 derived carbons were explored by collecting their isotherms up to 1 bar. A comparative analysis of CO_2 adsorption isotherms measured at 273 and 298 K for each class of ALP-6 derived carbons as well as parent polymer is illustrated in Figures 3.12 A-F. As shown in Figure 3.12 A, at 273 K the low temperature carbonized samples at 600 and 700 °C exhibit slightly lower CO_2 uptake at 1 bar

compared to ALP-6 while ALPDCD800 features slight improvement in final uptake. As evidenced by Figure 3.12 D, at 298 K ALPDC800 features noticeable improvement in uptake while ALPDCD600 and ALPDCD700 show almost similar uptake to the parent molecule. All three KOH activated carbons show substantial enhancement in final uptake owing to the generation of micropores and evolution of basic nitrogen and oxygen surface groups during chemical activation. However, the ALPDCK500 with the highest microporosity and heteroatom level presents a lower rate of increase in uptake at pressures higher than 0.4 bar. By contrast, ALPDCK600 and ALPDCK700 demonstrate steady rise in CO_2 uptake for the entire pressure range thanks to the existence of larger micropores and narrow mesopores despite their lower nitrogen content (Figure 3.12 B and Figure 3.12 E). At 1 bar the ALPDCK600 features the highest CO_2 uptake values of 8.3 and 5.2 mmol g^{-1} at 273 and 298 K, respectively, which are comparable to the highest heteroatom doped microporous carbon reported to date.[5, 10, 24-27] Similarly, three $ZnCl_2$ activated carbons show superior adsorption capacity at 1 bar with respect to ALP-6 (Figure 3.12 C and Figure 3.12 F). The highest CO_2 uptakes, 6.2 mmol g^{-1} and 3.9 mmol g^{-1} were achieved on ALPDCZ500 at 273 and 298 K, respectively.

In order to investigate the binding affinity of ALP-derived carbons for CO_2, isosteric heats of adsorption (Q_{st}) were calculated by the virial method using CO_2 adsorption isotherms collected at 273 and 298 K.[28] The plots of Q_{st} (kJ mol^{-1}) as a function of CO_2 uptake (mmol g^{-1}) are shown in Figures 3.12 G-I and Q_{st} values at zero coverage are provided in Table 3.3. The polymer precursor features the intermediate isosteric heat of adsorption of 28.5 kJ mol^{-1} at zero loading. After direct carbonization the Q_{st} values significantly increased to 34.7-36.3 kJ mol^{-1}. This dramatic improvement in Q_{st} can be explained by collapsing of the initial microporosity in ALP-6 and providing much smaller pores, which are more beneficial for interaction with CO_2 molecules.

The Q_{st} values of 37.2, 32.0 and 25.4 kJ mol^{-1} were obtained for samples which are KOH activated at 500, 600 and 700 °C, respectively. The decreasing trend with relatively large steps in Q_{st} of ALPDCKs can be rationalized by noticeable loss of the heteroatom content and pore widening upon increasing the temperature. Considering the fact that $ZnCl_2$ activated carbons possess almost identical amounts of heteroatom, the Q_{st} values are just controlled by the pore size altercation. Both ALPDCZ600 and ALPDZ700 samples show the highest Q_{st} values of 34 kJ mol^{-1} evidently because of higher percentage of micropores.

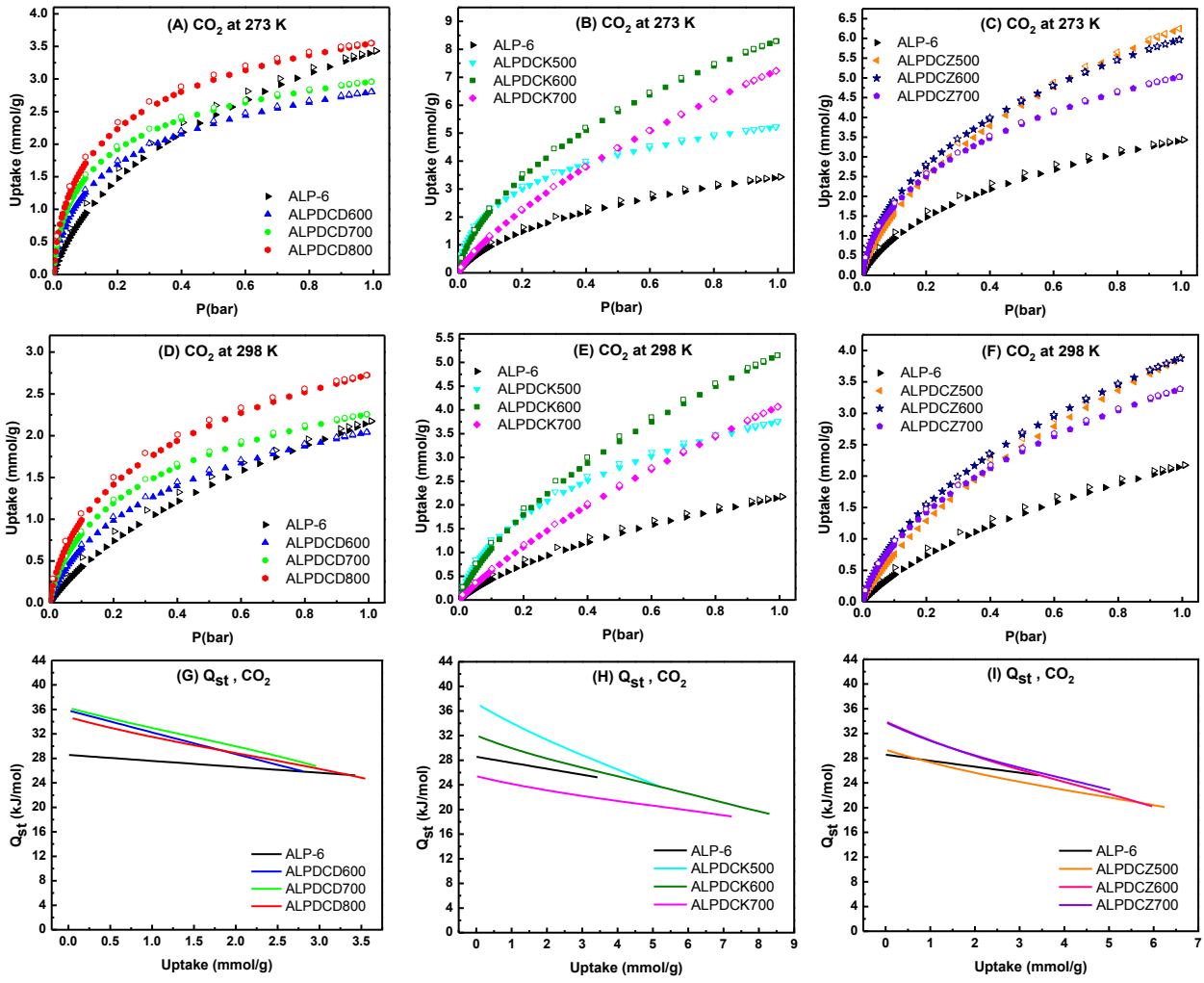

Figure 3.12 CO_2 adsorption isotherms at (A-C) 273 K and (D-F) 298 K, and (G-I) CO_2 isosteric heats of adsorption for ALP-6 derived carbons and ALP-6.

Table 3.3. Gas Uptakes, Isosteric Heats of Adsorption, and Selectivity (CO_2/N_2 and CO_2/CH_4) ALP-6 Derived Carbons and ALP-6 [a]

	CO_2					CH_4			Selectivity	
	0.15 bar		1.0 bar			1.0 bar				
Sample	273 K	298 K	273 K	298 K	Q_{st}	273 K	298 K	Q_{st}	CO_2/N_2	CO_2/CH_4
ALP-6	1.2	0.6	3.4	2.2	28.6	1.0	0.60	19.0	45 (48)	10 (7)
ALPDCD600	1.5	0.8	2.8	2.0	35.8	1.2	0.7	25.2	89 (54)	12 (8)
ALPDCD700	1.7	1.0	3.0	2.3	36.3	1.4	1.0	24.8	79 (54)	9 (8)
ALPDCD800	2.0	1.2	3.5	2.7	34.7	1.7	1.2	24.3	64 (42)	9 (7)
ALPDCK500	2.7	1.5	5.2	3.8	37.2	1.7	1.1	22.5	115 (62)	18 (11)
ALPDCK600	2.9	1.5	8.3	5.2	32.0	2.4	1.4	20.3	62 (36)	13 (8)
ALPDCK700	1.8	0.9	7.2	4.1	25.4	2.4	1.5	18.2	22 (14)	5 (4)
ALPDCZ500	2.1	1.0	6.2	3.9	29.4	1.9	1.1	21.1	47 (27)	10 (6)
ALPDCZ600	2.4	1.3	6.0	3.9	34.0	2.0	1.2	21.2	70 (41)	12 (9)
ALPDCZ700	2.2	1.2	5.0	3.4	33.8	1.8	1.1	22.2	74 (45)	13 (9)

[a] Gas uptake in mmol g^{-1}, isosteric heats of adsorption (Q_{st}) in kJ mol^{-1} and selectivity mol mol^{-1} at 273 K (298 K)

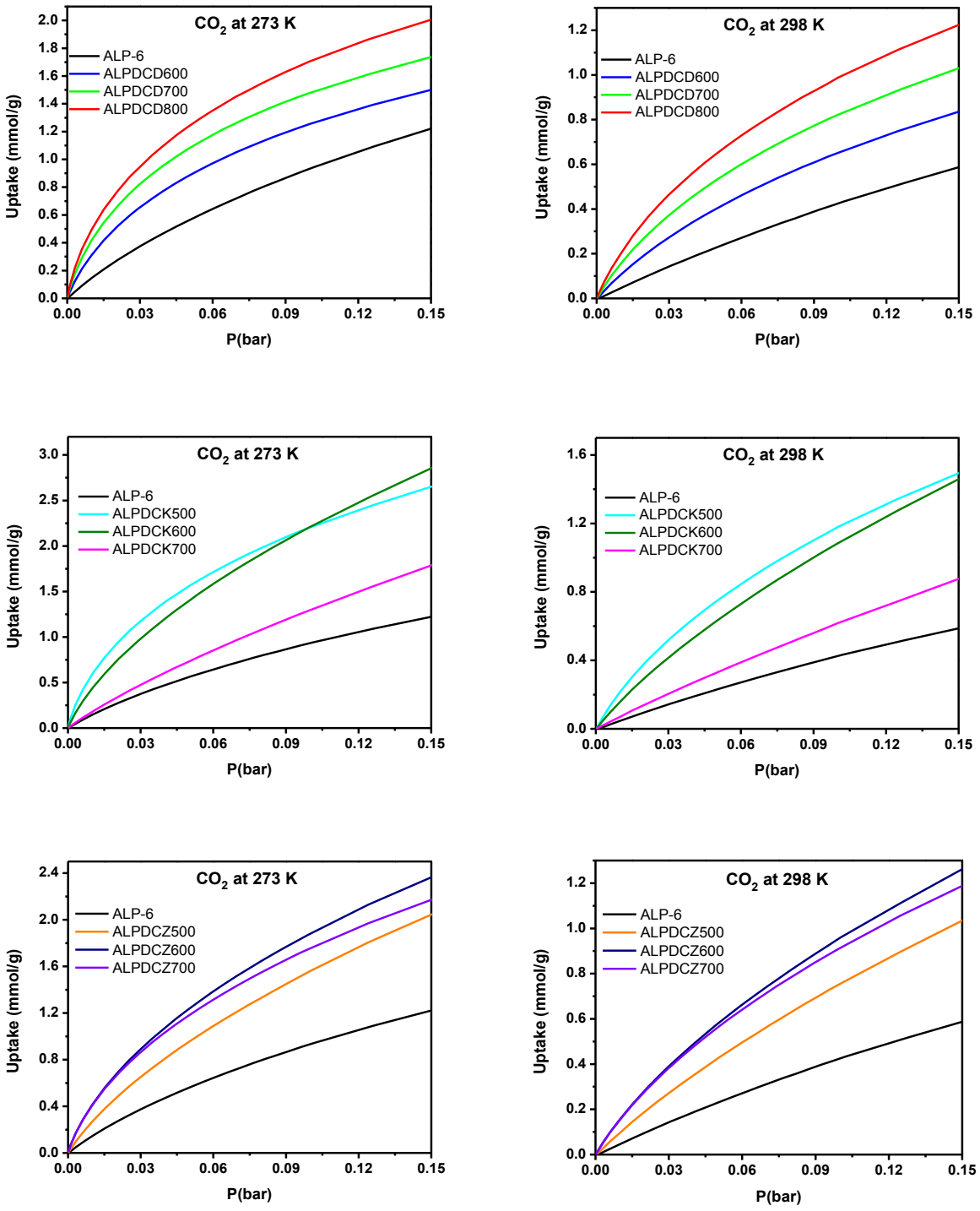

Figure 3.13. Low pressure (<0.15 bar) CO_2 capture capacity for ALP-6 derived carbons and ALP-6 at 273 K and 298 K.

To have a more accurate assessment about merit of our ALP-6 derived carbons as sorbents for the practical CO_2 capture and separation, their CO_2 adsorption behavior should be studied at low pressure region of their isotherms which corresponds to CO_2 pressure in flue gas condition (3-15 % by volume).[29] Thus, low pressure uptake isotherms of each class of ALP-6 derived carbons as well as ALP-6 precursor at 273 and 298 K are presented in Figure 3.13. All studied carbon materials show improved CO_2 capture at 0.15 bar which further highlights the effectiveness of our carbonization and activation strategies. Namely, ALPDCD800, ALPDCK500 and ALPDCZ600 show substantial CO_2 uptake of 1.2, 1.5 and 1.3 mmol g^{-1} at 298 K / 0.15 bar, respectively, featuring a minimum of two times improvement compared to 0.6 mmol g^{-1} value for ALP-6 precursor (Figure 3.14). This result is coherent with Q_{st} observations and the fact that enhanced CO_2 uptake at low pressure is mostly governed by synergistic effect of high fraction of ultramicropores (V_0 in Table 3.1) and basic heteroatoms on the pore walls. The former provide stronger adsorption potential for confinement of the CO_2 molecule (kinetic size 3.3 Å)[30] while the latter introduce high charge density (N and O sites) to the carbon network and favor binding to polarizable acidic CO_2 through hydrogen bonding and/or Lewis acid-base interactions.[31-34]

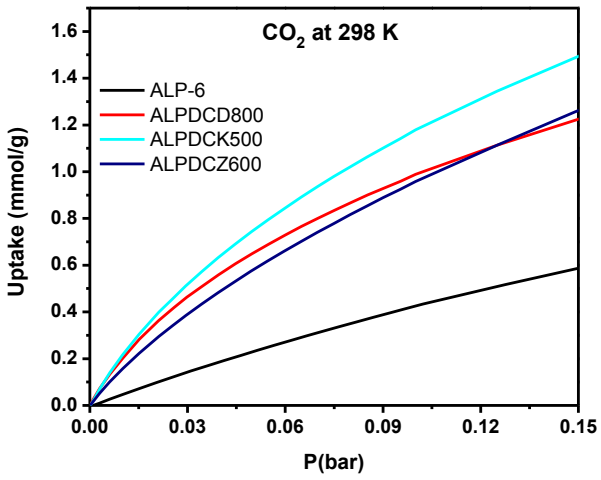

Figure 3.14. Low-pressure CO_2 comparison of selected ALPDCs and ALP-6 at 298 K.

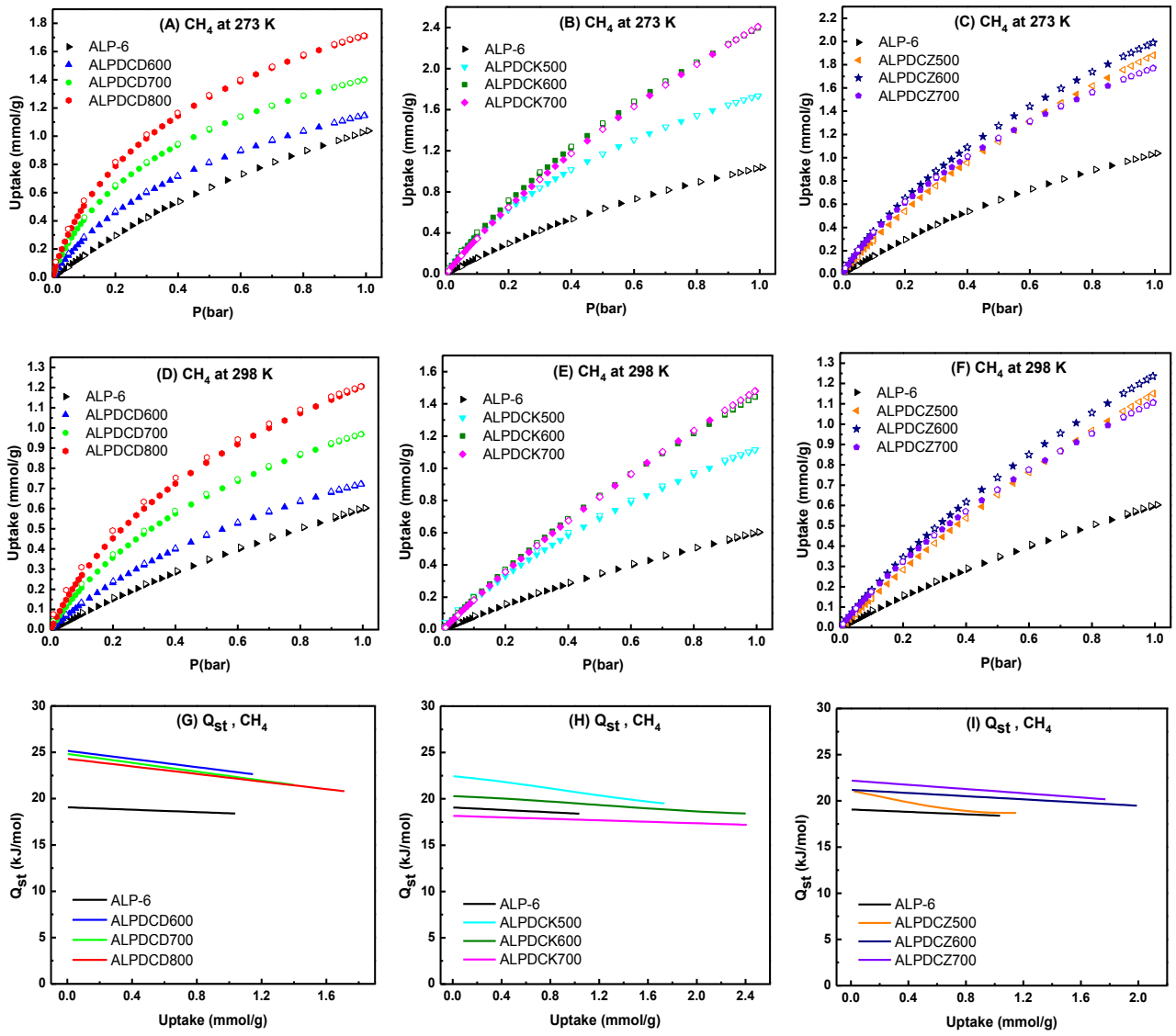

Figure 3.15. CH_4 adsorption isotherms at (A-C) 273 K and (D-F) 298 K, and (G-I) CH_4 isosteric heat of adsorption for ALP-6 derived carbons and ALP-6.

We also investigated the methane adsorption at 273 and 298 K and low pressure for gas separation studies. The results are displayed in Figures 3.15 (A-F) and summarized in Table 3.3. All ALP-6 derived carbons exhibit superior methane adsorption performance for the entire pressure range in comparison with the polymer precursor. The role of basic heteroatom can be

ruled out due to the very low polarizability of methane (26×10^{-25} cm^3).[35] Therefore, the improvement of methane uptake can be solely correlated with modified textural properties after carbonization/activation. A closer observation of methane isotherms for three classes of carbons reveals that direct carbonized samples show higher uptake at low pressures (up to 0.2 bar) while ALPDCZ and ALPDCK series exhibit greater uptake at higher pressures (0.2-1 bar). Moreover, none of the studied carbons reaches to saturation uptake at 1 bar pressure range suggesting a higher CH_4 capacity could be achieved by increasing the pressure above 1 bar. From the last two statements, it can be concluded that methane uptake at very low pressures is governed by narrow pores. As the pore size increases, the higher amount of methane will also be adsorbed at higher pressure. The measured methane heats of adsorption (Figures 3.15 G-I and Table 3.3) further validate previously explained adsorption trend where direct carbonized samples presented extremely high heat of adsorption ranging 24.3-25.3 kJ mol^{-1} at zero coverage. This high amount of energy compared to 19 kJ mol^{-1} for ALP-6 can be justified by increasing the number of very small pores generated by shrinkage of the primary porosity.

3.3.4. Selective Adsorption of CO_2 over N_2 and CH_4. To this end, we showed that transformation of azo-linked polymer to heteroatom doped carbons resulted in improvement of CO_2 adsorption capacity. However, for the practical application such as separation of CO_2 from flue gas, landfill gas and natural gas, selective adsorption of CO_2 over other gases in the mixture (mainly N_2 and CH_4) also needs to be fulfilled along with high uptake value. Excellent uptake of studied carbons at low pressure, high amounts of basic heteroatoms and abundance of microporosity would be expected to afford high selectivity for CO_2 over N_2 and CH_4. The selectivity was probed using the initial slope ratios measured according to Henry's law constant

for single component adsorption components at low pressure coverage. Subsequently, N_2 isotherms at 273 and 298 K were also collected and presented together with previously measured CO_2 and CH_4 isotherms in Figure 3.16 and Figure 3.17. It is clearly observed that the amount of CO_2 adsorbed is much higher than for CH_4 and N_2 in all tested pressure range. The initial slopes calculation for ALP-6 derived carbons at 273 and 298 K are shown in Figure 3.18 and Figure 3.19 and selectivity values of CO_2/N_2 and CO_2/CH_4 are provided in Table 3.3. The analogous trend of selectivity results to Q_{st} values at low loading indicates the importance of heteroatom and ultramicropores. It should be emphasized that since N_2 and CH_4 are not able to interact with basic functionalities through hydrogen bond and/or dipole-quadrupole, it is expected that any decrease in heteroatoms content reduce the CO_2 selectivity values. In other words, CO_2-philic sites (N and O) are considered as key parameters for the selective CO_2 adsorption over N_2 and CH_4.[36] Thus, it is believed that basic functional groups on the pore walls of carbons play more important role than pore size in selectivity. As in direct carbonized samples, the ALPDCD600 sample shows the highest CO_2/N_2 and CO_2/CH_4 of 89 and 12 at 273K, respectively. Further increase in carbonization temperature resulted in elimination of more basic surface groups and decline of selectivity values. The ALPDCK500 carbon features remarkable CO_2 selectivity values of 118 (over N_2) and 18 (over CH_4) at 273 K, mainly due to collaborating effect of narrow micropores and high level of heteroatoms (~ 30 wt% total). Considering the similar amount of total heteroatom in all three $ZnCl_2$ activated carbons, the highest selectivity was observed for ALPDCZ700, which has smaller pores. These values reaches up to 74 and 13 for CO_2/N_2 and CO_2/CH_4 at 273 K, respectively.

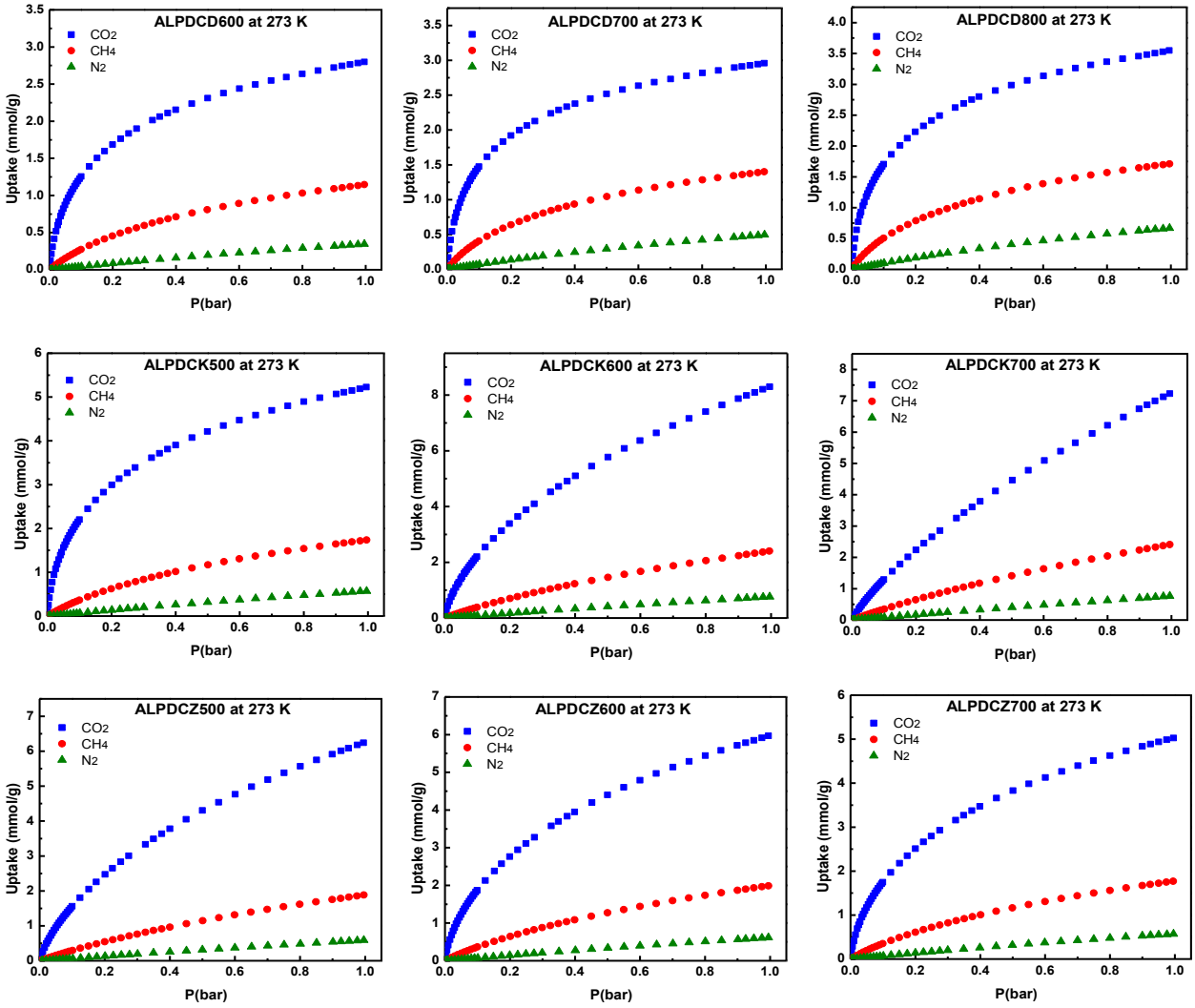

Figure 3.16. Experimental pure component curves for ALP-6 derived carbons at 273 K; CO_2 (blue), CH_4 (red) and N_2 (green).

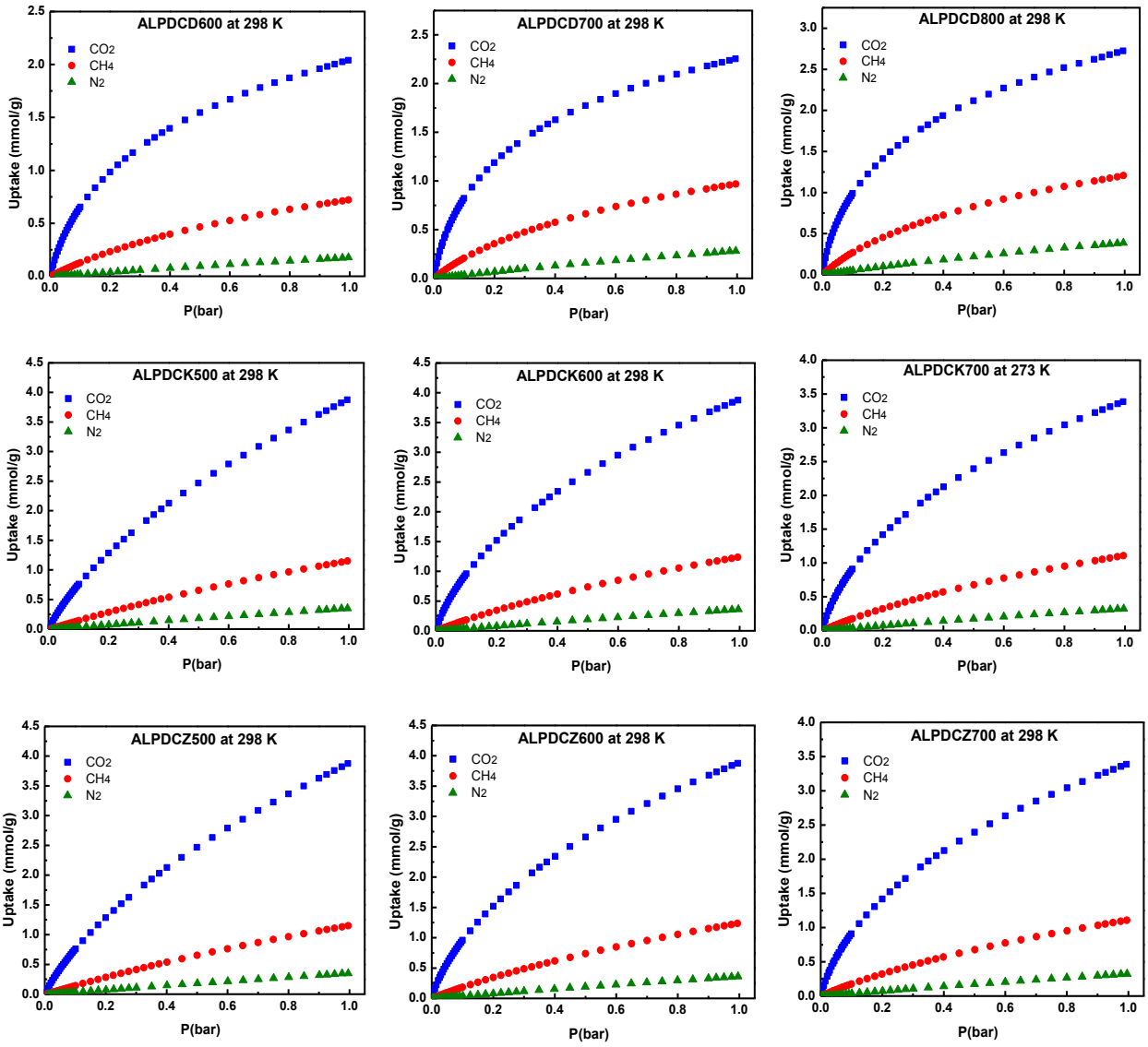

Figure 3.17. Experimental pure component curves for ALP-6 derived carbons at 298 K; CO_2 (blue), CH_4 (red) and N_2 (green).

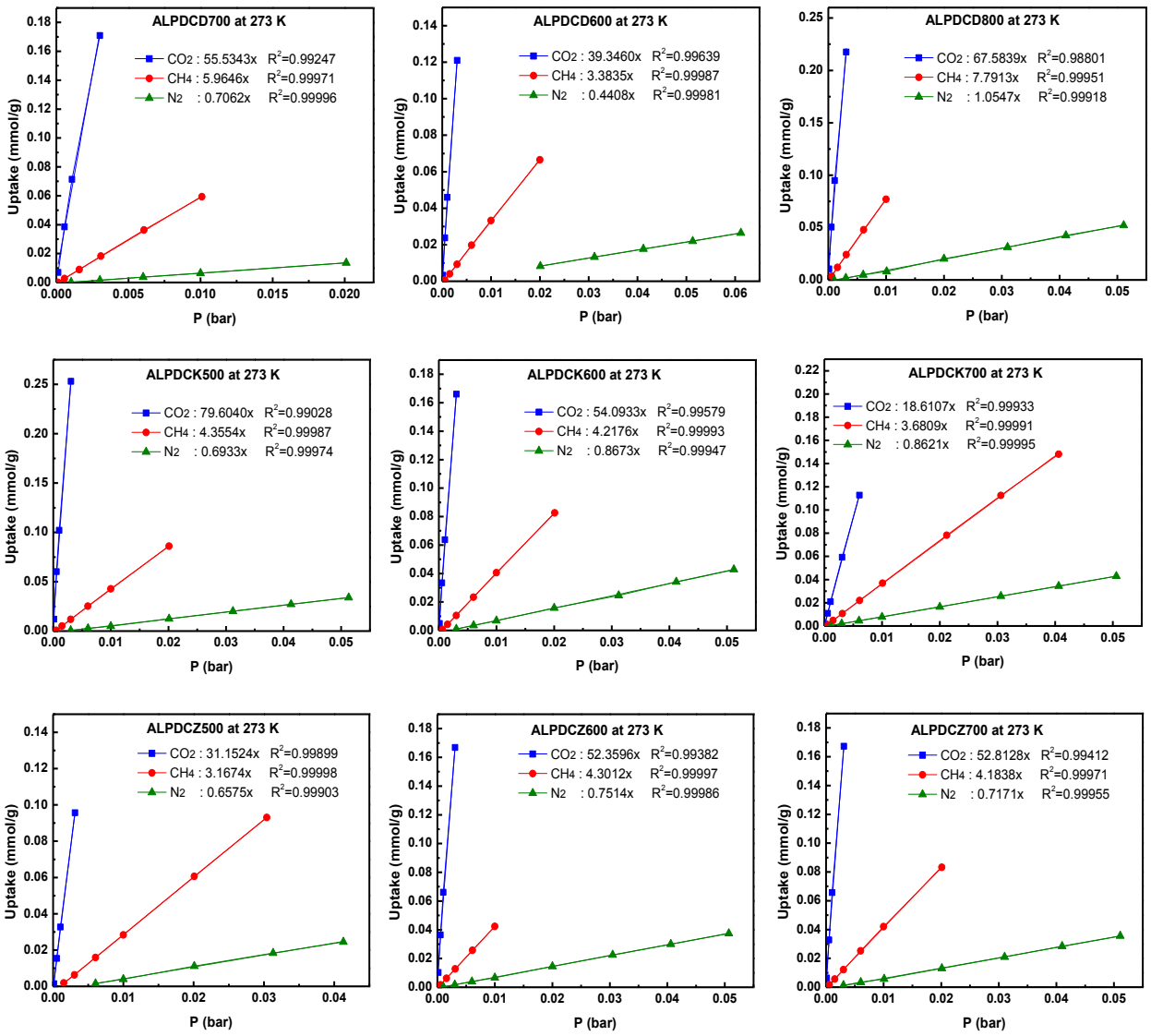

Figure 3.18. CO_2/N_2 and CO_2/CH_4 adsorption selectivity for ALP-6 derived carbons using the Henry's law constant in the linear low pressure range. CO_2 (blue), CH_4 (red) and N_2 (green) isotherms collected at 273 K.

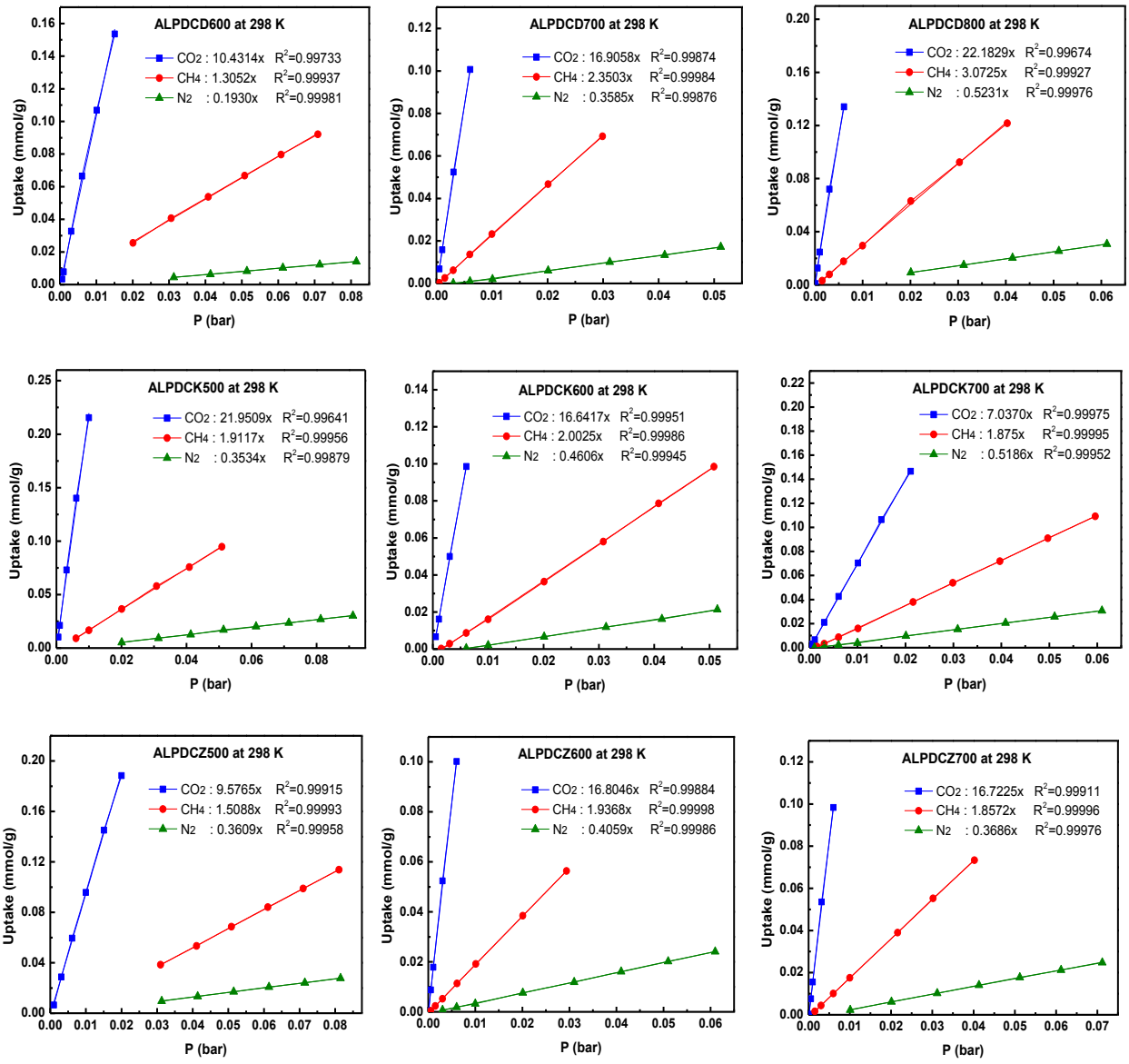

Figure 3.19. CO_2/N_2 and CO_2/CH_4 adsorption selectivity for ALP-6 derived carbons using the Henry's law constant in the linear low pressure range. CO_2 (blue), CH_4 (red) and N_2 (green) isotherms collected at 298 K.

3.4 Conclusion

Three different strategies based on direct carbonization, $ZnCl_2$ and KOH activation were applied to transform an azo-linked polymer (ALP-6) into microporous heteroatom doped carbons. By adjusting the activation temperature, a diverse range of textural properties such as surface area, pore volume and well-developed microporosity was modulated. The resultant carbons contained high amount of Lewis basic functionalities (nitrogen and oxygen), which vary with activation methods and pyrolysis temperatures. The carbon materials show high CO_2 adsorption capacity with value as high as 5.2 mmol g^{-1} at 1 bar and 1.5 mmol g^{-1} at 0.15 bar and 298 K. This high CO_2 uptake capacity is obtained due to the combined effect of high levels of narrow microporosity and a high density of oxygen and nitrogen basic functionalities of the pores. Moreover, the prepared carbons discriminate CO_2 from other gases with relatively similar sizes such as CH_4 and N_2 to attain high selectivity levels of 115 for CO_2/N_2 and 18 for CO_2/CH_4 at 273 K. Thus, microporous carbons derived from ALP-6 are highly desirable for practical applications such as selective CO_2 capture from flu and landfill gas as well as natural gas upgrading.

3.5 References

1. Shen, W.; Fan, W., Nitrogen-Containing Porous Carbons: Synthesis and Application. *J. Mater. Chem. A* **2013**, *1*, 999-1013.

2. Paraknowitsch, J. P.; Thomas, A., Doping Carbons Beyond Nitrogen: An Overview of Advanced Heteroatom Doped Carbons with Boron, Sulphur and Phosphorus for Energy Applications. *Energy Environ. Sci.* **2013**, *6*, 2839-2855.

3. Aijaz, A.; Fujiwara, N.; Xu, Q., From Metal–Organic Framework to Nitrogen-Decorated Nanoporous Carbons: High CO_2 Uptake and Efficient Catalytic Oxygen Reduction. *J. Am. Chem. Soc.* **2014**, *136*, 6790-6793.

4. Gadipelli, S.; Guo, Z. X., Tuning of ZIF-Derived Carbon with High Activity, Nitrogen Functionality, and Yield - A Case for Superior CO_2 Capture. *ChemSusChem* **2015**, *8*, 2123-32.

5. Wang, J.; Senkovska, I.; Oschatz, M.; Lohe, M. R.; Borchardt, L.; Heerwig, A.; Liu, Q.; Kaskel, S., Highly Porous Nitrogen-Doped Polyimine-Based Carbons with Adjustable Microstructures for CO_2 Capture. *J. Mater. Chem. A* **2013**, *1*, 10951-10961.

6. Rabbani, M. G.; Sekizkardes, A. K.; Kahveci, Z.; Reich, T. E.; Ding, R.; El-Kaderi, H. M., A 2D Mesoporous Imine-Linked Covalent Organic Framework for High Pressure Gas Storage Applications. *Chem. Eur. J.* **2013**, *19*, 3324-8.

7. Yang, X.; Yu, M.; Zhao, Y.; Zhang, C.; Wang, X.; Jiang, J.-X., Remarkable Gas Adsorption by Carbonized Nitrogen-Rich Hypercrosslinked Porous Organic Polymers. *J. Mater. Chem. A* **2014**, *2*, 15139-15145.

8. Wang, C.; Luo, H.; Jiang, D. E.; Li, H.; Dai, S., Carbon Dioxide Capture by Superbase-Derived Protic Ionic Liquids. *Angew. Chem., Int. Ed.* **2010**, *49*, 5978-81.

9. Zhang, S.; Dokko, K.; Watanabe, M., Carbon Materialization of Ionic Liquids: From Solvents to Materials. *Mater. Horiz.* **2015**, *2*, 168-197.

10. Chen, G.; Wang, X.; Li, J.; Hou, W.; Zhou, Y.; Wang, J., Direct Carbonization of Cyanopyridinium Crystalline Dicationic Salts into Nitrogen-Enriched Ultra-Microporous Carbons toward Excellent CO_2 Adsorption. *ACS Appl. Mater. Interfaces* **2015**, *7*, 18508-18518.

11. Zhu, H.; Yin, J.; Wang, X.; Wang, H.; Yang, X., Microorganism-Derived Heteroatom-Doped Carbon Materials for Oxygen Reduction and Supercapacitors. *Adv. Funct. Mater.* **2013**, *23*, 1305-1312.

12. Fan, X.; Zhang, L.; Zhang, G.; Shu, Z.; Shi, J., Chitosan Derived Nitrogen-Doped Microporous Carbons for High Performance CO_2 Capture. *Carbon* **2013**, *61*, 423-430.

13. Arab, P.; Rabbani, M. G.; Sekizkardes, A. K.; İslamoğlu, T.; El-Kaderi, H. M., Copper(I)-Catalyzed Synthesis of Nanoporous Azo-Linked Polymers: Impact of Textural Properties on Gas Storage and Selective Carbon Dioxide Capture. *Chem. Mater.* **2014**, *26*, 1385-1392.

14. Arab, P.; Parrish, E.; Islamoglu, T.; El-Kaderi, H. M., Synthesis and Evaluation of Porous Azo-Linked Polymers for Carbon Dioxide Capture and Separation. *J. Mater. Chem. A* **2015**, *3*, 20586-20594.

15. Wang, J.; Kaskel, S., KOH Activation of Carbon-Based Materials for Energy Storage. *J. Mater. Chem.* **2012**, *22*, 23710-23725.

16. Caturla, F.; Molina-Sabio, M.; Rodríguez-Reinoso, F., Preparation of Activated Carbon by Chemical Activation with $ZnCl_2$. *Carbon* **1991**, *29*, 999-1007.

17. Molina-Sabio, M.; Rodríguez-Reinoso, F., Role of Chemical Activation in the Development of Carbon Porosity. *Colloids Surf., A* **2004**, *241*, 15-25.

18. Olivares-Marín, M.; Fernández-González, C.; Macías-García, A.; Gómez-Serrano, V., Preparation of Activated Carbon from Cherry Stones by Chemical Activation with $ZnCl_2$. *Appl. Surf. Sci.* **2006**, *252*, 5967-5971.

19. Hu, X.; Radosz, M.; Cychosz, K. A.; Thommes, M., CO_2-Filling Capacity and Selectivity of Carbon Nanopores: Synthesis, Texture, and Pore-Size Distribution from Quenched-Solid Density Functional Theory (QSDFT). *Environ. Sci. Technol.* **2011**, *45*, 7068-7074.

20. Pels, J. R.; Kapteijn, F.; Moulijn, J. A.; Zhu, Q.; Thomas, K. M., Evolution of Nitrogen Functionalities in Carbonaceous Materials During Pyrolysis. *Carbon* **1995**, *33*, 1641-1653.

21. Hulicova-Jurcakova, D.; Seredych, M.; Lu, G. Q.; Bandosz, T. J., Combined Effect of Nitrogen- and Oxygen-Containing Functional Groups of Microporous Activated Carbon on its Electrochemical Performance in Supercapacitors. *Adv. Funct. Mater.* **2009**, *19*, 438-447.

22. Tian, Z.; Dai, S.; Jiang, D.-e., Stability and Core-Level Signature of Nitrogen Dopants in Carbonaceous Materials. *Chem. Mater.* **2015**, *27*, 5775-5781.

23. Rodríguez-Reinoso, F.; Molina-Sabio, M., Activated Carbons from Lignocellulosic Materials by Chemical and/or Physical Activation: An Overview. *Carbon* **1992**, *30*, 1111-1118.

24. Sevilla, M.; Valle-Vigón, P.; Fuertes, A. B., N-Doped Polypyrrole-Based Porous Carbons for CO_2 Capture. *Adv. Funct. Mater.* **2011**, *21*, 2781-2787.

25. Ashourirad, B.; Sekizkardes, A. K.; Altarawneh, S.; El-Kaderi, H. M., Exceptional Gas Adsorption Properties by Nitrogen-Doped Porous Carbons Derived from Benzimidazole-Linked Polymers. *Chem. Mater.* **2015**, *27*, 1349-1358.

26. Wahby, A.; Ramos-Fernandez, J. M.; Martinez-Escandell, M.; Sepulveda-Escribano, A.; Silvestre-Albero, J.; Rodriguez-Reinoso, F., High-Surface-Area Carbon Molecular Sieves for Selective CO_2 Adsorption. *ChemSusChem* **2010**, *3*, 974-81.

27. Wickramaratne, N. P.; Jaroniec, M., Importance of Small Micropores in CO_2 Capture by Phenolic Resin-Based Activated Carbon Spheres. *J. Mater. Chem. A* **2013**, *1*, 112-116.

28. Czepirski, L.; JagieŁŁo, J., Virial-Type Thermal Equation of Gas—Solid Adsorption. *Chem. Eng. Sci.* **1989**, *44*, 797-801.

29. Lee, K. B.; Sircar, S., Removal and Recovery of Compressed CO_2 from Flue Gas by a Novel Thermal Swing Chemisorption Process. *AIChE J.* **2008**, *54*, 2293-2302.

30. Presser, V.; McDonough, J.; Yeon, S.-H.; Gogotsi, Y., Effect of Pore Size on Carbon Dioxide Sorption by Carbide Derived Carbon. *Energy Environ. Sci.* **2011**, *4*, 3059-3066.

31. Liu, Y.; Wilcox, J., Effects of Surface Heterogeneity on the Adsorption of CO_2 in Microporous Carbons. *Environ. Sci. Technol.* **2012**, *46*, 1940-1947.

32. Hao, G. P.; Li, W. C.; Qian, D.; Lu, A. H., Rapid Synthesis of Nitrogen-Doped Porous Carbon Monolith for CO_2 Capture. *Adv. Mater.* **2010**, *22*, 853-7.

33. Sekizkardes, A. K.; Altarawneh, S.; Kahveci, Z.; İslamoğlu, T.; El-Kaderi, H. M., Highly Selective CO_2 Capture by Triazine-Based Benzimidazole-Linked Polymers. *Macromolecules* **2014**, *47*, 8328-8334.

34. Rabbani, M. G.; El-Kaderi, H. M., Template-Free Synthesis of a Highly Porous Benzimidazole-Linked Polymer for CO_2 Capture and H_2 Storage. *Chem. Mater.* **2011**, *23*, 1650-1653.

35. Herm, Z. R.; Krishna, R.; Long, J. R., CO_2/ CH_4, CH_4/H_2 and CO_2/CH_4/H_2 Separations at High Pressures Using Mg_2(DOBDC). *Microporous Mesoporous Mater.* **2012**, *151*, 481-487.

36. Patel, H. A.; Hyun Je, S.; Park, J.; Chen, D. P.; Jung, Y.; Yavuz, C. T.; Coskun, A., Unprecedented High-Temperature CO_2 Selectivity in N_2-Phobic Nanoporous Covalent Organic Polymers. *Nat. Commun.* **2013**, *4*, 1357.

Chapter 4: Heterocyclic Building Block Transformation to Nanoporous Carbons: Toward a Very High Surface Area and CO_2 Uptake

4.1 Introduction

In order to incorporate nitrogen into the carbon matrix, employing a single source precursor of carbon and desired elements followed by activation/carbonization is considered as an efficient strategy. Progressively, the main effort during recent years has been focused on utilizing synthetic polymers (POPs, MOFs…) or biomasses as single source precursors of carbon and desired heteroatoms.[1-4] However, using a synthetic porous polymer as sole precursor has been somewhat restricted due to vigorous reaction condition (toxic organic solvents and chemicals) and multistep nature of synthesis.[5-6] On the other hand, the biomasses also demand steps of preparation such as cleaning, drying, grinding and pre-carbonization to be applicable as single source precursors.[7-8] The recently established method of carbonization of ionic liquids[9] and organic salts[10] has overcome these drawbacks but the control over porous structure remains a challenge. However, the utilization of simple organic building blocks as precursors has been ignored so far and the role of heteroatom in the feasibility of their chemical activation has not been investigated. In this chapter, we report a facile, template/solvent free and one-step synthesis of nanoporous carbons through KOH activation of benzimidazole (BI) building block as a low-cost, commercially available and highly enriched nitrogen (24 wt%) single source precursor. Textural and chemical properties as well as CO_2 capture and working capacity of prepared carbons will be investigated.

4.2 Experimental

4.2.1 Materials and Methods. Benzimidazole and potassium hydroxide were purchased from TCI America and Alfa Aesar, respectively. To minimize the effect of ambient moisture, various ratios of as received BI and KOH were mixed inside glovebox prior to carbonization. The mixtures then were transferred to a temperature-programmed tube furnace and carbonized at elevated temperature under Ar flow. The obtained benzimidazole derived carbons are designated as "BIDC-x-y," where "x" indicates KOH to BI weight ratio and "y" represents applied activation temperature. To examine the textural and chemical characteristics of carbons more accurately, four representative samples were synthesized by tuning the relative amount of KOH to BI (0.5, 1, 2 and 3) at 700 °C. It is worth mentioning that any KOH to BI ratio less than 0.5 resulted in under activation and mostly sublimed precursor while ratios more than 4 led to formation of totally burnt and over activated products. The 700 °C temperature was adopted as optimum activation temperature, which can retain considerable amounts of nitrogen and develop porous structure simultaneously according to our previous studies.

4.2.2 Characterization and Measurements. Elemental microanalyses were performed at the Midwest Microlab, LLC. To obtain Scanning Electron Microscopy (SEM) images, each sample was dispersed onto a sticky carbon surface attached to a flat aluminum sample holder. Then, the sample was coated with platinum at a pressure of 1×10^{-5} mbar in a nitrogen atmosphere for 90 s before imaging. SEM images were taken on a Hitachi SU-70 Scanning Electron Microscope. TEM images were recorded on a JEOL 2010 apparatus operated at an accelerating voltage of 200 kV. Samples were dispersed in ethanol and then drop cast onto a 200 mesh carbon-coated copper grid. Powder X-ray diffraction data were collected on a Panalytical X'pert pro multipurpose diffractometer (MPD). Samples were mounted on a sample holder and measured using Cu Kα.

X-ray photoelectron spectroscopy (XPS) analysis was performed on a ThermoFisher ESCALAB 250 spectrometer employing Al Kα (1486.68 eV) X-ray source equipped with a hemispherical analyzer. Atmospheric gas (N_2, CO_2 and CH_4) sorption measurements were carried out on a Quantachrome Autosorb iQ volumetric analyzer using UHP grade adsorbates. Prior to the adsorption analyses the samples were degassed at 200 °C for 12 h.

4.2.3 Working Capacity Calculation. The pure component isotherms of CO_2 were fitted with the dualsite Langmuir (DSL) isotherm model with a temperature dependent parameter. CH_4 and N_2 isotherms were fitted to single site Langmuir isotherms. Fitting parameters were used to calculate IAST selectivities and then sorbent selection parameters. Details about the calculations were explained previously.[11-12]

Dual site Langmuir model = $q_A + q_B$; Single site Lagmuir model = q_A

$$q = q_A + q_B = \frac{q_{sat,A} * (b_A * \exp\left(\frac{E_A}{R * T}\right) * p}{1 + b_A * \exp\left(\frac{E_A}{R * T}\right) * p} + \frac{q_{sat,B} * (b_B * \exp\left(\frac{E_B}{R * T}\right) * p}{1 + b_B * \exp\left(\frac{E_B}{R * T}\right) * p}$$

where, q is total molar loading; q_{sat} is saturation loading, mol kg^{-1}; p is total system pressure, Pa; R is ideal gas constant, 8.314 J mol^{-1} K^{-1}; b is Langmuir constant, Pa^{-1}; T is absolute temperature,K. Subscripts A and B refers to site A and site B, respectively.

4.3 Results and Discussion

4.3.1 Organic Molecule Conversion to Carbon. The carbonization of sole benzimidazole building block results in complete mass loss at around 400 °C due to sublimation of the organic moiety as evidenced by its TGA (red curve in Figure 4.1.a). However, it is shown that the hydrogen present in NH group of benzimidazole is sufficiently acidic to react with different bases to form N-metal benzimidazole salts.[13] This unique property of benzimidazole originates from the high stability of the corresponding ions due to resonance. Moreover, benzimidazole has high degree of stability at high temperatures and harsh acidic/basic conditions.[14] In order to suppress the evaporation of BI building blocks and ensure subsequent activation, we took advantage of this fact and mixed BI building units with KOH prior to high temperature carbonization. Heating the mixture of BI and KOH to the melting point of benzimidazole leads to reaction of KOH with molten BI to yield potassium-N benzimidazole salt.

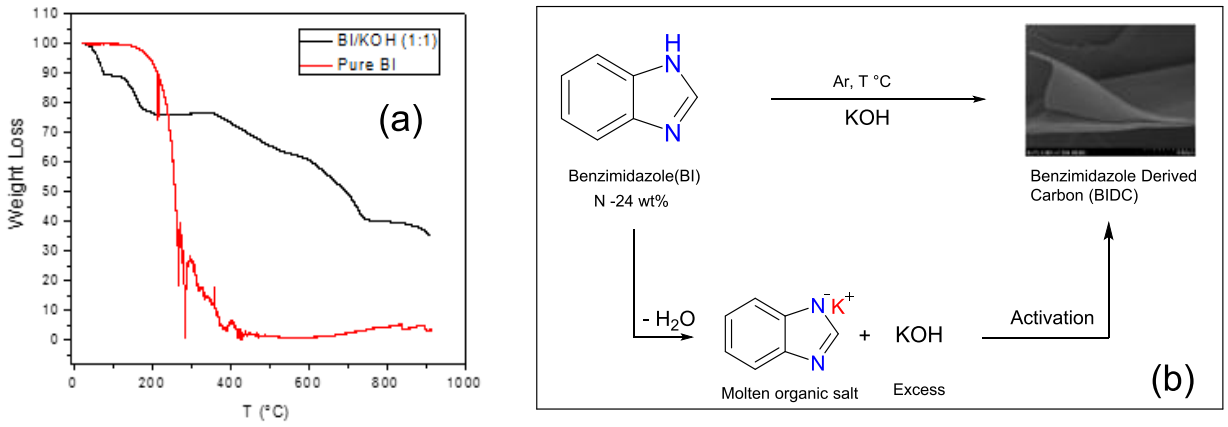

Figure 4.1. (a) TGA graph of bare BI and BI-KOH mixture, (b) Schematic representation of BI building blocks transformation to a heteroatom doped porous carbon.

The activation/carbonization of non-volatile molten salt proceeds by means of excess KOH present in the system and further heating of the mixture according to well established mechanisms such as etching (by redox reactions), gasification (by evolving gaseous species such as H_2O and CO_2) and expansion of carbon framework (by metallic potassium).[15] The TGA results of bare BI and BI-KOH mixture, which further support this finding, are shown in Figure 4.1(a). The transformation of BI to heteroatom-doped carbon is also depicted schematically in Figure 4.1(b).

4.3.2 Textural Properties. The N_2 (77 K) adsorption isotherms were collected to assess textural properties of activated carbons (Figure 4.2) and the results are summarized in Table 4.1 in detail. Notably, all prepared carbons features unexpectedly high Brunauer−Emmett−Teller (BET) surface area (1316-4171 $m^2\ g^{-1}$) and large total pore volume (0.53-2.39 $cm^3\ g^{-1}$) with respect to their nonporous precursor (Figure 4.3). The samples which are activated at KOH/BI of 0.5 and 1 show microporous type-I behavior featured by a sharp rise in very low pressure area ($<10^{-3}$ bar) and a plateau for the rest of their pressure range. On the other hand, BIDC-2-700 and BIDC-3-700 represent a hybrid of type I−IV isotherms with gradual increase of uptake after rapid initial rise indicating the generation of narrow mesopores (2-5 nm). The pore size distribution (PSD) analysis from N_2 isotherms (77 K) based on quenched solid density functional theory (QSDFT) model, which is widely employed for carbons with heterogeneous pore walls[16] also supported the existence of micropores for all samples. The PSD curves are distributed around 6.4 Å (for BIDC-0.5 and BIDC-1), 8.5 Å and 9.3 Å (for BIDC-2-700 and BIDC-3-700, respectively). The former is slightly lower than twice of the kinetic size of CO_2 (3.3 Å) and is expected to be beneficial to effective carbon dioxide capture. Unfortunately, due to extremely slow diffusion mechanism of nitrogen molecules at cryogenic temperature and very low pressure, obtaining reliable information

below 6 Å is a tedious and time-consuming process. Consequently, CO_2 isotherms (at 273 K) and non-local density functional theory (NLDFT) model were employed to assess the distribution of ultramicropores. The overall cumulative pore volume and pore size distribution for all BIDCs are depicted in Figure 4.4.

The ratio of micropore volume to total pore volume (V_{Mic}/V_{Tot}) calculated from cumulative pore volume of PSD curves, can be regarded as a reasonable indication for microporosity level. The obtained percentage of microporosity not only confirms the results by nitrogen isotherms shape, but also reveals that the sample BIDC-1-700 is consist of pure micropores. It is noteworthy to mention that the introduction of mesopores into the BIDC-2-700 and BIDC-3-700 does not occur at the expense of micropores conversion to larger pores, since the volume of micropores is steadily increasing. In other words, the newly formed mesopores will be added to the initially formed micropores as the amount of KOH increases.[17]

Table 4.1. Textural Properties and CHN Elemental Analysis of BIDCs

Sample	S_{BET} $m^2\ g^{-1}$	V_{Tot} [a] $cm^3\ g^{-1}$	$V_{Mic,DFT}$ [b] $cm^3\ g^{-1}$	$V_{Tot,DFT}$ [b] $cm^3\ g^{-1}$	V_0 [c] $cm^3\ g^{-1}$	C wt%	H wt%	N wt%
BIDC-0.5-700	1316	0.53	0.47 (96)	0.49	0.30	66.0	1.2	14.5
BIDC-1-700	2642	1.06	0.97 (100)	0.97	0.43	69.0	1.2	10.7
BIDC-2-700	3477	1.61	0.85 (57)	1.48	0.28	72.6	0.5	5.1
BIDC-3-700	4171	2.39	0.87 (39)	2.23	0.25	74.1	0.2	3.5

[a] Total pore volume at P/P_o = 0.95. [b] Determined by PSD assuming slit-shaped pores and QSDFT model from N_2 adsorption data at 77 K; the values in parentheses are the percentage of micropores volume relative to total pore volume. [c] Pore volume of ultramicropores (<0.7 nm) obtained from CO_2 adsorption data at 273 K.

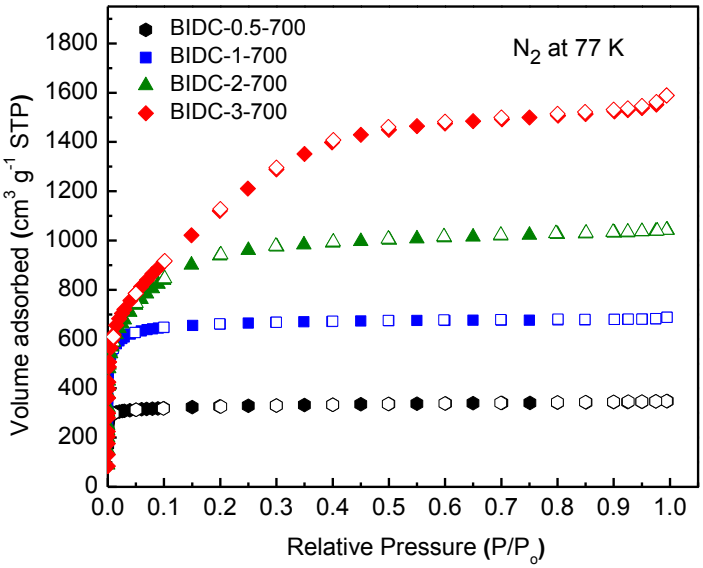

Figure 4.2. Nitrogen adsorption isotherms of BIDCs at 77 K.

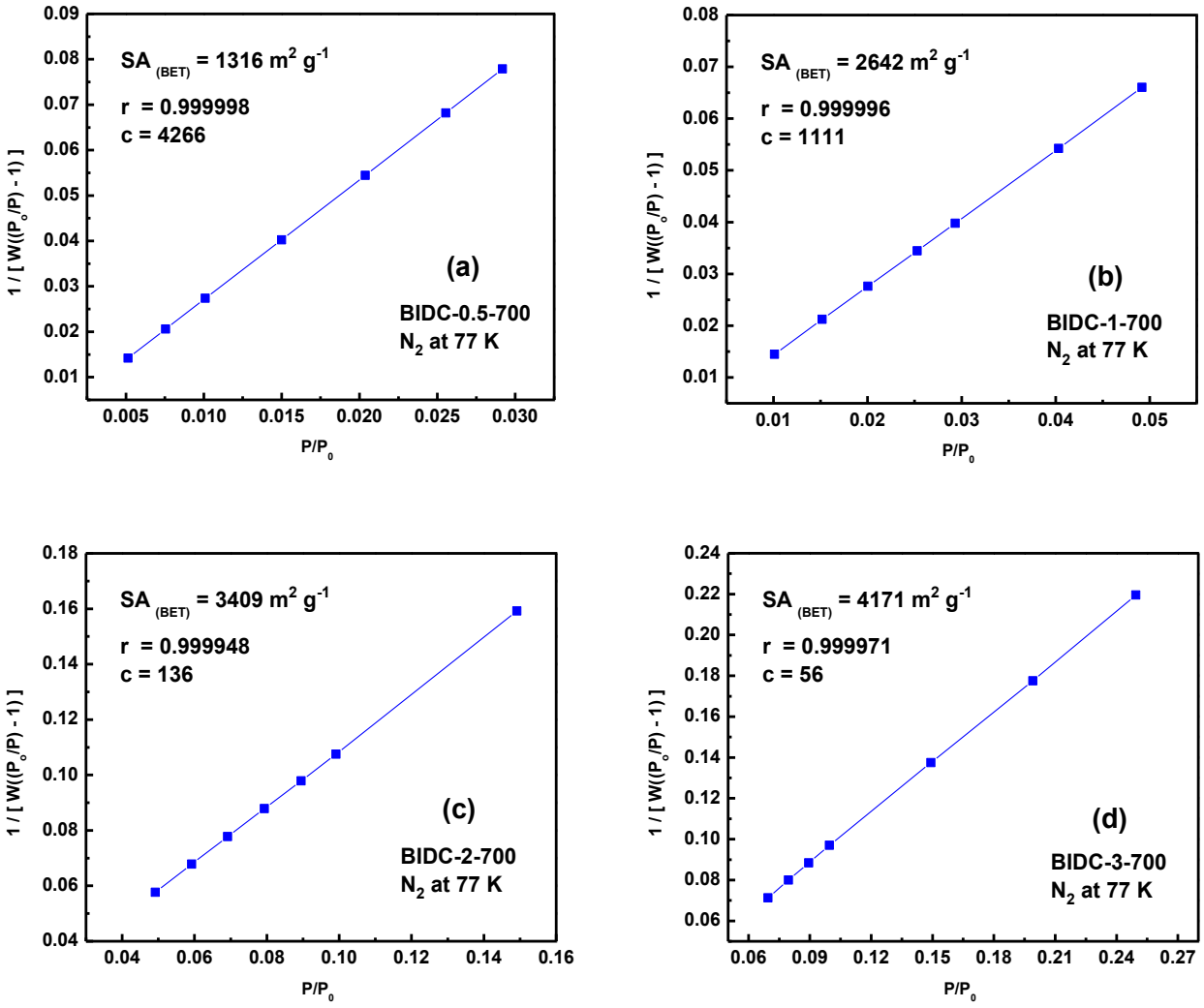

Figure 4.3. BET plots calculated from the N_2 adsorption isotherms at 77 K for (a) BIDC-0.5-700, (b) BIDC-1-700, (c) BIDC-2-700 and (d) BIDC-3-700 (W = Weight of gas adsorbed at P/P_0, r = Correlation coefficient, c = C constant).

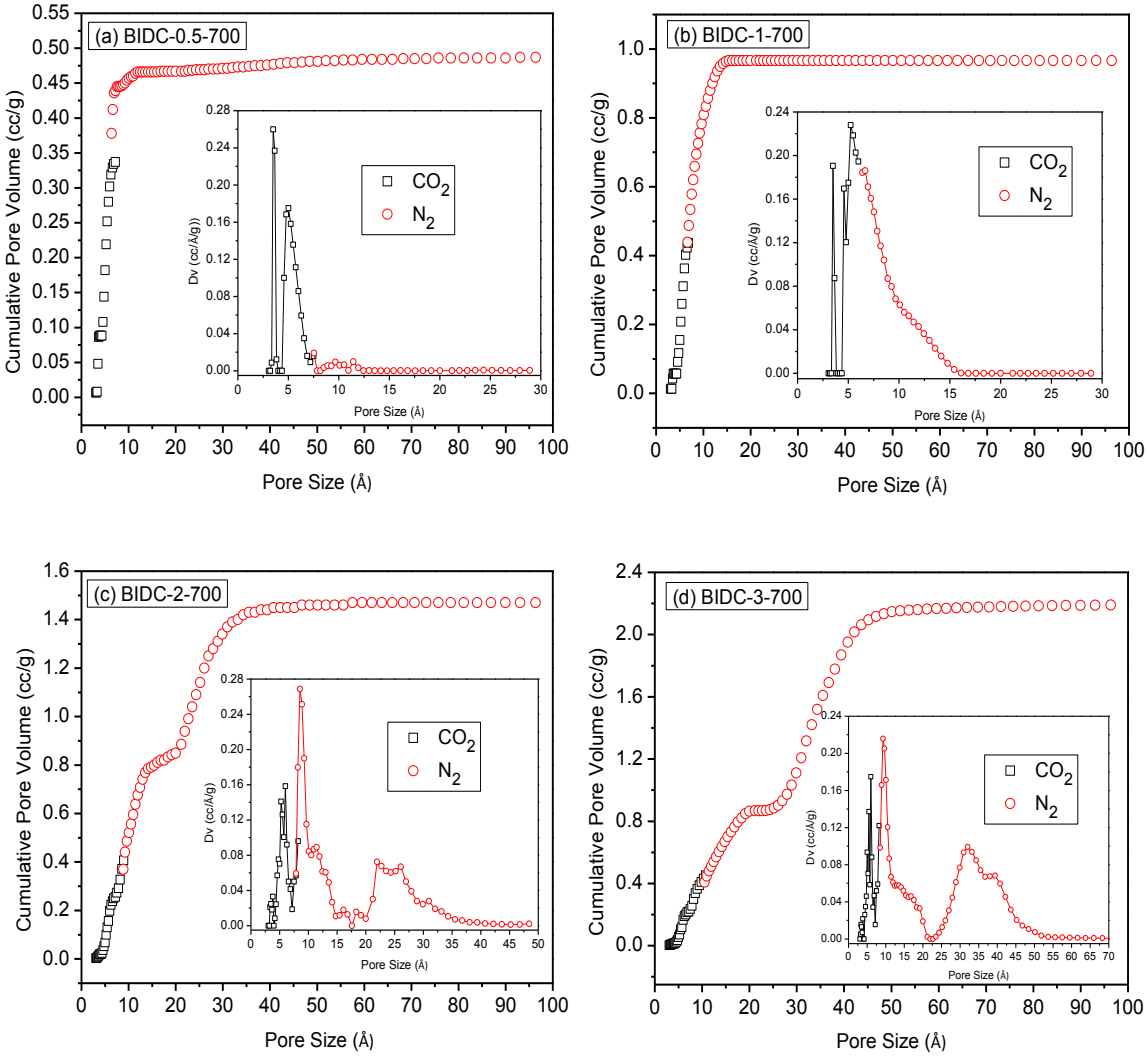

Figure 4.4. Cumulative pore volume and (inset) pore size distribution for N_2 (calculated by using a slit pore QSDFT model) and CO_2 (calculated by using a slit pore NLDFT model) for (a) BIDC-0.5-700, (b) BIDC-1-700, (c) BIDC-2-700 and (d) BIDC-3-700.

4.3.3 Morphology and Crystal Structure. The scanning electron microscopy (SEM) images reveal sheet-like morphology for BIDCs with diverse thickness and rough topography. These sheet-like structures are very different from huge blocks of BI precursors confirming complete destruction of precursor and its transformation to porous carbon (Figure 4.5). The ratio of KOH does not have any significant effect on the texture and morphology of the porous carbon indicating changes take place in much more smaller scale. To confirm uniform distribution of nitrogen and oxygen heteroatoms into the carbon framework, the SEM elemental mapping was also carried out. The results for BIDC-0.5-700 and BIDC-1-700 with highest level of heteroatoms are demonstrated in Figure 4.6 and Figure 4.7, respectively, which represent homogenous distribution of oxygen and nitrogen heteroatoms. The transmission electron microscopy images of BIDCs (Figure 4.8) evidence mainly disordered slit-shape micropores randomly distributed all over the microstructure. The so-called "worm-like" interlocked pore structure is formed by stacking of curved graphene layers.

The structure of BIDCs was investigated by wide-angle X-ray diffraction (XRD). As illustrated in Figure 4.9, no sharp peaks are observed in the XRD pattern, which is indicative of the amorphous nature of BIDCs. The parent BI building block, however, features well-resolved crystalline peaks. This further validates the total destruction of initial crystalline building blocks caused by salt formation and subsequent carbonization. Moreover, the target temperature of 700 °C was not high enough to graphitize newly formed porous carbon sheets.

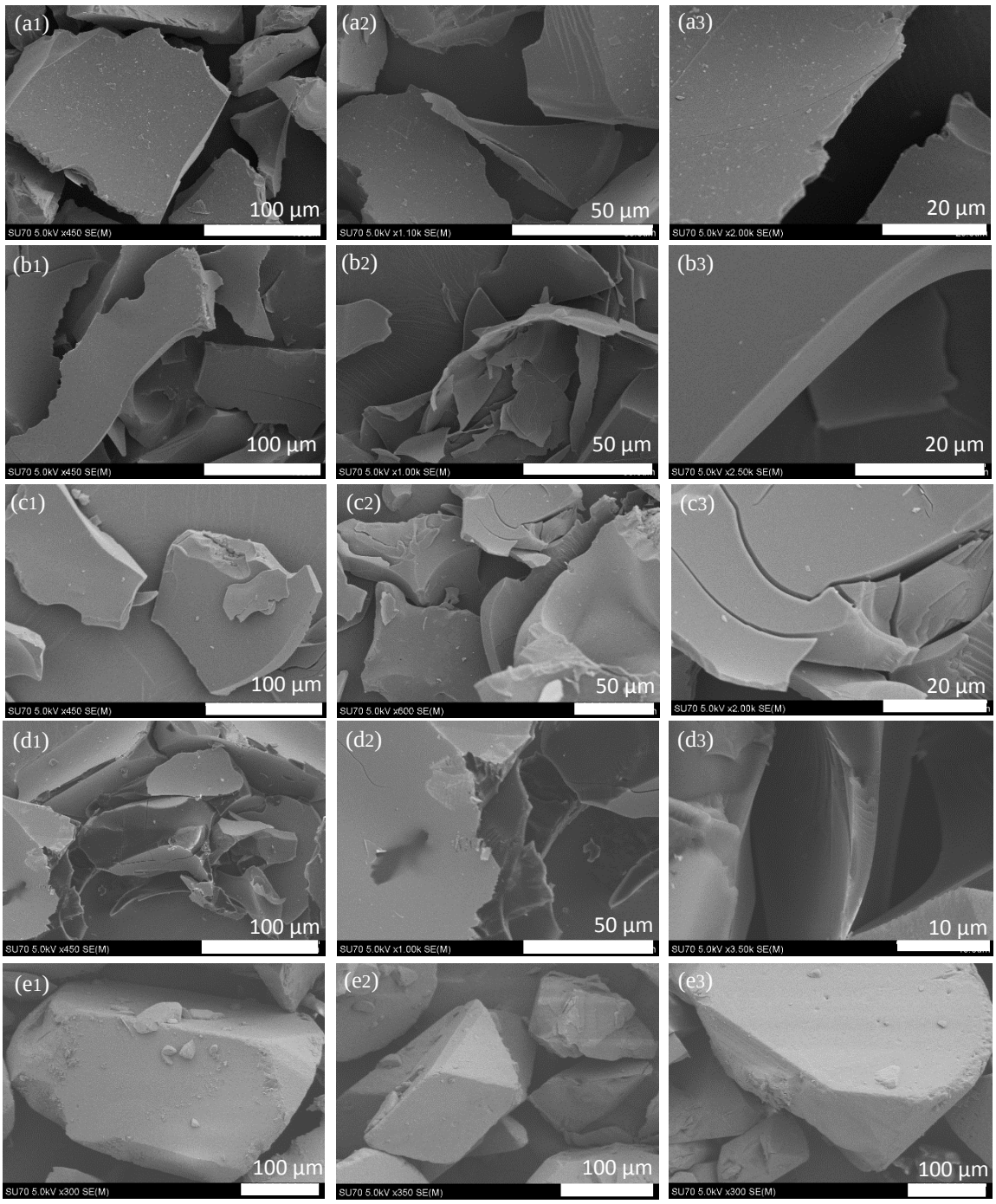

Figure 4.5. SEM images of BIDCs with different magnifications. (a1-a3) BIDC-0.5-700, (b1-b3) BIDC-1-700, (c1-c3) BIDC-2-700, (d1-d3) BIDC-3-700 and (e1-e3) BI.

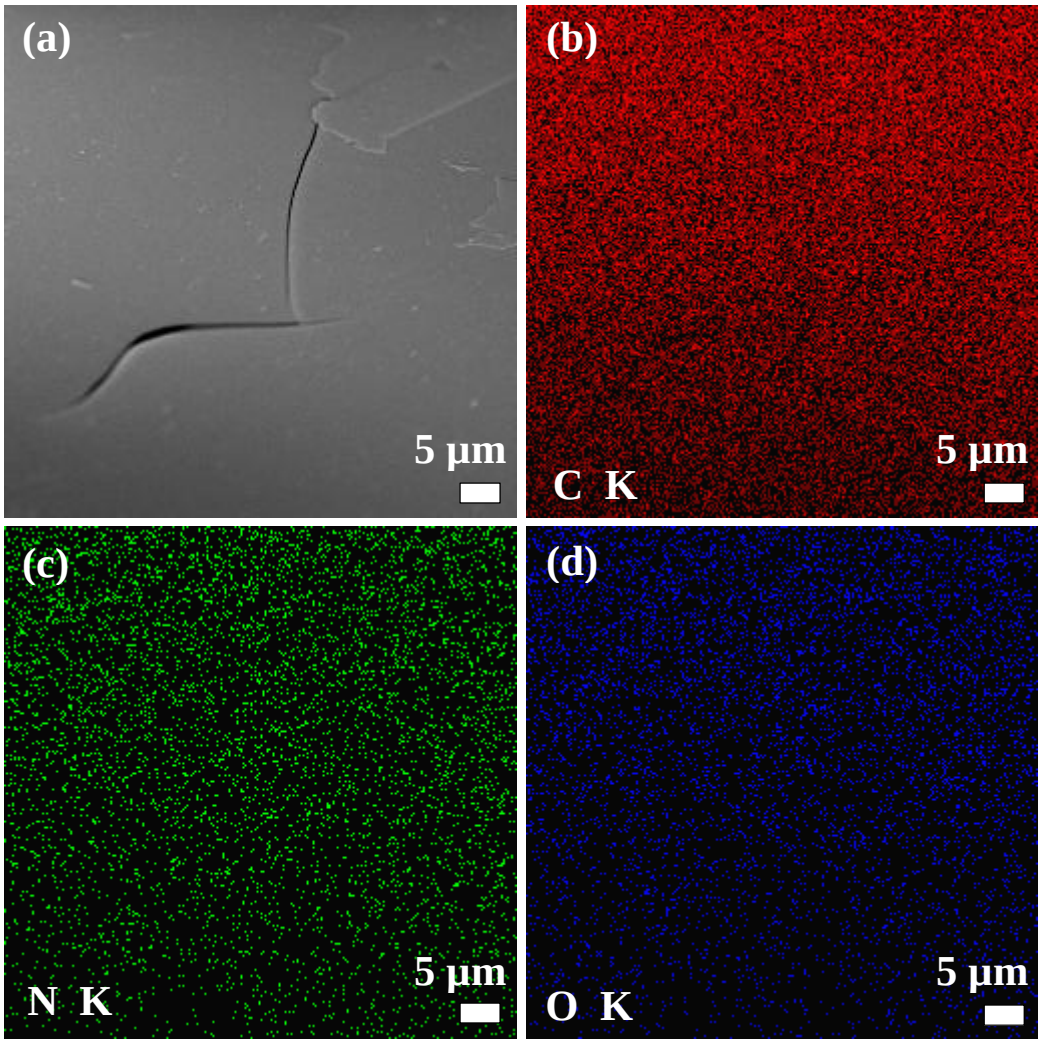

Figure 4.6. (a) SEM image and (b) carbon (c) nitrogen and (d) oxygen elemental mapping for BIDC-1-700.

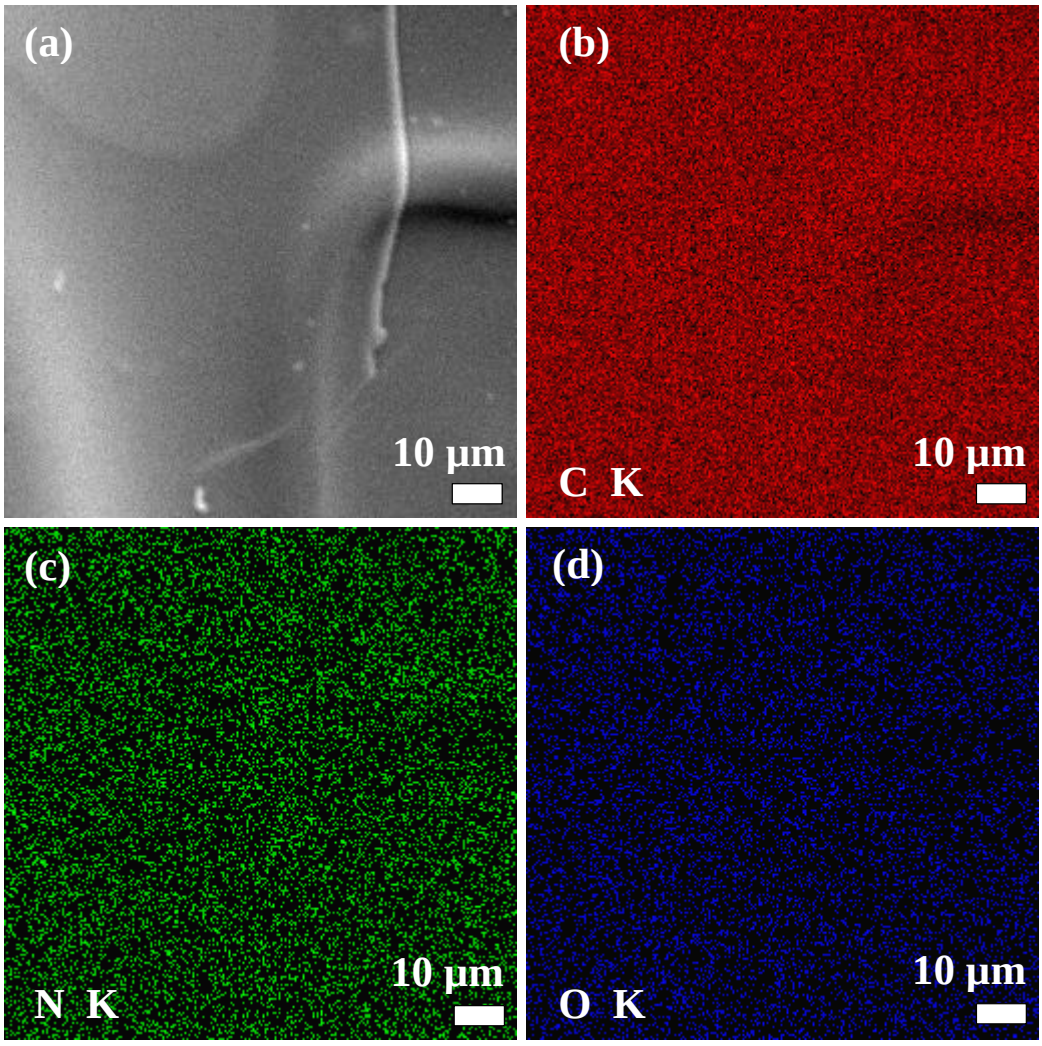

Figure 4.7. (a) SEM image and (b) carbon (c) nitrogen and (d) oxygen elemental mapping for BIDC-1-700.

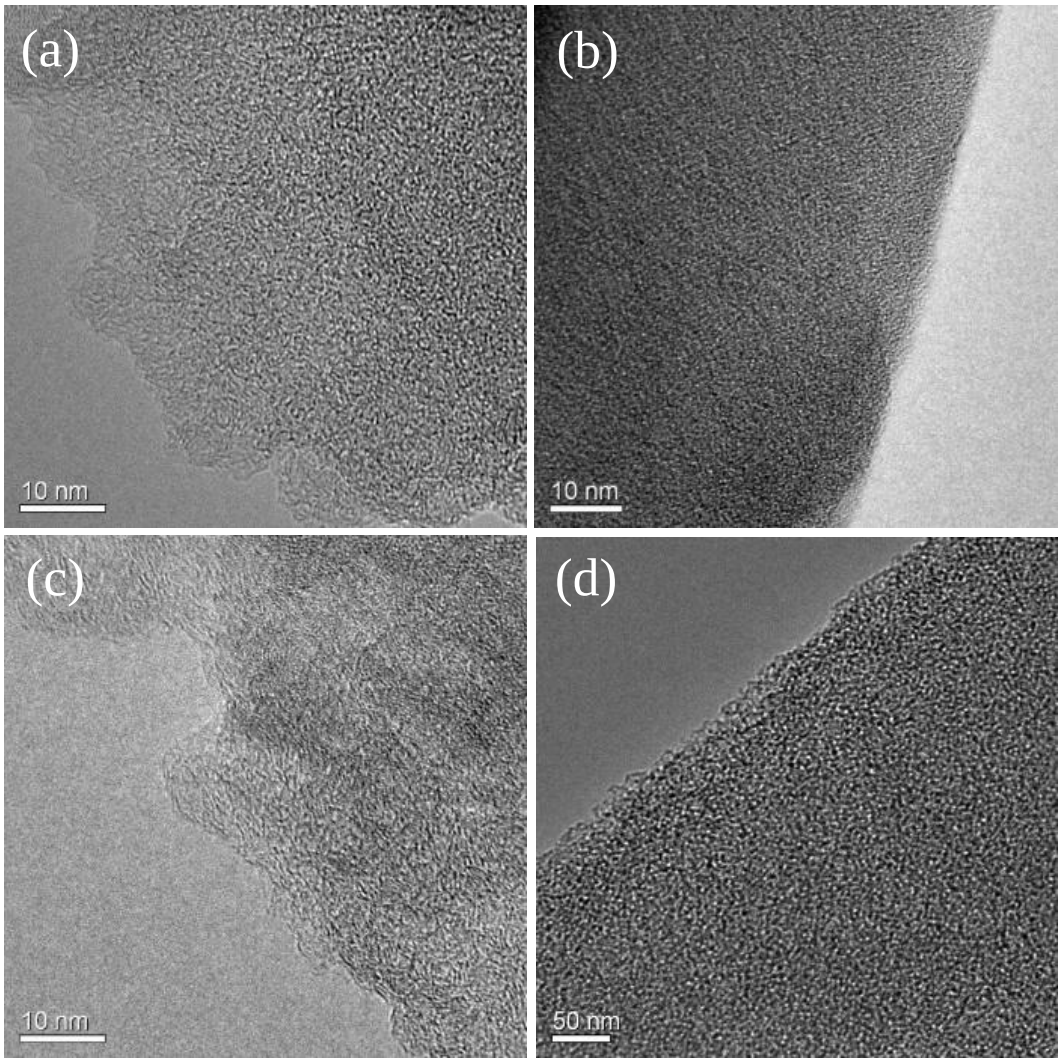

Figure 4.8. High resolution TEM images of BIDCs with different magnifications. (a) BIDC-0.5-700, (b) BIDC-1-700, (c) BIDC-2-700 and (d) BIDC-3-700.

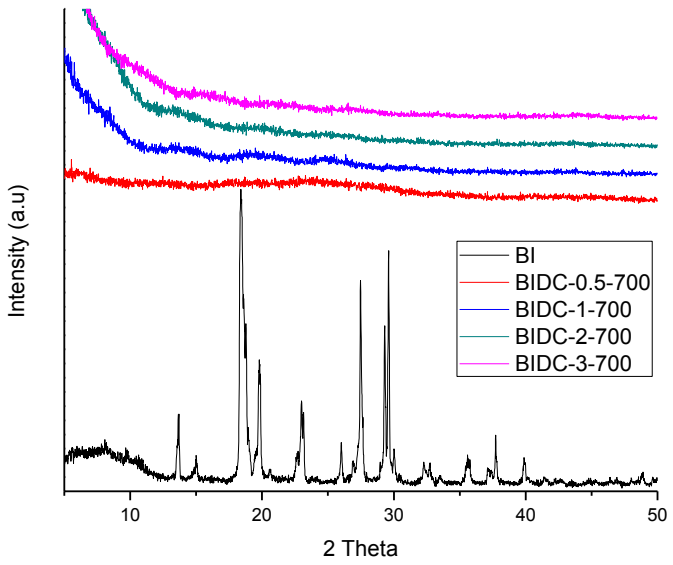

Figure 4.9. XRD patterns of BIDCs and BI precursor.

4.3.4 Composition Study of BIDCs. The chemical compositions of carbons are evaluated by CHN elemental analysis and results are shown in Table 4.1. The X-ray photoelectron spectroscopy (XPS) survey of all four prepared carbons confirmed the presence of the C 1s peak, N 1s peak, and O 1s peak at 284, 400 and 530 eV, respectively (Figure 4.10). The nature of oxygen and nitrogen moieties on the surface of prepared BIDCs was further investigated by deconvolution of their 1s core level spectra. For oxygen, three main contributions are visible in the high-resolution O 1s: i) C=O quinone type oxygen at 531 eV (O-I), ii) C–OH phenol and/or C–O–C ether groups at 533 eV (O-II) and iii) COOH carboxylic groups and/or water at 536 eV (O-III).[18] Similarly, for nitrogen four peaks around 398, 400, 401 and 405 eV represent pyridinc (N-6), pyrrolic and/or pyridonic (N-5), quaternary (N-Q) and pyridine-N-oxide (N-X), respectively.[19] Owing to the oxidative condition of chemical activation by KOH and relatively high temperature (> 600 °C), the pyridonic nitrogen most likely has the major contribution to N-5 species (Figure 4.11).

Deconvoluted N 1s and O 1s spectra of BIDCs are also shown in Figures 4.12 and 4.13, respectively.

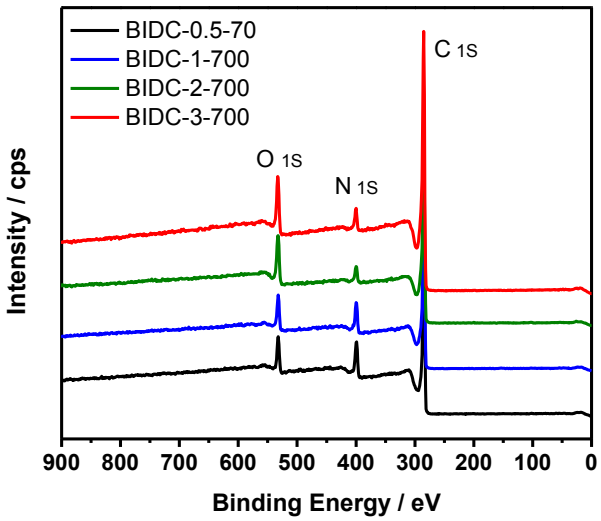

Figure 4.10. X-ray photoelectron spectroscopy (XPS) survey spectra of BIDCs.

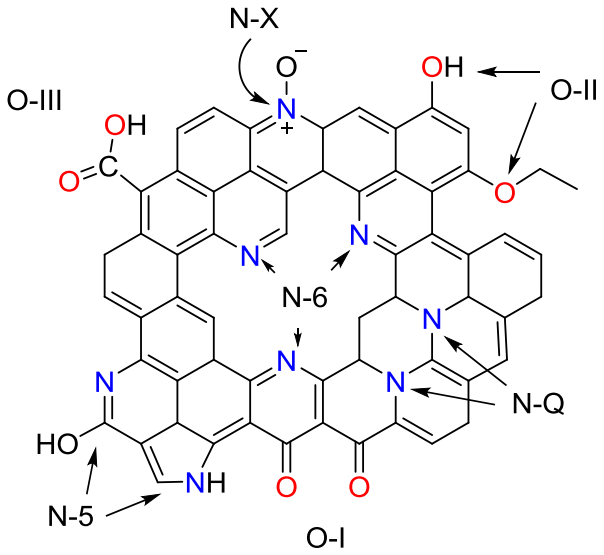

Figure 4.11. Schematic illustration of various nitrogen and oxygen functionalities on the pore walls of a typical porous carbon.

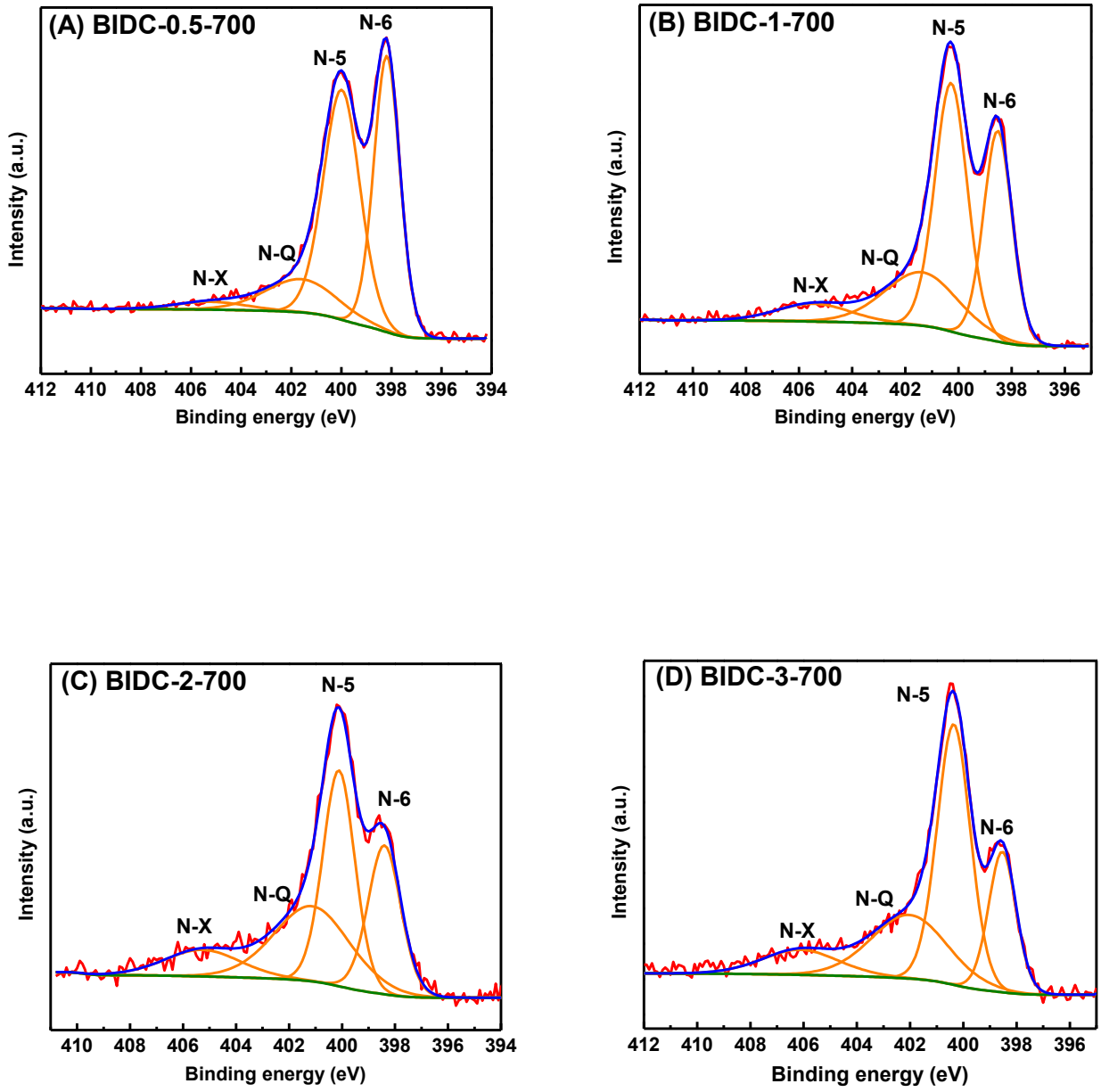

Figure 4.12. High resolution deconvoluted N 1s spectra of (A) BIDC-0.5-700, (B) BIDC-1-700, (C) BIDC-2-700 and (D) BIDC-3-700.

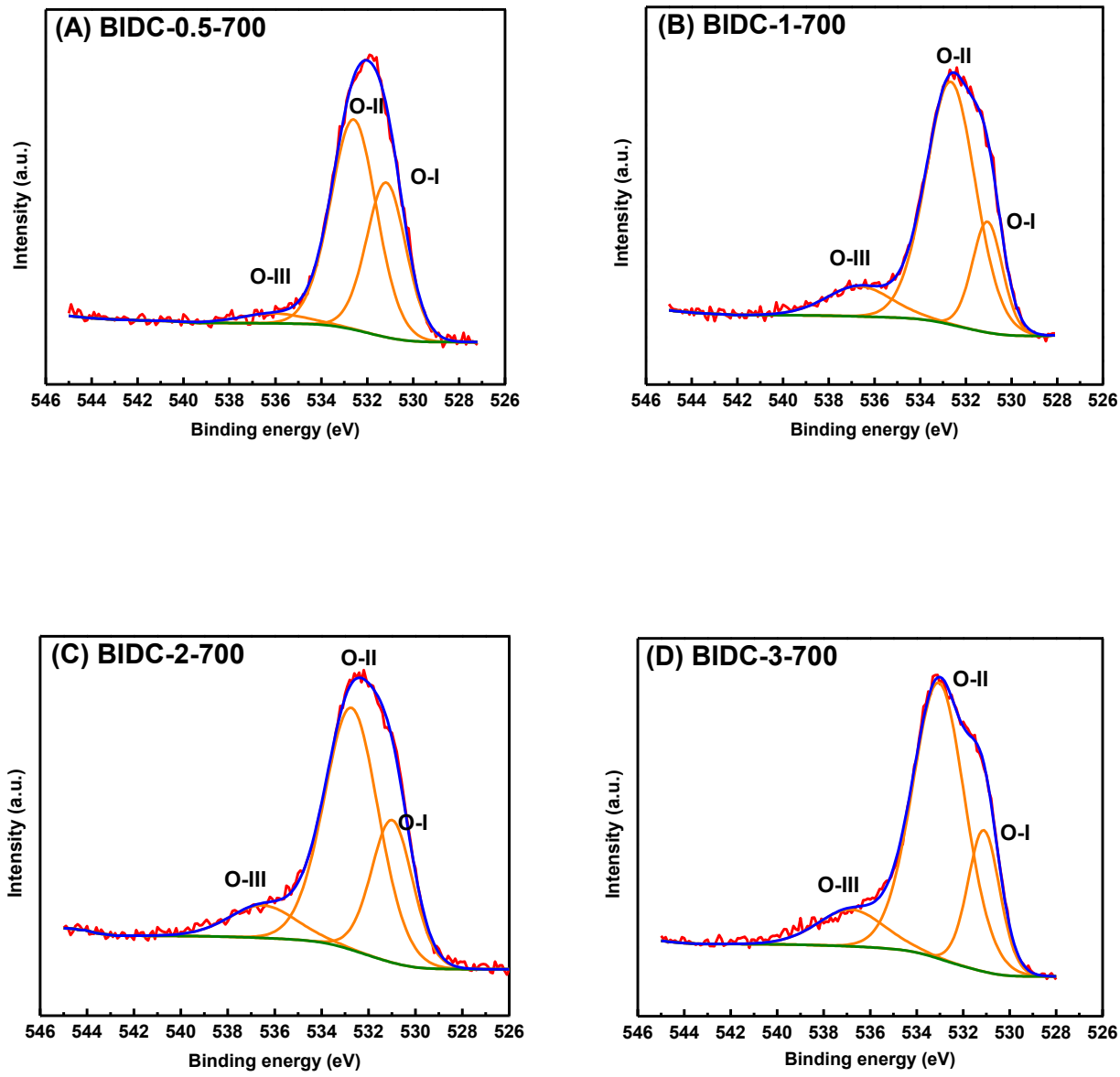

Figure 4.13. High resolution deconvoluted O 1s spectra of (A) BIDC-0.5-700, (B) BIDC-1-700, (C) BIDC-2-700 and (D) BIDC-3-700.

4.3.5 CO_2 Capture Performance. Owing to the high level of heteroatom surface groups and large micropore volume of BIDCs, we decided to evaluate their performance as CO_2 adsorbent at low pressure (0-1 bar). Accordingly, their CO_2 capture capacity are measured at 273, 298, and 323 K up to 1 bar (Figure 4.14 a-c) and the uptake values at 0.15 and 1 bar are listed in Table 4.2. It should be noted that the adsorption capacity at 0.15 bar is of great significance because it represents the typical partial pressure of CO_2 in flue gas. These results clearly demonstrate the outstanding CO_2 uptake capacity of BIDCs even at high temperatures. At 273 K and 1 bar, all samples exhibit CO_2 capture value greater than 6 mmol g^{-1} which among them the BIDC-1-700 sample reaches a remarkable value of 10.1 mmol g^{-1}. The BIDC-1-700 sample also shows the highest overall uptake of 6.2 and 3.3 mmol g^{-1} at 298 and 323 K, respectively. Such a high capture capacity outperforms quite most of the activated carbons under similar condition. Only Nandi *et al*. reported greater value of 11.5 mmol g^{-1} at 273 K and 1 bar for a polyacrylonitrile-derived carbon.[20] However, they take advantage of physical activation with CO_2 gas at very high temperature with a complex and multistep procedure to achieve such a high capture capacity. In contrast, our strategy is facile, straightforward and reproducible. At 0.15 bar the trend is slightly different and BIDC-0.5-700 features the highest capture capacity of 3.5, 1.9 and 1.0 mmol g^{-1} at 273, 298 and 323 K, respectively.

Table 4.2. Gas Uptakes in mmol g^{-1} and Isosteric Heats of Adsorption (Q_{st}) in kJ mol^{-1}

	CO_2 at 0.15 bar			CO_2 at 1 bar			Q_{st}
Sample	273 K	298 K	323 K	273 K	298 K	323 K	
BIDC-0.5-700	3.5	1.9	1.0	7.2	5.1	3.2	33.1
BIDC-1-700	3.3	1.6	0.8	10.1	6.2	3.3	30.3
BIDC-2-700	1.7	0.8	0.4	6.8	3.9	2.1	25.3
BIDC-3-700	1.3	0.7	0.3	6.0	3.4	1.7	21.8

To investigate the strength of the interaction between CO_2 molecules and BIDCs, isosteric heat of adsorption (Q_{st}) was calculated by fitting CO_2 adsorption isotherms at 273 and 298 K to the virial equation. At zero coverage the values of Q_{st} decrease from 33 to 22 kJ mol^{-1} as the KOH to BI ratio increases from 0.5 to 3 (Figure 4.14 d). This further confirms that the highest measured isosteric heat of adsorption for BIDC-0.5-700 is mainly due to interaction of its nitrogen functionalities (14.5 wt%) with CO_2 molecules. The impact of nitrogen functionalities on CO_2 uptake enhancement of numerous porous polymers and carbons has been fully investigated.[21-23] In general, nitrogen functionalities on the pore walls are able to anchor CO_2 molecules either thorough dipole-quadropole interaction or hydrogen bonding. It is worth mentioning that formation of oxygen functionalities in KOH activated carbons is unavoidable as confirmed earlier by XPS analysis. Nevertheless, the role of oxygen functionalities in CO_2 adsorption of activated carbons is widely underestimated. The oxygen basic groups can contribute positively to higher level of adsorption with similar mechanisms of nitrogen functionalities.[24-25] The Q_{st} observation well explains the relationship between heteroatoms doping level and low pressure CO_2 uptake. However, the outstanding overall CO_2 capture capacity of prepared carbons cannot be solely rationalized by basic functional groups. It has been proven that narrow micropores can effectively strengthen the interaction between pore walls and CO_2 molecules.[7, 26-27] Thus, the ultrahigh CO_2 uptake can be correlated to the synergistic effect of basic dopants (oxygen and nitrogen) and narrow micropores developed during chemical activation. More specifically, Presser *et al.*[28] showed that in order to achieve a high CO_2 uptake for carbide-derived carbons (CDCs) at 1 bar, pores smaller than 8 Å are preferred while at lower pressure of 0.1 bar pores smaller than 5 Å are needed. Thus, the excellent performance of BIDC-1-700 in spite of almost similar level of heteroatom and percentage microporosity to BIDC-0.5-700 must be driven by higher volume of

ultramicropores (V_0 in Table 4.1). The difference between low pressure and final (1 bar) CO_2 uptake values of these two samples also can be observed in their CO_2 isotherms by an intersection point. It can be deduced that at relative pressures lower than intersection point surface heterogeneity is more beneficial to the CO_2 uptake, whereas narrow micropores play more important role at higher pressures. This intersection point takes place at relative pressures of 0.2 bar for 273 K isotherm and shifts to higher values of 0.5 and 0.8 bar for 298 K and 323 K isotherms, respectively. This further indicates that at higher temperatures the CO_2 uptake is more controlled by electrostatic interaction rather than physical adsorption through weak van der Waals interaction.

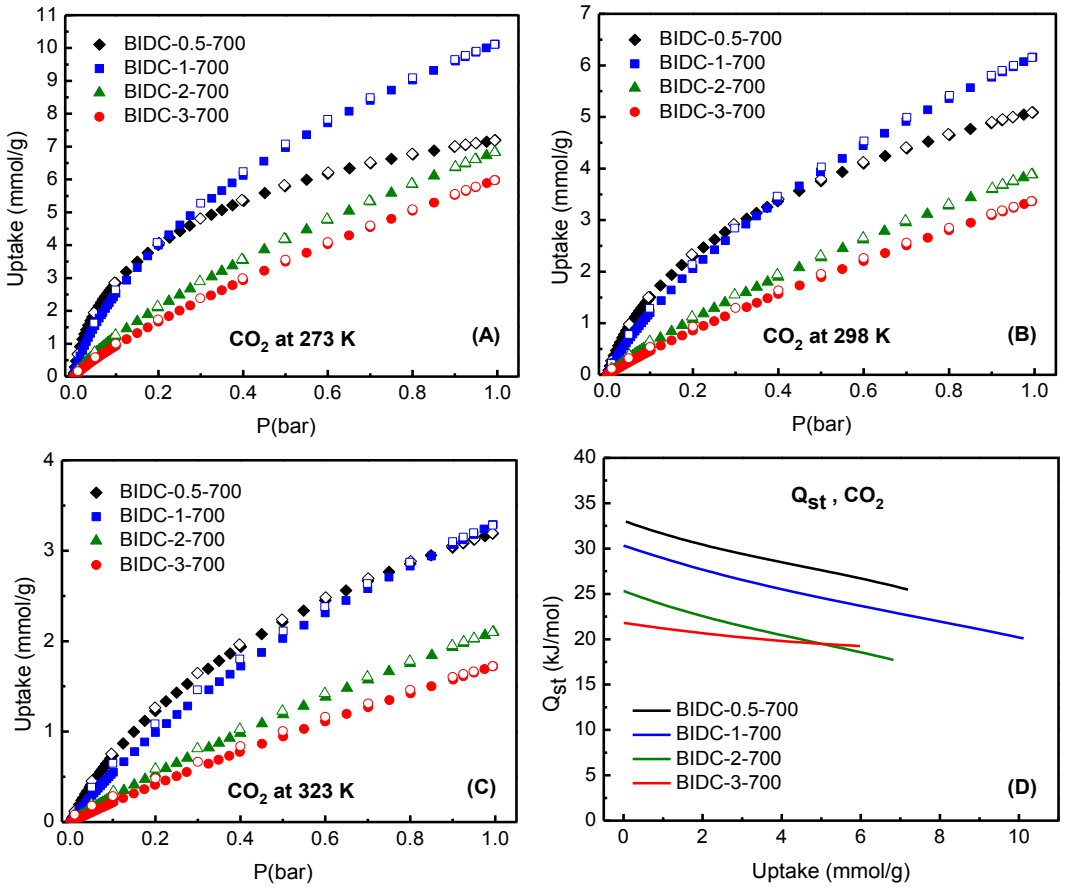

Figure 4.14. CO_2 adsorption isotherms at (a) 273 K, (b) 298 K, (c) 323 K and (d) isosteric heat of adsorption for BIDCs.

4.3.6 Working Capacity. The fact that BIDCs showed remarkable CO_2 uptakes at ambient temperature and pressure encouraged us to perform the calculation of sorbent evaluation criteria described by Bae and Snurr.[29] These criteria should be considered together for a comprehensive evaluation of sorbents as it gives insight into the trade-off between gas uptake and selectivity. Therefore, this analysis helps us to attain the best candidate for different industrial conditions yet it only requires the use of pure gas isotherms. These five criteria can be summarized as *CO_2 uptake under adsorption conditions* (N_1^{ads}); *working CO_2 capacity (ΔN_1)*, difference between CO_2 uptake capacity at the adsorption pressure (N_1^{ads}) and the desorption pressure (N_1^{des}); *regenerability (R),* ($\Delta N_1/N_1^{ads}$) × 100 %; s*electivity under adsorption conditions* (α_{12}^{ads}); *sorbent selection parameter (S)* is defined as $S=(\alpha_{12}^{ads})^2/(\alpha_{12}^{des}) \times (\Delta N_1/\Delta N_2)$ where superscripts ads and des represent the adsorption and desorption conditions, respectively. Since the *S* value combines the selectivity and the working capacity (uptake) of the gases, it provides an insight into trade-off between these two parameters.

Landfill gas-fired power plants are feasible alternative to coal-fired power plant as the former has much lower carbon footprint. However, landfill gas contains up to 50% CO_2 which needs to be separated in order to increase the energy density.[30] Here, we considered the landfill gas composition as equimolar mixture of CO_2 and CH_4, and vacuum swing process that operates between 1 bar (adsorption pressure) and 0.1 bar (desorption pressure). As shown in Table 4.3, BIDC-1-700 shows the highest working capacity (3.27 mol kg^{-1}) among all listed in the same table. The combined effect of high N-content, high micropore volume and high surface area in BIDC-1-700 resulted in remarkable CO_2 uptake (3.86 mol kg^{-1}) at 298 K and 0.5 bar, and therefore a noteworthy working capacity of CO_2 (3.27 mol kg^{-1}). Despite the presence of open metal sites in Ni-MOF-74, its CO_2 working capacity (3.16 mol kg^{-1}) is lower than that of BIDC-1-700 under the

same conditions.[29] In addition, BIDC-1-700 presents 83.7% regenerability value, which is 65% higher, compared to Ni-MOF-74 caused by optimal Q_{st} value of the former. The lower surface area of TBILP-2 and SNU-Cl-va results in higher selectivity and therefore higher *S* values compared to BIDC-1-700, however, the former present much lower working capacity.[22, 31] High working capacity and moderate selectivity of BIDC-1-700 result in high *S* value, which makes it a promising solid adsorbent for carbon dioxide separation from methane rich gases.

Table 4.3. Adsorbents for VSA in Landfill Gas (CO_2/CH_4: 50/50) Separation at 298 K, P_{ads} = 1 bar and P_{des} = 0.1 bar

Adsorbent	N_1^{ads}	ΔN_1	**% R**	α_{12}^{ads}	***S***
BIDC-0.5-700	3.74	2.84	75.8	7.0	47
BIDC-1-700	3.91	3.27	83.7	6.1	38
BIDC-2-700	2.20	1.90	86.5	3.9	15
BIDC-3-700	1.79	1.58	87.9	3.2	11
Ni-MOF-74	6.23	3.16	50.7	8.5	21
Zeolite-13X	3.97	1.97	49.6	13.2	19
TBILP-2	2.20	1.84	83.7	7.6	63
BILP-12	2.01	1.71	85.3	6.0	34
SNU-Cl-va	1.51	1.21	80.6	9.7	84
Dimide-POP	1.39	1.05	76.0	5.8	16

Table 4.4. Adsorbents for VSA in Flue Gas (CO_2/N_2 : 10/90) Separation at 298 K, P_{ads} = 1 bar and P_{des} = 0.1 bar

Adsorbent	N_1^{ads}	ΔN_1	**% R**	α_{12}^{ads}	***S***
BIDC-0.5-700	1.60	1.37	85.5	36	138
BIDC-1-700	1.19	1.05	87.9	25	67
BIDC-2-700	0.55	0.49	88.7	13	18
BIDC-3-700	0.42	0.37	89.2	10	11
HKUST-1	0.62	0.55	89.0	20	46
TBILP-2	0.67	0.59	88.3	42	192
BILP-12	0.55	0.49	88.7	27	73
ZIF-78	0.60	0.58	96.3	35	396
SNU-Cl-va	0.47	0.41	87.3	38	262

Another industrially important gas mixture that needs to be separated from CO_2 is flue gas. For flue gas separation, the CO_2/N_2 mixture is considered to be 10/90 and adsorption and desorption pressures are taken to be 1 bar and 0.1 bar, respectively. Additionally, the VSA is considered to be more economically viable compared to temperature swing adsorption (TSA) for flue gas separation.[32] Since the partial pressure of CO_2 is lower in the flue gas compared to landfill gas, the initial CO_2 uptake (at 0.1 bar) is much more important. High percentage of micropore volume and CO_2-philic sites are known to increase CO_2 uptakes at lower partial pressures. The BIDC-0.5-700 sample consists of 14.5 wt% nitrogen atoms and 96% micropores and exhibits significant CO_2 uptake (1.52 mol kg^{-1}) at 0.1 bar and 298 K. Therefore, the working capacity of the BIDC-0.5-700 is ~30% higher compared to BIDC-1-700 despite much higher surface area of the latter. High binding affinity (33.1 kJ mol^{-1}) for CO_2 in BIDC-0.5-700 results in high CO_2 over N_2 selectivity (35.8) and thus, a remarkable sorbent selection parameter, *S,* value. ZIF-78 and SNU-Cl-va samples present the highest *S* but because of their low CO_2 working capacities, their practical use is limited. Experimental data and corresponding fittings of CO_2, CH_4, and N_2 adsorption isotherms for all BIDC samples are presented in Figures 4.15-4.18.

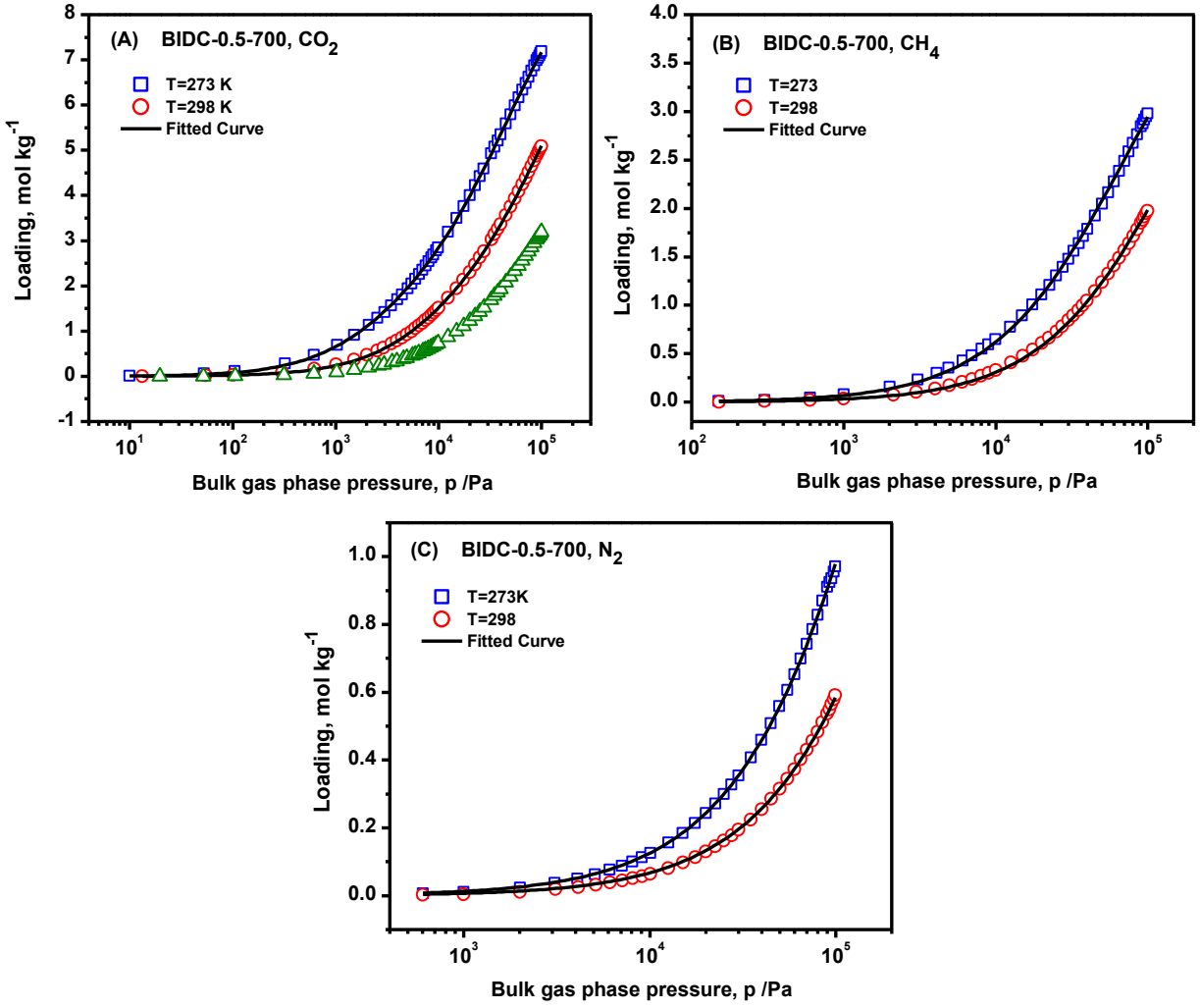

Figure 4.15. Experimental data (symbol) and corresponding fittings (solid line) of CO_2 (A), CH_4 (B), and N_2 (C) adsorption isotherms in BIDC-0.5-700 at low pressures (0-1 bar).

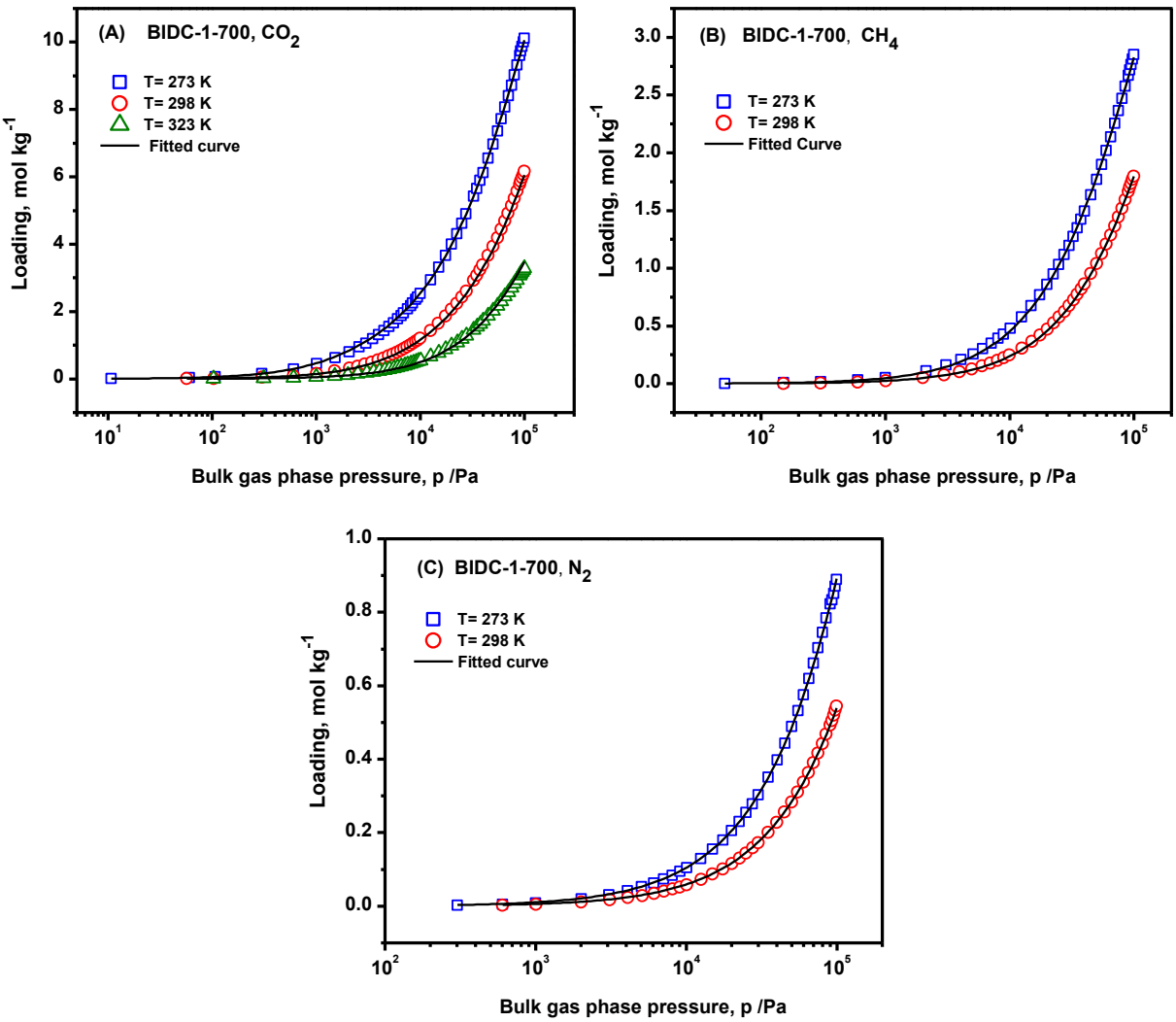

Figure 4.16. Experimental data (symbol) and corresponding fittings (solid line) of CO_2 (A), CH_4 (B), and N_2 (C) adsorption isotherms in BIDC-1-700 at low pressures (0-1 bar).

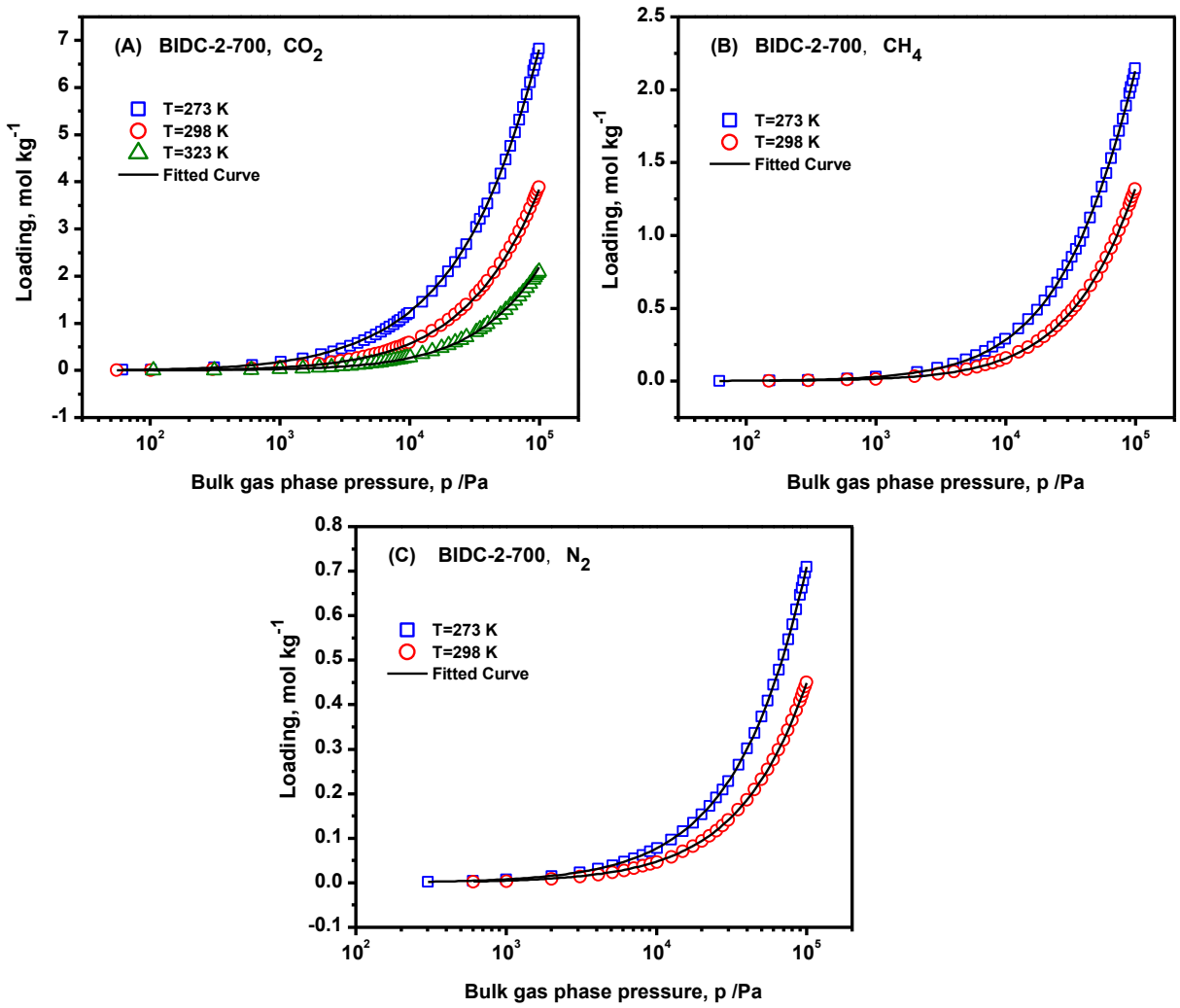

Figure 4.17. Experimental data (symbol) and corresponding fittings (solid line) of CO_2 (A), CH_4 (B), and N_2 (C) adsorption isotherms in BIDC-2-700 at low pressures (0-1 bar).

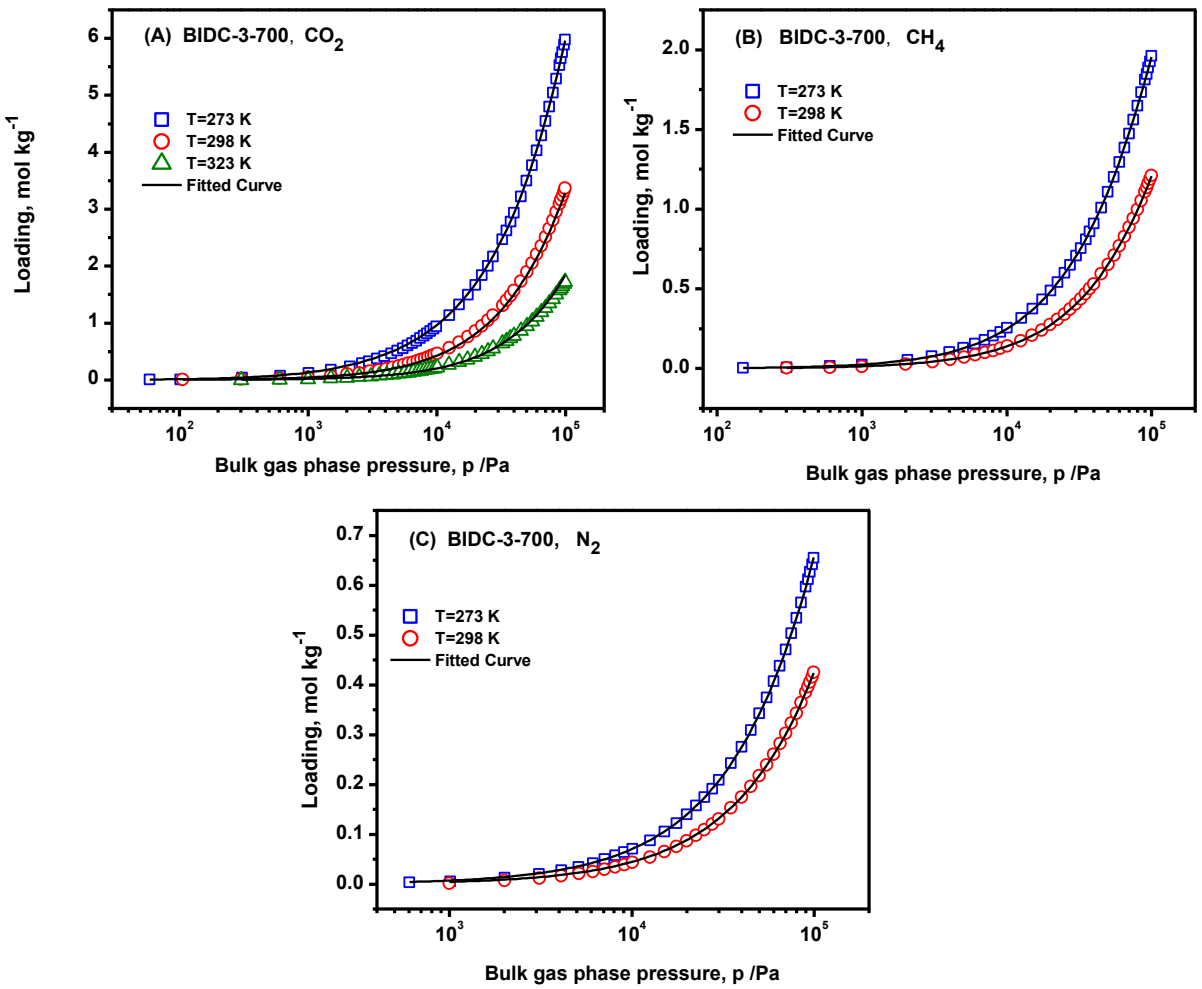

Figure 4.18. Experimental data (symbol) and corresponding fittings (solid line) of CO_2 (A), CH_4 (B), and N_2 (C) adsorption isotherms in BIDC-3-700 at low pressures (0-1 bar).

4.4 Conclusion

In summary, the synthesis of novel oxygen and nitrogen-doped activated carbons has been demonstrated by a facile, solvent-free, cost-effective, and readily reproducible approach. The heteroatom doped porous carbons were synthesized by one-step chemical activation of inexpensive benzimidazole building unit, which serves as a single source precursor of both carbon and nitrogen. The synthesis parameters can be adjusted to tailor the textural properties and heteroatom contents in order to achieve the best gas sorption properties. The BIDC-1-700, with a high amount of dopants and fine micropores exhibited outstanding CO_2 capture performance of 10.1 and 6 mmol g^{-1} at 273 and 298 K, respectively. Moreover, BIDCs feature high working capacity values for practical separation applications of CO_2 from N_2 and CH_4. In particular, for CO_2 separation from land fill gas, the BIDC-1-700 sample featured a very high working capacity (3.27 mol kg^{-1}) which is comparable to values obtained by MOFs with open metal sites. The synthetic approach is reproducible and scalable and can easily be extended to other building blocks, which meet the criteria.

4.5 References

1. Toyao, T.; Fujiwaki, M.; Miyahara, K.; Kim, T. H.; Horiuchi, Y.; Matsuoka, M., Design of Zeolitic Imidazolate Framework Derived Nitrogen-Doped Nanoporous Carbons Containing Metal Species for Carbon Dioxide Fixation Reactions. *ChemSusChem* **2015**, *8*, 3905-12.

2. Gadipelli, S.; Guo, Z. X., Tuning of ZIF-Derived Carbon with High Activity, Nitrogen Functionality, and Yield - A Case for Superior CO_2 Capture. *ChemSusChem* **2015**, *8*, 2123-32.

3. Kim, J.; Oliver, A. G.; Hicks, J. C., Enhanced CO_2 Capture Capacities and Efficiencies with N-Doped Nanoporous Carbons Synthesized from Solvent-Modulated, Pyridinedicarboxylate-Containing Zn-MOFs. *CrystEngComm* **2015**, *17*, 8015-8020.

4. Modak, A.; Bhaumik, A., Porous Carbon Derived via KOH Activation of a Hypercrosslinked Porous Organic Polymer for Efficient CO_2, CH_4, H_2 Adsorptions and High CO_2/N_2 Selectivity. *J. Solid State Chem.* **2015**, *232*, 157-162.

5. Wang, J.; Senkovska, I.; Oschatz, M.; Lohe, M. R.; Borchardt, L.; Heerwig, A.; Liu, Q.; Kaskel, S., Highly Porous Nitrogen-Doped Polyimine-Based Carbons with Adjustable Microstructures for CO_2 Capture. *J. Mater. Chem. A* **2013**, *1*, 10951-10961.

6. Ashourirad, B.; Sekizkardes, A. K.; Altarawneh, S.; El-Kaderi, H. M., Exceptional Gas Adsorption Properties by Nitrogen-Doped Porous Carbons Derived from Benzimidazole-Linked Polymers. *Chem. Mater.* **2015**, *27*, 1349-1358.

7. Sevilla, M.; Fuertes, A. B., CO_2 Adsorption by Activated Templated Carbons. *J. Colloid Interface Sci.* **2012**, *366*, 147-154.

8. Wang, J.; Heerwig, A.; Lohe, M. R.; Oschatz, M.; Borchardt, L.; Kaskel, S., Fungi-Based Porous Carbons for CO_2 Adsorption and Separation. *J. Mater. Chem.* **2012**, *22*, 13911-13913.

9. Paraknowitsch, J. P.; Zhang, J.; Su, D.; Thomas, A.; Antonietti, M., Ionic Liquids as Precursors for Nitrogen-Doped Graphitic Carbon. *Adv. Mater.* **2010**, *22*, 87-92.

10. Sevilla, M.; Parra, J. B.; Fuertes, A. B., Assessment of the Role of Micropore Size and N-Doping in CO_2 Capture by Porous Carbons. *ACS Appl. Mater. Interfaces* **2013**, *5*, 6360-6368.

11. Myers, A. L.; Prausnitz, J. M., Thermodynamics of Mixed-Gas Adsorption. *AIChE J.* **1965**, *11*, 121-127.

12. Sekizkardes, A. K.; Islamoglu, T.; Kahveci, Z.; El-Kaderi, H. M., Application of Pyrene-Derived Benzimidazole-Linked Polymers to CO_2 Separation under Pressure and Vacuum Swing Adsorption Settings. *J. Mater. Chem. A* **2014**, *2*, 12492-12500.

13. Grevy, J. M.; Tellez, F.; Bernés, S.; Nöth, H.; Contreras, R.; Barba-Behrens, N., Coordination Compounds of Thiabendazole with Main Group and Transition Metal Ions. *Inorg. Chim. Acta* **2002**, *339*, 532-542.

14. Wright, J. B., The Chemistry of the Benzimidazoles. *Chem. Rev.* **1951**, *48*, 397-541.

15. Wang, J.; Kaskel, S., KOH Activation of Carbon-Based Materials for Energy Storage. *J. Mater. Chem.* **2012**, *22*, 23710-23725.

16. Hu, X.; Radosz, M.; Cychosz, K. A.; Thommes, M., CO_2-Filling Capacity and Selectivity of Carbon Nanopores: Synthesis, Texture, and Pore-Size Distribution from Quenched-Solid Density Functional Theory (QSDFT). *Environ. Sci. Technol.* **2011**, *45*, 7068-7074.

17. Kuhn, P.; Forget, A.; Su, D.; Thomas, A.; Antonietti, M., From Microporous Regular Frameworks to Mesoporous Materials with Ultrahigh Surface Area: Dynamic Reorganization of Porous Polymer Networks. *J. Am. Chem. Soc.* **2008**, *130*, 13333-13337.

18. Hulicova-Jurcakova, D.; Seredych, M.; Lu, G. Q.; Bandosz, T. J., Combined Effect of Nitrogen- and Oxygen-Containing Functional Groups of Microporous Activated Carbon on Its Electrochemical Performance in Supercapacitors. *Adv. Funct. Mater.* **2009**, *19*, 438-447.

19. Pels, J. R.; Kapteijn, F.; Moulijn, J. A.; Zhu, Q.; Thomas, K. M., Evolution of Nitrogen Functionalities in Carbonaceous Materials During Pyrolysis. *Carbon* **1995**, *33*, 1641-1653.

20. Nandi, M.; Okada, K.; Dutta, A.; Bhaumik, A.; Maruyama, J.; Derks, D.; Uyama, H., Unprecedented CO_2 Uptake over Highly Porous N-Doped Activated Carbon Monoliths Prepared by Physical Activation. *Chem. Commun.* **2012**, *48*, 10283-10285.

21. Rabbani, M. G.; El-Kaderi, H. M., Template-Free Synthesis of a Highly Porous Benzimidazole-Linked Polymer for CO_2 Capture and H_2 Storage. *Chem. Mater.* **2011**, *23*, 1650-1653.

22. Arab, P.; Rabbani, M. G.; Sekizkardes, A. K.; İslamoğlu, T.; El-Kaderi, H. M., Copper(I)-Catalyzed Synthesis of Nanoporous Azo-Linked Polymers: Impact of Textural Properties on Gas Storage and Selective Carbon Dioxide Capture. *Chem. Mater.* **2014**, *26*, 1385-1392.

23. Sevilla, M.; Valle-Vigón, P.; Fuertes, A. B., N-Doped Polypyrrole-Based Porous Carbons for CO_2 Capture. *Adv. Funct. Mater.* **2011**, *21*, 2781-2787.

24. Torrisi, A.; Mellot-Draznieks, C.; Bell, R. G., Impact of Ligands on CO_2 Adsorption in Metal-Organic Frameworks: First Principles Study of the Interaction of CO_2 with Functionalized Benzenes. I. Inductive Effects on the Aromatic Ring. *J. Chem. Phys.* **2009**, *130*, 194703.

25. Liu, Y.; Wilcox, J., Effects of Surface Heterogeneity on the Adsorption of CO_2 in Microporous Carbons. *Environ. Sci. Technol.* **2012**, *46*, 1940-1947.

26. Wickramaratne, N. P.; Jaroniec, M., Activated Carbon Spheres for CO_2 Adsorption. *ACS Appl. Mater. Interfaces* **2013**, *5*, 1849-1855.

27. Zhang, Z.; Zhou, J.; Xing, W.; Xue, Q.; Yan, Z.; Zhuo, S.; Qiao, S. Z., Critical Role of Small Micropores in High CO_2 Uptake. *Phys. Chem. Chem. Phys.* **2013**, *15*, 2523-2529.

28. Presser, V.; McDonough, J.; Yeon, S.-H.; Gogotsi, Y., Effect of Pore Size on Carbon Dioxide Sorption by Carbide Derived Carbon. *Energy Environ. Sci.* **2011**, *4*, 3059-3066.

29. Bae, Y.-S.; Snurr, R. Q., Development and Evaluation of Porous Materials for Carbon Dioxide Separation and Capture. *Angew. Chem., Int. Ed.* **2011**, *50*, 11586-11596.

30. Farha, O. K.; Bae, Y.-S.; Hauser, B. G.; Spokoyny, A. M.; Snurr, R. Q.; Mirkin, C. A.; Hupp, J. T., Chemical Reduction of a Diimide Based Porous Polymer for Selective Uptake of Carbon Dioxide Versus Methane. *Chem. Commun.* **2010**, *46*, 1056-1058.

31. Xie, L.-H.; Suh, M. P., High CO_2-Capture Ability of a Porous Organic Polymer Bifunctionalized with Carboxy and Triazole Groups. *Chem._Eur. J.* **2013**, *19*, 11590-11597.

32. Chaffee, A. L.; Knowles, G. P.; Liang, Z.; Zhang, J.; Xiao, P.; Webley, P. A., CO_2 Capture by Adsorption: Materials and Process Development. *Int. J. Greenhouse Gas Control* **2007**, *1*, 11-18.

Chapter 5: Concluding Remarks

The research shown in this dissertation provides reasonable clues as to why activated carbons with a high level of porosity and heteroatom are attractive materials in the field of gas storage and separation. The objective of this dissertation is to gain systematic knowledge about outcomes of task-specific precursors, their transformation into heteroatom-doped carbons and the gas adsorption behavior of final products. The important outcomes of this research study are summarized below.

First, a specific benzimidazole-linked polymer, BILP-5, was selected as a single source precursor of carbon and nitrogen. Five different carbons were synthesized by physical mixing of BILP-5 and KOH inside the glovebox and subsequent heating under Ar atmosphere. Isolation of black fine powders after acid washing validated the successful transformation of BILP-5 into a porous carbon. Inspired by carbons prepared from BILP-5, we deliberately targeted an azo-lined polymer, ALP-6 as the next precursor. ALP-6 not only benefits from the higher nitrogen level and easier synthetic procedure but also features robust nitrogen linkage. In order to convert ALP-6 to microporous carbon, the synthetic strategies were expanded to $ZnCl_2$ and KOH activation as well as direct carbonization under mild temperatures. To this end, four different classes of doped carbons synthesized by employing porous organic polymers as precursors. However, complex steps as well as low yield and toxic features of organic polymer synthesis encouraged us to use more sustainable precursors. Accordingly, the possibility of carbonization of molecular

benzimidazole as a non-porous organic building block and highly rich in nitrogen was evaluated in our last work. Considering the successful conversion of BILP-5 to carbon and the protic nature of benzimidazole molecules, KOH was employed as both neutralizing and activating agent. By varying the ratio of KOH to benzimidazole precursor and thermolysis temperature, a new family of carbons were obtained.

Secondly, all carbons were subjected to elemental analysis and X-ray photoelectron spectroscopy (XPS) for compositional studies. These crucial characterization steps not only confirmed successful doping of nitrogen into final carbons but also provided quantitative levels of heteroatoms. In addition to nitrogen doping originated from the precursor, oxygen groups were also realized on the pore walls of carbons. Regardless of precursor used, deconvolution of nitrogen spectra confirmed the presence of pyridinic, pyrrolic/pyridonic and pyridine-N-oxide in all carbons. Elemental analysis results confirmed that the amount of nitrogen dopants in the bulk of final carbons depends upon the selected precursor and synthesis temperature. For example, benzimidazole with 24 wt% initial nitrogen content retained 3.5-14.5 wt% after activation. Retaining 4.7-14.3 wt% of nitrogen in carbon derived from ALP-6 precursor with an initial nitrogen level of 14.7 wt% further validated the robustness of nitrogen-nitrogen linkage with respect to nitrogen-carbon bonds.

Thirdly, the heteroatom-doped carbons were subjected to nitrogen sorption studies at 77 K to evaluate their porosity parameters. These studies revealed superior textural properties (surface area and pore volume) of prepared carbons when compared to their parent precursors. The surface area and pore volume of carbons derived from non-porous benzimidazole precursors range between 1316-4171 $m^2 g^{-1}$ and 0.53-2.39 $cm^3 g^{-1}$, respectively. The initial rapid uptake in nitrogen isotherms confirmed the microporous nature of all prepared carbons. The pores size distribution

curves featured the dominant pore size around 0.9 nm for all carbons. Nevertheless, carbons activated at relatively high temperature consisted of additional narrow mesopore (2-4 nm) while low temperature synthesized carbons were made of mainly ultramicropores (<0.7 nm). The low pressure CO_2 and CH_4 adsorption capacity of carbons were also thoroughly investigated. The results confirmed superior performance of carbons with higher amount of fine micropores and heteroatoms. A benzimidazole derived carbon synthesized under KOH/BI=1 and 700 °C condition exhibited remarkably high CO_2 uptake of 10.1 mmol g^{-1} at 273 K and 1 bar. It is found that, electron-rich oxygen and nitrogen functional groups anchor CO_2 acidic molecules and contribute more positively to physisorption process. In general, the cooperative effect of developed microporosity and high heteroatoms level account for excellent CO_2 adsorption performance of carbons. In contrast to CO_2 capture, the adsorption of less polarizable methane molecule just governed by pore size of carbons. Small pore size resulted in higher methane uptake at lower pressure. Accordingly, wider pores contributed more to adsorption at higher relative pressures.

Finally, the merit of carbons for selective CO_2 separation from N_2 and CH_4 gas mixtures was evaluated by initial slopes of their single-component sorption isotherms. The results indicated higher selectivity for carbons with higher amounts of heteroatom and narrow microspores. However, the drop in CO_2 selective adsorption of highly activated carbons was observed at the expense of nitrogen loss, increase in surface area, and pore enlargement. This trend is found to be consistent with isosteric heat of adsorption data at zero loading. Among different classes of prepared carbons, ALP-6 based carbon showed superior selectivity values. Namely, ALPDCK500 was able to reach ultrahigh selectivity levels of 115 for CO_2/N_2 and 18 for CO_2/CH_4 at 273 K.

Extending of our research work can be classified into two main categories: applications and materials/methods. As mentioned earlier in the introduction section, the polarity induced by

basic heteroatoms makes resultant carbons attractive materials for capturing polarizable molecule besides CO_2. As such, the adsorption behavior of SO_2, NO_2 and water vapor can be investigated by using our porous carbons. In addition, the conductive nature of carbons coupled with modified surface chemistry by dopants makes them promising electrode materials for energy storage applications. Addressing the materials and methods aspects, a wide range of task-specific organic building blocks can be converted to carbons. The importance of molecular precursor becomes more prominent when sustainability, scalability, reproducibility and simplicity of procedure is considered.

In summary, we have introduced five series of heteroatom-doped carbons by one-pot activation or carbonization of a single source precursor. The precursors were chosen based on either presence of nitrogen in pyridinic/pyrrolic positions or robustness of nitrogen linkage. Chemical activation by KOH and $ZnCl_2$ as well as direct carbonization was applied to transform precursors to highly porous and heteroatom doped carbons. Overall, the research works presented in this dissertation open a new chapter of using efficient and sustainable materials and methods in the field of gas storage and separation. Although our prepared carbons featured remarkable gas sorption properties, there is still much more room for additional scientific investigations. With further research and effort, the molecule-derived carbons can be commercialized and used in relevant industrial applications.